Thinking of $(1,1)$ knots using elastic bands on peg-boards and combed glazing on the mille-feuille

by

Mihai Marian

BSc. Mathematics, McGill University, 2018

A THESIS SUBMITTED IN PARTIAL FULFILLMENT
OF THE REQUIREMENTS FOR THE DEGREE OF

Master of Science

in

THE FACULTY OF GRADUATE AND POSTDOCTORAL STUDIES
(Mathematics)

The University of British Columbia
(Vancouver)

August 2020

The following individuals certify that they have read, and recommend to the Faculty of Graduate and Postdoctoral Studies for acceptance, the thesis entitled:

Thinking of $(1,1)$ knots using elastic bands on peg-boards and combed glazing on the mille-feuille

submitted by **Mihai Marian** in partial fulfillment of the requirements for the degree of **Master of Science** in **Mathematics**.

Examining Committee:

Liam Watson, Mathematics
Supervisor

Benedict Williams, Mathematics
Supervisory Committee Member

Abstract

Despite the analytic underpinnings of Heegaard Floer theory and its refinement to knots, there is an interesting class of knots, the $(1,1)$ knots, which have the special property that their knot Floer homology can be computed naïvely, straight from the definition, using only combinatorial techniques. In this thesis, we survey $(1,1)$-knots, describe their knot Floer homology, and focus in particular on the landscape of the manifolds obtained by Dehn surgery on these knots. More precisely, J. Greene, S. Lewallen and F. Vafaee recently described a simple criterion for determining if a $(1,1)$ knot admits a nontrivial surgery to an L-space, using the orientation of the curves in a doubly pointed genus-1 Heegaard diagram for the knot. This characterization is formally very similar to a characterization due to J. Hanselman, J. Rasmussen and L. Watson, using a graphical calculus they developed for working with the bordered Floer theory. We relate these two perspectives, by providing in the final chapter a novel proof of Greene et al.'s criterion using the graphical calculus, recently expanded by A. Kotelskiy, Watson and C. Zibrowius.

Lay Summary

Three-dimensional spaces are complicated! As arrogant humans, it behooves us to build frameworks to understand these complications. One framework, Heegaard Floer theory, uses the simple idea that the path taken by a marble dropped on a surface tells a lot about the shape of the surface. Analogously, Heegaard Floer theory organizes all possible paths of marbles floating in a three-dimensional space with a single massive source of gravity. Within this framework, we consider a specific topic: how knots can be used to build new spaces out of old. Two marbles sitting at the same point, maximally far away from the source, eventually reach it, if nudged, and their trajectories form a knot in the space. There are two different methods for telling whether such a knot can be used to build L-spaces, which are the simplest possible spaces in Heegaard Floer theory, and this thesis discusses and bridges these methods.

Preface

Chapters 2 and 3 and section 4.1 form standard material, extant in textbooks, and included for the purpose of having this thesis be self-contained; the author's only possible contribution is in the presentation. The rest of chapter 4 and all of chapter 6 is an exposition of work found in parts of [Ras05], [GLV18], [HRW16], [HRW18] and [KWZ20]; some arguments, unless clearly referenced from other sources, are the author's own. Chapters 5 and 7 consist of original, unpublished, independent work of the author, spurred by conversations with the author's advisor.

Table of Contents

Abstract . . . . . **iii**

Lay Summary . . . . . **iv**

Preface . . . . . **v**

Table of Contents . . . . . **vi**

List of Figures . . . . . **viii**

Acknowledgments . . . . . **x**

1 Introduction **1**

2 Some 3-manifold Topology **4**

2.1 Heegaard Diagrams 5

2.2 The Morse Theory Perspective 10

2.3 $(1,1)$ Knots and their Diagrams 15

2.3.1 The Bridge Number of Knots 16

2.3.2 (g,b) Knots 18

3 Knot Floer Homology **24**

3.1 General Definition 25

3.1.1 *CFK* the Vector Space 26

3.1.2 *CFK* the Type D Structure 27

3.1.3 Variations on a Theme 30

3.1.4 Spin^c Structures 31
3.1.5 CFK the Chain Complex 32
3.2 Simplifications in Genus 1 33
3.2.1 $CFK = CFK$ 37
3.3 Some Sample Computations 38

4 On $(1,1)$ L-space Knots 42
4.1 An Overview of Dehn Surgery 43
4.2 The Normal Form 46
4.3 Sketch of the Proof of Theorem 4.2.7 51
4.3.1 The Staircase Characterization 51
4.3.2 The Proof 53
4.4 Algorithmic Implementation 56
4.4.1 Discussion 59

5 The Structure of Bigons in $(1,1)$ Diagrams 60
5.1 From $(1,1)$ to CFK 61
5.2 The Knot $K(19,2,1,7)$ 62
5.3 Purity Conjecture 67

6 Immersed Curves 70
6.1 The Immersed Curve $\widehat{HF}$ 71
6.1.1 2-surgery on the Right-handed Trefoil Knot 76
6.2 The  Formalism 79
6.2.1 The Basis Simplification Algorithm 83
6.2.2 Monotonicity 85

7 The Reproof 87
7.1 Coherence of $\mathcal{D}$ is equivalent to monotonicity of Υ 88
7.2 Υ detects L-space knots 95

8 Conclusion 96

Bibliography 98

List of Figures

Figure 2.1 A genus 2 Heegaard diagram 9
Figure 2.2 A doubly-pointed Heegaard diagram 15
Figure 2.3 Two projections of 4_1 in bridge position. 18
Figure 2.4 The knot described by fig. 2.2. 20
Figure 2.5 A $(1,1)$ diagram for the trefoil after a Dehn twist. 21
Figure 2.6 The knot 6_2 with candidate γ and τ coloured. 22
Figure 2.7 $(1,1)$ diagrams. 22
Figure 2.8 A torus with a β curve for 6_2. 23
Figure 2.9 A $(1,1)$ diagram for 6_2. 23

Figure 3.1 A bigon removal. 34
Figure 3.2 A bigon from x to y. 35
Figure 3.3 A $(1,1)$ diagram and a lift of β. 37
Figure 3.4 $(1,1)$ diagram for $\mathbb{U}$. 38
Figure 3.5 $(1,1)$ diagrams for the trefoil knots. 39
Figure 3.6 $(1,1)$ diagram for 4_1 and $CFK(4_1)$. 41
Figure 3.7 The complex $CFK^-(4_1)$. 41

Figure 4.1 Two homological bases for $H_1(\partial\nu(K);\mathbb{Z})$. 44
Figure 4.2 A generic $(1,1)$ diagam in normal form 47
Figure 4.3 An application of D_α, the Dehn twist along α. 48
Figure 4.4 Oriented $(1,1)$ diagrams for the two trefoil knots 50
Figure 4.5 A $(1,1)$ diagram for 8_{19} and $CFK(8_{19})$. 53
Figure 4.6 The pair $(\widetilde{\beta},\widetilde{\alpha})$ for the diagram $\mathcal{D}(5,1,1,1)$. 55

Figure 4.7 Identities satisfied by the indices of intersection points . . 58

Figure 5.1 $(1,1)$ diagram for $K(19,2,1,7)$ 63
Figure 5.2 A sketch of the bigon B'. 64
Figure 5.3 The bigon $\bullet_{18} \xrightarrow{U^4} \bullet_{10}$. 66
Figure 5.4 A bigon B in H^+ s.t. $n_w(B) = 0$. 67
Figure 5.5 Two possible cases for γ. 68

Figure 6.1 Mnemonic for immersing $\widehat{CFD}(Y)$ into T_Y. 74
Figure 6.2 The immersed curve $\widehat{HF}$ for the right-handed trefoil. . . . 75
Figure 6.3 $\widehat{HF}(D^2 \times S^1)$, with the standard framing. 75
Figure 6.4 The curves $\widehat{HF}(K^c)$ and $h(\ell)$. 76
Figure 6.5 An example of a train track in  80
Figure 6.6 The type D structure $CFK(\mathcal{D}(5,2,1,0))$. 82
Figure 6.7 The simplified type D structure $CFK(\mathcal{D}(5,2,1,0))$. 82
Figure 6.8 The immersed curve invariant $\gamma(4_1)$. 83
Figure 6.9 An illustration of $\gamma(8_{19})$. 85

Figure 7.1 Sketch of the snail from R_{j-2} to R_j 90
Figure 7.2 Sketch of the possible snails in the base case $h = k = 0$ . . 91
Figure 7.3 The disc transformation applied to a subarc of $\widetilde{\beta}$. 92
Figure 7.4 Possible extensions of the snail from case (1). 93
Figure 7.5 Possible γ with $(\Psi(i))$ an alternating string of 1 and 0. . . 94

Acknowledgments

I am privileged to have a mentor as supportive, amicable and communicative as I do. I extend my gratitude to Liam Watson, for teaching me much more than how to turn type D structures into immersed curves in surfaces. I hope to one day be as generous, open-minded and knowledgeable an advisor as he is.

I am also grateful to the professors at UBC and, in particular, to Ben Williams, not only for his generous help and advice, beyond what is expected of a second reader on a lengthy MSc. thesis, but also for instilling in me the importance of clarity and organization through his lectures.

Of course, I would not have been able to work on this project if it hadn't been for profs. Przytycki, Wise and Kamran at McGill, who introduced me to the wonderful jungle of 3-manifolds and mentored me in my final years of undergraduate studies.

Thanks go to my friends, Tristan, Ruby, James, Adriane and Chloé at home, who, perhaps unwittingly, shaped me in my formative years, and my friends Sebastian, Kim and Liam, who formed the best possible bubble here in Vancouver. Conversations with Niny and my office-mates Santanil, Max, Sebastian and Ben helped inform some of the exposition; we had a good thing going before we no longer could. Special thanks to Sebastian for reading and critiquing some of this beast.

Finally, and most importantly, I am lucky to have a loving and supportive

family, starting with my amazing grandmother Aurelia who has four years of education but made sure that her sons stayed in school, and including my parents Marcel and Laura, my sister Andra and her husband Tom, and my Naomi, who inexplicably put up me for all this time and helped me with my code.

Chapter 1

Introduction

Our objects of study in this thesis are circles embedded in lens spaces (i.e. knots in lens spaces), and our framework is Heegaard Floer theory. This is in spirit a (3+1)-dimensional TQFT and it specializes to a powerful homological theory for knots, called knot Floer homology; the original theory is due to P. Ozsváth and Z. Szabó in [OS04c], and the knot Floer homology was discovered by them in [OS04a] and independently by J. Rasmussen over the course of his PhD, [Ras03]. More recently, in the last decade, the Heegaard Floer theory has been expanded by R. Lipshitz, P. Ozsváth and D. Thurston to 3-manifolds with connected boundary into what is known as *bordered Heegaard Floer theory*, [LOT18]. This expansion has been been given a very pretty geometric interpretation by J. Hanselman, J. Rasmussen and L. Watson in [HRW16], in the case of 3-manifolds with torus boundary: to such a manifold one can associate a collection of curves immersed in the boundary, and these curves, up to regular homotopy, form an invariant. The Heegaard Floer homology of the gluing of two manifolds along their torus boundary can then be obtained by overlapping their immersed curve invariants and by organizing the geometric data of the intersection between these two collections of curves. This interpretation makes it especially easy to compute the Heegaard Floer homology of a manifold obtained by Dehn

surgery on a knot, and it makes it even easier to check whether a manifold obtained by Dehn surgery on a knot is an L-space, i.e. a (Heegaard Floer) homology lens space; these are the 3-manifolds with the simplest possible Heegaard Floer homology.

Without using the bordered theory, J. Greene, S. Lewallen and F. Vafaee proved in [GLV18] that, for the special family of so-called $(1,1)$ knots, it is possible to check easily whether a knot admits surgeries to L-spaces by looking at its knot diagram in the torus. The purpose of this thesis is to give a novel proof of Greene, Lewallen and Vafaee's characterization using the immersed curve invariants constructed in [HRW16] and [KWZ20]. This is done in Theorems 7.1.1 and 7.2.1, under an additional technical assumption on the $(1,1)$ knots. This assumption is a conjectured property that $(1,1)$ knots seem to have, but that seems to require some hard work beyond the scope of this thesis to prove directly. The hope is that this novel proof brings the immersed curve invariants closer to the $(1,1)$ diagram, which is not an invariant in itself.

The length of this thesis is due to the background chapters whose purpose is twofold: to have this work be as self-contained as possible and to offer arguments for some facts which are either considered folklore or cannot easily be found in the literature. The rationale for including such a long discussion and exposition prior to the main work is mainly selfish, for the author to convince himself that he knows what he is talking about, but it is also to provide a hopefully useful service to the envisioned reader, who is a graduate student that could make use of pointers and meta-commentary to navigate the presently immense field of Heegaard Floer theory.

Structure of the Thesis

In chapter 2, we review Heegaard diagrams and Morse theory, the goal being to explain how a Heegaard diagram for a 3-manifold M is equivalent to a family of Morse functions on M. This then allows us to describe the con-

struction of Heegaard diagrams that specify knots embedded in 3-manifolds. With section 2.3, we finish by specializing this construction to define $(1,1)$ knots, also known as 1-bridge knots in lens spaces; we also explain at the end how to draw a doubly pointed Heegaard diagram, known as a $(1,1)$ diagram, describing a given $(1,1)$ knot in S^3.

In chapter 3, we first sketch the definition of the type D structure $CFK(K)$ for an arbitrary knot, partly so as to give the reader an idea of the analytic difficulties that this project eschews. We stop along the way to define the other Heegaard Floer invariants, as they can be easily extracted from $CFK(K)$. We then provide an alternate definition of CFK for $(1,1)$ knots and finish by computing this invariant for the small knots.

In chapter 4, after reviewing Dehn surgery in section 4.1, we describe a normal form for $(1,1)$ knots in section 4.2 and in the next section we present the main argument in [GLV18]. In the last section, we present the author's implementation of the algorithm described in [GLV18].

Chapter 5 consists one large worked example, accompanied by a few lemmas and a conjecture describing the fine structure of bigons in $(1,1)$ diagrams, on which the work of chapter 7 relies.

In chapter 6, we introduce the immersed curve invariants from [HRW16] and [KWZ20], which is the framework we use in chapter 7.

Finally, chapter 7 is devoted to a novel proof of the main result in [GLV18]. Section 7.1 contains a combinatorial argument by induction, in which the brunt of the work is an analysis of the possible bigons in a $(1,1)$ diagram; this relies crucially on chapter 5. Section 7.2 is essentially a restatement in our context of the work done in [HRW16] and [HRW18] towards rapid computation of Dehn surgery.

On Notation. The symbol $\simeq$ is used to denote isomorphism in the obvious category that we are working in. We can commit this abuse because we are almost never working with two different categories that have the same objects.

Chapter 2

Some 3-manifold Topology

In this chapter, we will standardize the notation used throughout and briefly describe the objects we are working with. The manifolds mentioned are compact, connected, orientable, topological 3-manifolds, unless otherwise specified; they are also assumed to have empty boundary in Chapters 2 to 4. Of course, to each such manifold corresponds a unique smooth structure, which we allow ourselves to use freely, especially in section 2.2. For a proof of the existence of unique smooth structures, see theorem 35.3 of [Moi77], together with theorems 3.10.8 and 3.10.9 of [Thu97].

The point of section 2.1 is to explain how a 3-manifold needs to be packaged in order to feed it to the Heegaard Floer machinery. This packaging is known as a Heegaard diagram. In section 2.2 we explain how to understand Heegaard diagrams in terms of Morse theory and use this to extend Heegaard diagrams to also package knots embedded in 3-manifolds. In section 2.3 we introduce the class of $(1,1)$ knots and describe how to obtain Heegaard diagrams in this context.

2.1 Heegaard Diagrams

The 3-manifold topology we need is the theory of Heegaard splittings and its relationship to Morse theory. The latter is given in Theorem 2.2.11 and offers an important perspective.

I have been made aware that the material in this section is not easy to understand the first time around. I believe however that once one becomes accustomed to visualizing the point at infinity in S^3, one becomes comfortable enough to pretend they can visualize 3-manifolds arising from Heegaard diagrams. To this end, consider the simplest possible Heegaard splitting (definition 2.1.3 is not necessary to understand it):

Example 1. Think of S^3 as the 1-point compactification of $\mathbb{R}^3$. This can be done very explicitly by defining S^3 to be $\{x \in \mathbb{R}^4 : \|x\| = 1\}$ and by applying stereographic projection to identify $S^3 \setminus \{(0,0,0,1)\}$ with $\mathbb{R}^3$. Then the north pole of S^3, i.e. the point $(0,0,0,1)$, is the point at infininty for $\mathbb{R}^3$. The projection decomposes S^3 as the union of two balls which we can see in $\mathbb{R}^3$ as follows: the equator of S^3 gets mapped to the unit sphere $S^2 \subset \mathbb{R}^3$, and the northern and southern hemispheres get mapped to the unbounded and bounded components of $\mathbb{R}^3 \setminus S^2$, respectively. This decomposition of S^3 into two 3-balls is a genus 0 Heegaard splitting of S^3.

Remark. The decomposition in the previous example is in fact the only possible genus 0 Heegaard splitting, due to Alexander's trick, which says that every self-homeomorphism of S^2 can be extended to a homeomorphism of the 3-ball (cf. Theorem 1.4 in [Sav12]).

The reader interested in 3-manifold topology and knot theory is strongly encouraged to look at the many expositions given by the masters, which the author cannot try to emulate: a good selection is [FM97], [Rol03], [Sav12]. For what follows, we assume the reader understands the notions of tubular neighbourhood, isotopy and homotopy (of functions) and is aware of the basic results of geometric topology, such as the existence of tubular (open)

neighbourhoods for submanifolds $N \hookrightarrow M$, which we denote by $\nu(N)$.

Definition 2.1.1. Let M be a connected 3-manifold and $\Sigma \subset M$ and embedded surface. We say that Σ **splits** M if $M \setminus \nu(\Sigma)$ has two connected components.

Note that surfaces don't always split 3-manifolds, even when everything is orientable: consider $S^2 \times \{*\} \subset S^2 \times S^1$. Suppose that M is a manifold-with-boundary. A standard way of building a new manifold-with-boundary is by attaching a ball B to M by specifying a homeomorphism from a submanifold of ∂B to a submanifold of ∂M. When the chosen submanifold of ∂B is a thickened sphere, this is called a k-handle attachment.

Definition 2.1.2. Let M be a 3-manifold-with-boundary. A **k-handle attached** to M is a copy of $D^k \times D^{3-k}$ attached along an embedding $\partial D^k \times D^{3-k} \hookrightarrow \partial M$.

For example, attaching a 0-handle is taking a disjoint union with a ball, since $\partial D^0 = \varnothing$.

Definition 2.1.3. A genus g **handlebody**, for $g \in \mathbb{N}$, is a 3-manifold homeomorphic to a 3-ball with g 1-**handles** attached.

Remark. Equivalently, a handlebody is a 3-manifold homeomorphic to a regular neighbourhood of a bouquet of g circles (embedded in $\mathbb{R}^3$).

If U, V are two handlebodies of genus g, their boundaries are abstractly homeomorphic, so we may form a closed manifold as a quotient $U \sqcup V \big/ \sim$, where $\sim$ is the identification of the boundaries given by some choice of homeomorphism $h \colon \partial V \xrightarrow{\sim} \partial U$. To make the dependence on h explicit, we also denote this quotient by

$$U \cup_h V,$$

and we say that this consists of a Heegaard splitting for $M = U \cup_h V$. More formally:

Definition 2.1.4. A **Heegaard splitting** is a pair (M, Σ), where M is a

manifold and Σ is a closed embedded surface that splits M into a disjoint union of two handlebodies, each of the same genus as Σ.

Remark. Σ is necessarily closed and oriented.

For our purposes, we think of 3-manifolds through their Heegaard splittings. It is thus reassuring to have the following theorem, which is a consequence of the deep result that 3-manifolds admit triangulations (Theorem 35.3 in [Moi77].

Theorem 2.1.5 (Theorem 1.1 [Sav12], Theorem 9.C.2 in [Rol03])**.** *Every closed connected orientable manifold M admits a Heegaard splitting.*

Proof sketch. Let $f\colon K \to M$ be a triangulation. Note that since M is compact and 3-dimensional, K is a finite 3-dimensional complex. Let $K^{(1)}$ be the 1-skeleton of K and consider its image $M_1 := f(K^{(1)})$. Let $\nu(M_1)$ be a regular neighbourhood of M_1. The closure $\overline{\nu(M_1)}$ is a handlebody H_1 of genus $1 - \chi(K^{(1)})$. The complement $M \setminus \nu(M_1)$ is another handlebody of the same genus (this is not obvious); call it H_2. We thus have a Heegaard splitting $M = H_1 \sqcup H_2/\sim$. □

Remark. Alternatively, the theorem above can be obtained using Morse theory, which requires a smooth structure, so this approach also uses the triangulation theorem (see the footnote at the beginning of the chapter). We discuss Morse theory in section 2.2.

While it is nice to split 3-manifolds into handlebodies with the goal of applying some divide and conquer heuristic, it is still nicer to know what 3-manifold is obtained by a specific gluing of two handlebodies. In this vein, we have the following result, which forms the main connection between the study of mapping class groups of surfaces and 3-manifold topology:

Proposition 2.1.6 (Theorem 8.2.3 in [Hir76])**.** *Suppose U, V are manifolds with boundary and $\psi_0, \psi_1\colon \partial U \xrightarrow{\sim} \partial V$ are isotopic homeomorphisms (i.e. ψ_0 and ψ_1 are homotopic through homeomorphisms). Then we have the*

homeomorphism

$$U \cup_{\psi_0} V \simeq U \cup_{\psi_1} V.$$

Definition 2.1.7. Fix a surface Σ. The **mapping class group** of Σ, $\mathrm{MCG}(\Sigma)$ is defined to be the group of self-homeomorphisms of Σ modulo isotopy.

With this definition, Proposition 2.1.6 states that the image of $h \in \mathrm{Homeo}(\Sigma)$ under the quotient $\mathrm{Homeo}(\Sigma) \to \mathrm{MCG}(\Sigma)$ determines $U \cup_h V$. Whereas a Heegaard splitting is a decomposition of a 3-manifold into handlebodies, a Heegaard diagram is the information required to construct a 3-manifold M as a Heegaard splitting, starting with an orientable surface Σ, which is to become the surface along which M is split. If Σ is to determine M up to homeomorphism, it requires some decorations. These are attaching circles:

Definition 2.1.8. Let U be a genus g handlebody. A collection of **attaching circles** is a set $\boldsymbol{\alpha} = \{\alpha_1, \ldots, \alpha_g\}$ of g pairwise disjoint, closed curves embedded in ∂U such that:

1. The α_i bound embedded and pairwise disjoint discs in U.
2. The α_i are linearly independent in $H_1(\partial U; \mathbb{Z})$.

Remark. The homological linear independence of $\boldsymbol{\alpha}$ may be replaced with the condition that $\Sigma_\alpha := \partial U \setminus \cup\boldsymbol{\alpha}$ is connected, by the following rapid argument. If Σ_α is disconnected, then some proper subset $S \subset \boldsymbol{\alpha}$ bounds a subsurface of ∂U, so the union of the elements of S is null-homologous. Conversely, if Σ_α is connected, then $\partial U \setminus \nu(\cup\boldsymbol{\alpha})$ is a sphere with $2g$ open discs removed, by the classification of surfaces; these $2g$ boundary components can be identified with the cocores of a standard handle decomposition of U, and thus obviously generate a copy of $\mathbb{Z}^{\oplus g}$ in $H_1(\partial U; \mathbb{Z})$.

Definition 2.1.9. Let g be a nonnegative integer. A **Heegaard diagram** of genus g is a triple $(\Sigma_g, \boldsymbol{\alpha}, \boldsymbol{\beta})$, where Σ_g is a genus g closed, orientable surface, $\boldsymbol{\alpha}$ and $\boldsymbol{\beta}$ are g-tuples of circles embedded in Σ_g such that $\boldsymbol{\alpha}$ is a set of attaching circles for a handlebody U_α and $\boldsymbol{\beta}$ is a set of attaching circles

for U_β; $\boldsymbol{\alpha}$ and $\boldsymbol{\beta}$ are understood to be empty if $g = 0$.

Example 2. Figure 2.1 shows a genus 2 Heegaard diagram. It is not hard to see first that this is the Heegaard diagram for a manifold M with $\pi_1(M) \simeq \mathbb{Z}/2\mathbb{Z} \oplus \mathbb{Z}/2\mathbb{Z}$, and second that M is a connected sum of two manifolds with fundamental group isomorphic to $\mathbb{Z}/2\mathbb{Z}$. To check that M is homeomorphic to $\mathbb{R}P^2 \# \mathbb{R}P^3$ would require some work beyond the scope of this thesis. For many more examples, see [FM97] and [Sav12].

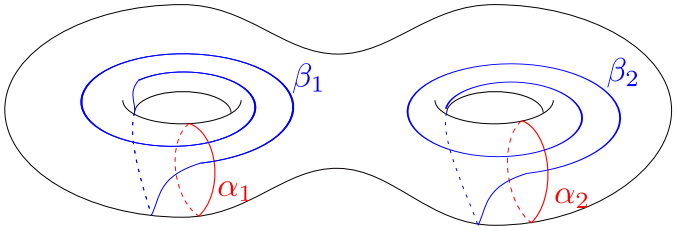

Figure 2.1: A genus 2 Heegaard diagram for the 3-manifold $\mathbb{R}P^3 \# \mathbb{R}P^3$, with the α curves drawn in red and the β curves in blue.

Remark. A set of attaching circles $\boldsymbol{\alpha} \subset \Sigma_g$ specifies a genus g handlebody. If we also have a homeomorphism $h \colon \Sigma_g \to \Sigma_g$, this provides us with a Heegaard diagram: simply define $\boldsymbol{\beta} := \{h(\alpha_1), \ldots, h(\alpha_g)\}$ to be the set of attaching circles for the second handlebody.

Construction 2.1.10. A Heegaard diagram $(\Sigma, \boldsymbol{\alpha}, \boldsymbol{\beta})$ of genus g specifies a closed oriented 3-manifold M split along Σ as follows: thicken the diagram to $\Sigma \times [0, 1]$ and push the α curves to $\Sigma \times \{0\}$ and the β curves to $\Sigma \times \{1\}$. Next, attach a 2-handle to each $\alpha_i \times \{0\}$ and each $\beta_i \times \{1\}$. This yields a 3-manifold with two boundary components, each of which is a sphere. By Alexander's trick, $\mathrm{MCG}(S^2) = 1$, so there is a unique way – up to isotopy – to fill these boundary components with 3-balls. This resulting manifold is M.

2.2 The Morse Theory Perspective

A unifying perspective on Heegaard decompositions is given by Morse theory. The classical introduction to this topic is [Mil63]. We refer to it, in particular to §2, for an explanation of the terms which we now use.

Definition 2.2.1. A **Morse function** on a smooth n-dimensional manifold M (n arbitrary) is a smooth map $f\colon M \to \mathbb{R}$ such that the critical points of f are nondegenerate. To each critical point p of f, there is associated a nonnegative integer called the **index** of f at p, defined to be the number of negative eigenvalues of the Hessian

$$\left(\frac{\partial^2 f}{\partial x^i \partial x^j}\bigg|_p \right)$$

computed in some coordinate chart. The index is independent of the choice of chart. A Morse function is called **self-indexing** if the index of every critical point p is $f(p)$.

The import of the index is the following result, known as *Morse's lemma*:

Theorem 2.2.2. *Let $p \in M$ be a critical point of f of index i. There exists a coordinate chart $(U, (x_1, \ldots, x_n))$ containing p in which f is equal to the map*

$$(x_1, \ldots, x_n) \mapsto -(x_1^2 + \cdots + x_i^2) + x_{i+1}^2 + \cdots + x_n^2.$$

In other words, we can model f in a neighbourhood of every critical point as a saddle given by a specific quadratic polynomial. As a corollary, one can see that nondegenerate critical points are isolated. More importantly, the indices of the critical points of f contain the information required to construct M using a sequence of handles:

Proposition 2.2.3 (§3 of [Mil63])**.** *Let $f\colon M \to \mathbb{R}$ be a Morse function, $p \in M$ a critical point of f and suppose $[a, b] \subset \mathbb{R}$ is an interval of regular*

values of f. Let also,

$$M^q = f^{-1}(-\infty, q],$$

$c = f(p)$ and let k be the index of p. Then

1. *M^a is diffeomorphic to M^b.*
2. *There exists $\epsilon > 0$ such that $M^{c+\epsilon}$ is diffeomorphic to $M^{c-\epsilon} \cup_h H$, where H is a k-handle $D^k \times D^{n-k}$ and $h\colon \partial D^k \times D^{n-k} \to M^{c-\epsilon}$ is an attaching map.*

Another offshoot of Theorem 2.2.2 is that, with the saddle model in hand, we immediately imagine M being split at a critical point p of index i into an i-dimensional submanifold and an $(n-i)$-dimensional submanifold: namely the submanifolds of points below and above p. To define these submanifolds rigorously, we require some auxiliary data:

Construction 2.2.4. Let $f\colon M \to \mathbb{R}$ be a Morse function and endow M with a Riemannian metric $\langle -, - \rangle$. This provides an explicit isomorphism $T_pM \xrightarrow{\sim} T_p^*M$ for every $p \in M$, given by

$$X_p \mapsto \langle -, X_p \rangle.$$

The image under this isomorphism of the 1-form df is the vector field ∇f, defined by the differential equation

$$\langle X, \nabla f \rangle = df(X)$$

for every $X \in \Gamma(TM)$. This determines a **downward**, or **descending, gradient flow**. Solutions $u\colon \mathbb{R} \to M$ to the equation

$$-\nabla f\big|_{u(s)} = u'(s)$$

are called **flow lines** and they package the Morse-theoretic information nicely (see Theorem 2.2.11).

Definition 2.2.5. The **unstable manifold** $W_f^u(p)$ is defined to be the

collection of flow-lines leaving p:

$$W_f^u(p) = \{p\} \cup \{u(s) \in M : \mathbb{R} \xrightarrow{u} M \text{ is a flow line of } \nabla f, \lim_{s \to -\infty} u(s) = p\}.$$

The stable manifold $W_f^s(p)$ is defined to be $W_{-f}^u(p)$.

Finally, we need to know that this data can be used to construct a homology theory for smooth manifolds:

Theorem 2.2.6. *Suppose we have a Morse function $f\colon M \to \mathbb{R}$. Define C_i to be the free Abelian group generated by the index i critical points of f. It is possible, with some extra auxiliary choices, to define a collection of maps*

$$\partial^m\colon C_i \to C_{i-1},$$

for all i, such that (C_*, ∂^m) forms a chain complex. Its homology, called the ***Morse homology*** *of M, is independent of the auxiliary choices and of the choice of Morse function.*

Theorem 2.2.7 (See ch.4 of [Sch93])**.** *Morse homology is naturally isomorphic to singular homology.*

Proposition 2.2.8. *Every closed, connected 3-manifold admits a self-indexing Morse function with a unique critical point of index 0 and a unique critical point of index 3.*

Proof. This is well-known, but not well-referenced. A theorem of M. Morse, proved in [Mor60], states that every compact, connected, smooth manifold admits a Morse function with a unique minimum and a unique maximum. Theorem 4.8 of [Mil16] states that, for every Morse function f on a compact, smooth manifold, there exists a self-indexing Morse function with the same critical points, each with the same index, as f. These theorems taken together prove the proposition. □

Definition 2.2.9. Let us call self-indexing Morse functions with unique maximum and minimum **nice**.

Remark. Let $f\colon M \to \mathbb{R}$ be a nice Morse function and let c_i be the number of index i critical points of f. Then, since Morse homology is isomorphic to singular homology and $\chi(M) = 0$ for odd-dimensional manifolds (cf. [Hir76] 6.3.6), it follows that the alternating sum of the c_i vanishes. Since $c_0 = c_3 = 1$, it follows that $c_1 = c_2$. We have shown:

Corollary 2.2.10. *Nice Morse functions on closed 3-manifolds have as many critical points of index 1 as critical points of index 2.*

If f is a nice Morse function, let $g(f)$ denote the number of critical points of index 1 of f. The relationship between Heegaard diagrams and Morse theory is given by the following theorem and its proof.

Theorem 2.2.11. *Every nice Morse function $f\colon M \to \mathbb{R}$ induces a Heegaard diagram for M of genus $g = g(f)$.*

Proof. Suppose first that we have a nice Morse function $f\colon M \to \mathbb{R}$ and let

$$F^a = f^{-1}(-\infty, a),$$

so F^a is simply $M^a \setminus \partial M^a$. Let $\{x_1, \ldots, x_g\}$ be the critical points of index 1 and let $\{y_1, \ldots, y_g\}$ be the critical points of index 2, where $g = g(f)$. We make the following definitions:

$$\begin{aligned} \Sigma &= f^{-1}(3/2) \\ \alpha_i &= W^s_f(x_i) \cap \Sigma \\ \beta_i &= W^u_f(y_i) \cap \Sigma \end{aligned}$$

and we claim that $(\Sigma, \{\alpha_1, \ldots, \alpha_g\}, \{\beta_1, \ldots, \beta_g\})$ forms a Heegaard diagram for M. To prove the claim we need to show the following

1. $\Sigma \simeq \Sigma_g$, the closed, orientable surface of genus g.
2. Σ splits M.
3. $U_\alpha := M^{3/2}$ and $U_\beta := M \setminus F^{3/2}$ are genus g handlebodies.

4. $\boldsymbol{\alpha} = \{\alpha_1, \ldots, \alpha_g\}$ is a set of attaching circles for U_α.

5. $\boldsymbol{\beta}$ is a set of attaching circles for U_β.

Claims 1 and 2 follow from the continuity of f and the compactness and orientability of M. Claims 3, 4 and 5 follow from proposition 2.2.3, since the α_i are cocores of 1-handles attached to $M^{1/2}$, which is a ball and the β_i are cocores of 2-handles attached to $M^{3/2}$. □

The converse of Theorem 2.2.11, namely that to every Heegaard diagram of genus g corresponds a family of nice Morse functions f with $g(f) = g$ and such that every f induces the given Heegaard diagram, also holds. We will not prove this however. Our new understanding of attaching circles in terms of flow lines and the following theorem enable us to associate Heegaard diagrams to knots, which is the essential step in defining knot Floer homology.

Theorem 2.2.12 (Corollary 4.17 in [Sch93])**.** *Let A be a closed submanifold of M and $f_A \colon A \to \mathbb{R}$ a Morse function. Then there exists a Morse function $f \colon M \to \mathbb{R}$ such that*

$$f|_A = f_A.$$

Furthermore, f may be chosen so that no trajectories of the negative gradient flow f leave A.

Construction 2.2.13. Given a knot $K \colon S^1 \hookrightarrow Y$, let $f|_K \colon K \to [0,3]$ be a Morse function with a unique maximum at $m^* \in K$ and a unique minimum at $m_* \in K$, with $f(m^*) = 3$ and $f(m_*) = 0$. By Theorem 2.2.12, $f|_K$ can be extended to a Morse function $f \colon Y \to \mathbb{R}$ such that no flow lines leave K, i.e. such that the critical points of f in K are precisely m_* and m^*. The function f may be perturbed into a nice Morse function $Y \to \mathbb{R}$ such that K is a union of two flow lines of ∇f from m^* to m_*. The Heegaard diagram associated to f decorated with the two points of intersection with K is called a **doubly pointed Heegaard diagram** for K. The two points are traditionally labelled w and z, but we also use • and ×.

Example 3. The figure below is a doubly pointed Heegaard diagram for the right-handed trefoil knot embedded in S^3. That the ambient manifold is S^3 can be checked by erasing the basepoints $\bullet$ and $\times$. We show that the knot described is the trefoil in construction 2.3.6, but the reader may already think about how to verify this, using construction 2.2.13.

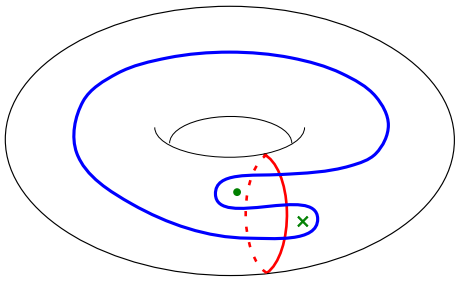

Figure 2.2: A doubly-pointed Heegaard diagram for the right-handed trefoil knot.

2.3 $(1,1)$ Knots and their Diagrams

The goal of this section is to provide a survey of the existing literature on $(1,1)$ knots. This class of knots was initially defined by H. Doll in his PhD thesis and in the publication [Dol92]. It has since been studied by the Japanese school of knot theory due to its relation with the class of knots with tunnel number 1; see [MS91], [Mat02], [CK03], for example. Interest in $(1,1)$ knots shifted geographically with the development of knot Floer homology in the early '00s, since the analytic difficulties present in the general theory all but vanish for $(1,1)$ knots, allowing for combinatorial or algorithmic methods to be applied. We are not the first to exploit this fact; see [Doy05], [GMM05], [Ras05], [Ord06], [Rác15].

As always, when considering a restricted class of objects with nicer-than-normal properties, one should make sure that the class is non-trivial. To

allay worries, note that the class of $(1,1)$ knots is not so restricted as to be uninteresting: other than 2-bridge knots and torus knots, which are all easily seen to be $(1,1)$, there exist non-alternating $(1,1)$ knots as well, such as 10_{161}, which is the worked example in [GMM05]. Additionally, H. Fujii showed in [Fuj96] that $(1,1)$ knots can have arbitrary Alexander polynomials by ingeniously constructing a parametrized family of $(1,1)$ knots. See also §3.1 of B. A. Rácz's PhD thesis [Rác15].

2.3.1 The Bridge Number of Knots

In this subsection we review the classical notion of bridge number, to motivate and put in context for the definition of $(1,1)$ knots. Bridge numbers were introduced by H. Schubert in [Sch54]. The reader may skip this discussion without loss of continuity. For the purpose of defining the bridge number, we need to remind the reader of some pedantic technicalities about knots.

First, a knot K in a 3-manifold Y is an *equivalence class* of smooth embeddings $K\colon S^1 \hookrightarrow Y$, under the equivalence relation: $K \sim K'$ if and only if there exists an orientation-preserving diffeomorphism $f\colon Y \to Y$ such that $f \circ K = K'$. For this subsection, $Y = S^3$, which we think of as $\mathbb{R}^3 \cup \{\infty\}$ (cf. Example 1 at the beginning of section 2.1).

Second, given a knot $[K]$, a knot diagram is a chosen projection π of $K(S^1)$ onto a plane $\mathcal{P} \subset S^3$, for a choice of $\mathcal{P}$ and representative $K \in [K]$. The choices are made so that the fibers of π have cardinality at most 2. The image $\pi(K(S^1))$ is also called a projection and it is decorated at the intersection points in order to preserve crossing information. See fig. 2.3 for two different projections of a given knot.

We can, and do, think of knots as equivalence classes of embedded circles in $\mathbb{R}^3$, since there do not exist smoothly embedded surjections $S^1 \to S^3$.

Definition 2.3.1. Let $\mathbb{R}^3$ have the height function $h\colon (x,y,z) \mapsto z$. The

bridge number of a knot $[K]$ is defined to be the smallest number of local maxima required in an embedding $K \in [K]$:

$$b[K] := \min_{K \in [K]} |\{p \in K(S^1) : h \text{ attains a local maximum at } p\}|.$$

A representative K of $[K]$ is said to be in **bridge position** if $h|_{K(S^1)}$ has precisely $b[K]$ local maxima.

Remark. If K is in bridge position, then its projection onto the xy-plane is a knot diagram that is distinguished by the following property: it has $b[K]$ strands such that all the crossings occur as undercrossings with one of the $b[K]$ strands crossing over. Note that one must be careful when projecting a knot that is in bridge position to the xy-plane so that no triple points get introduced. See the example below.

The bridge number is a difficult invariant to compute, but it is a good notion of complexity for knots. It can be shown for example that 2-bridge knots are alternating and it's not hard to show that the only knot with bridge number 1 is the unknot. Therefore a knot has bridge number 2 if it is nontrivial and has a representative with two local maxima. Proving that a knot has given bridge number is tricky if this number is suspected to be bigger than 2.

Example 4. The figure-8 knot, 4_1 in Rolfsen's table, is depicted in figure 2.3. 4_1 is non-trivial, so the picture on the left, which is the knot in bridge position, proves that $b[4_1] = 2$. The picture on the right is the projection of the figure-8 on the left onto the xy-plane. Subarcs of the knot are coloured to help read the picture. In order to avoid triple points, one must imagine the orange circles on the left sliding down the knot; this gives a reinterpretation of the crossings on the left as winding of the black and green arcs on the right.

The following proposition is the starting point for the generalization of bridge number which we need. A sketch of proof may be found in an algorithmic description of the passage from the left-hand projection to the

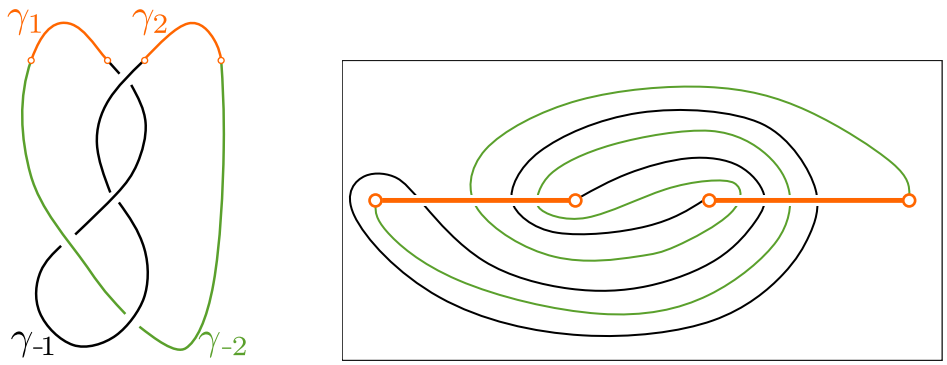

Figure 2.3: Two projections of 4_1 in bridge position. Left: in the yz-plane. Right: in the xy-plane.

right-hand projection in fig. 2.3.

Proposition 2.3.2. *Let $K \subset S^3$ be a knot in bridge position. Let P be a plane parallel to the xy plane that intersects K transversely in $2b[K]$ points. Such a plane splits K into $2b[K]$ arcs: $\gamma_1, \ldots, \gamma_{b[K]}$ above the plane and $\gamma_{-1}, \ldots, \gamma_{-b[K]}$ below. Then these arcs have the following property: each arc cobounds a properly embedded disc with an arc in P, in the sense that, for each γ_i, there exists an arc $\alpha \subset P$ and an embedding $(D, \partial D) \overset{\iota}{\hookrightarrow} (S^3, K \cup P)$ such that $\iota(\partial D) = \alpha \cup \gamma_i$.*

2.3.2 (g, b) Knots

We now return to the tradition of confounding knots $[K]$, representatives $K \in [K]$, their images $K(S^1)$ and, sometimes, their projections.

Definition 2.3.3. Let U be a handlebody and $\gamma \subset U$ a properly embedded arc (an embedded arc with $\partial\gamma = \gamma \cap \partial U$). If there exits a disc $D \subset U$ such that $\gamma \subset D$ and $\partial D \setminus \gamma \subset \partial U$, then γ is called **trivially embedded**.

Definition 2.3.4 ([Dol92])**.** A (g, b) knot is a knot $K \subset Y$, such that Y admits a genus g Heegaard decomposition with the property that K intersects the Heegaard surface Σ transversely in $2b$ points and $K \setminus \Sigma$ is a collection

of $2b$ trivially embedded arcs (in their corresponding handlebodies). (g, b) knots are often called b-bridge genus g knots. This defines $(1, 1)$ knots as 1-bridge genus-1 knots.

Notation. By $(1, 1)$ diagram, we mean a genus 1 doubly pointed Heegaard diagram.

In the context of Morse theory, we have the following reformulation:

Proposition 2.3.5. $(1, 1)$*-knots are precisely the knots* $K \subset Y$ *such that* K *admits a* $(1, 1)$ *diagram.*

Proof. Let $K \subset Y$ be a $(1, 1)$ knot. The statement is simply that, given a Morse function associated to K as in construction 2.2.13, the knot splits into 2 trivially embedded arcs. We show this now. Suppose that $f\colon Y \to \mathbb{R}$ is such a Morse function, so it has 4 critical points and it induces a genus-1 Heegaard decomposition on Y such that K is the union of two flow lines from the index 3 critical point to the index 0 critical point. Let $x, y \in Y$ be the index 1 and 2 critical points, respectively, and let $\{w, z\}$ be $K \cap f^{-1}(3/2)$. By Theorem 2.2.11, if we let $\alpha = W^u_f(x) \cap T^2$ and $\beta = W^s_f(y)$, then (T, α, β, w, z) forms a doubly pointed Heegaard diagram for $K \subset Y$. Let $A\colon [0, 1] \to T$ be an arc in T with $A(0) = w$, $A(1) = z$ and $A([0, 1]) \cap \alpha = \varnothing$. Then every point of $A([0, 1])$ flows down to the index 0 critical point, thus the union of the downwards flow lines over all $A(t)$ forms a disc exhibiting γ_α as a trivially embedded arc. Similarly, γ_β is trivially embedded. □

Remark. The ambient manifold Y of a $(1, 1)$ knot is restricted, because the only manifolds that admit a genus 1 Heegaard splitting are the Lens spaces $L_{p,q}$, S^3 and $S^2 \times S^1$, see §1 of [Sav12]. The knot is restricted as well, but there is no obvious alternate characterization of $(1, 1)$ knots.

Given a $(1, 1)$ diagram of a knot K in S^3 the following procedure produces a projection of K. The procedure is only given for knots in S^3 because it is not clear what a projection of a knot in an arbitrary manifold is.

Construction 2.3.6 (How to draw K, given its $(1, 1)$ diagram)**.** Let $\mathcal{D} =$

$(\Sigma, \alpha, \beta, w, z)$ be a $(1,1)$ diagram for a knot in S^3 and draw this diagram on a torus $S^1 \times S^1$ embedded as a surface of revolution in $\mathbb{R}^3$. Suppose furthermore that the pair (α, β) is isotopic in Σ to the pair $(\{*\} \times S^1, S^1 \times \{*\})$. Connect the $w = \bullet$ and $z = \times$ basepoints of the diagram by two arcs embedded in Σ: an arc $\gamma_a \subset \Sigma \setminus \alpha$ and an arc $\gamma_b \subset \Sigma \setminus \beta$. Keeping the endpoints fixed, push γ_a into the torus and push γ_b off of the torus. In other words, pick a nice Morse function inducing $\mathcal{D}$, and apply the gradient flow to push each arc into the handlebody inside of which it is trivially embedded.

Example 5. We apply the construction to the $(1,1)$ diagram in fig. 2.2 below. The reader may check that the resulting knot is the right-handed trefoil, 3_1 in Rolfsen's table.

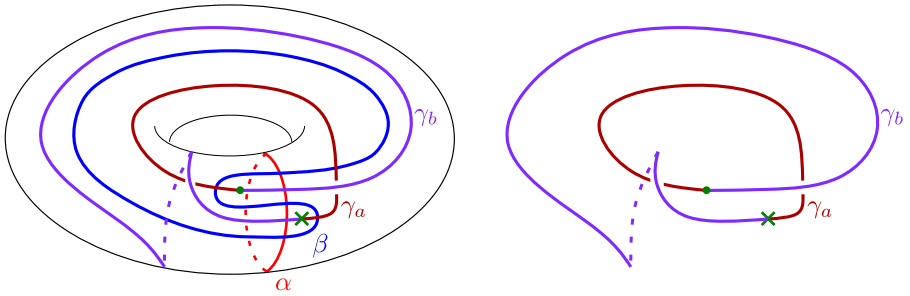

Figure 2.4: The knot described by fig. 2.2.

Remark. It is crucial that, fixing the embedding of (T^2, α) as a surface of revolution in $\mathbb{R}^3$ with $\alpha = \{*\} \times S^1$, the curve $\beta \subset T^2$ can be isotoped into the curve $S^1 \times \{*\}$. For example, by applying a Dehn twist along α to the diagram in fig. 2.2, we obtain the diagram in fig. 2.5. Note that this Dehn twist extends to a homeomorphism : $S^3 \xrightarrow{\sim} S^3$ that preserves the knot. The reader may check that applying construction 2.3.6 as in the example above to this Dehn twisted diagram yields a projection of the unknot. We refer to [Sav12] for a definition of **Dehn twist** along a curve. This is important to note for our discussion in section 4.2.

We now explain the heuristic method for obtaining a $(1,1)$ diagram of a knot $K \subset S^3$, starting with a projection. It is due to H. Goda, H. Matsuda and

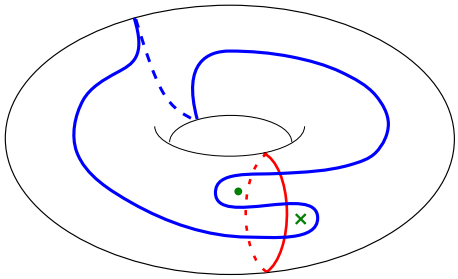

Figure 2.5: A $(1,1)$ diagram for the trefoil after a Dehn twist.

T. Morifuji in [GMM05] and an algorithmic implementation of it is the main result in Ording's PhD thesis [Ord06]. This method is illustrated below by its application to the knot 6_2 and it is intended to be read with illustrations figs. 2.6 to 2.9 in hand. Note that the method is not guaranteed to work, since not all knots $K \subset S^3$ are $(1,1)$.

1. Start by choosing a large closed arc $\gamma \subset K$ such that its endpoints can be connected by a short segment $(\tau, \partial\tau) \subset (S^3, K)$ with the property that a tubular neighbourhood of $\gamma \cup \tau$ is an unknotted solid torus in S^3, as in fig. 2.6. Call this tubular neighbourhood U_α and replace γ with the arc $K \cap U_\alpha$.

2. Let $T = \partial U_\alpha$ and let $U_\beta = \mathrm{cl}(S^3 \setminus U_\alpha)$ and note that U_α and U_β form a genus 1 Heegaard splitting of S^3 along the Heegaard surface T. Let also $\{w, z\} = K \cap T$; these will be the basepoints of the $(1,1)$ diagram.

3. Hopefully $K \cap U_\beta$ is trivially embedded in U_β, in which case K is a $(1,1)$ knot. If so, then there is a sequence of elements of $\mathrm{MCG}(T)$ which push the basepoints along generators of $\pi_1(T)$ such that, after applying this sequence of mapping classes, a disc exhibiting the trivial embedding of $K \setminus \gamma$ is apparent and it is possible to draw an attaching circle for U_β which does not intersect $K \setminus \gamma$; the attaching circle for U_β is drawn in blue in fig. 2.7.

4. Apply the inverse of the product of the mapping classes obtained above

to the β circle, as in fig. 2.7 and fig. 2.8.

5. Draw in the α circle, as in fig. 2.9 .

Example 6. The heuristic method applied to the knot 6_2.

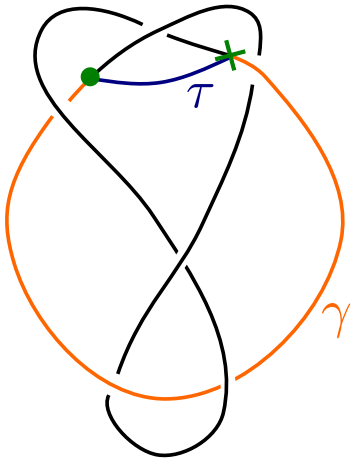

Figure 2.6: The knot 6_2 with candidate γ and τ coloured.

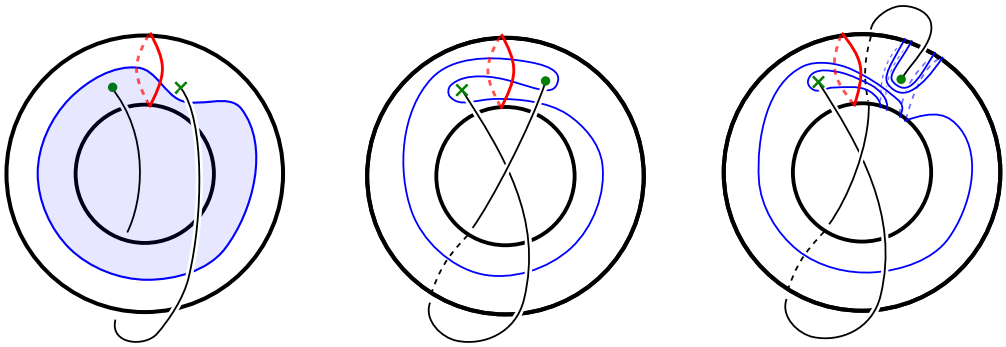

Figure 2.7: $(1,1)$ diagrams interpolating between the unknot and 6_2. The α curve is drawn in red and the β, in blue.

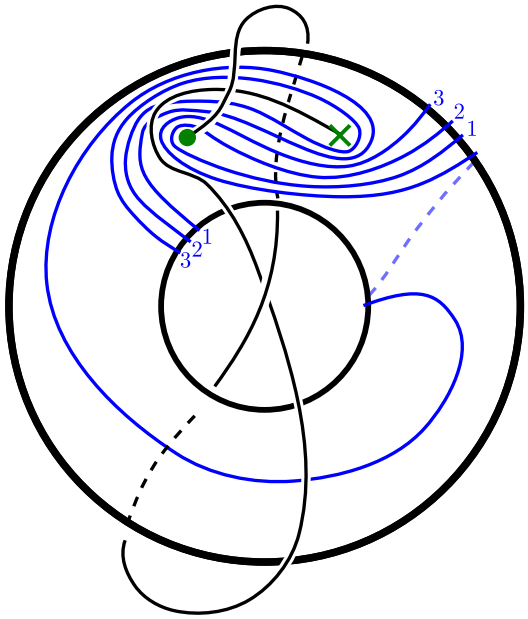

Figure 2.8: A torus with a β curve for 6_2. Note that the pairs of endpoints labeled 1, 2, 3 are connected by straight arcs behind the torus; these are not drawn, in order to keep the diagram readable.

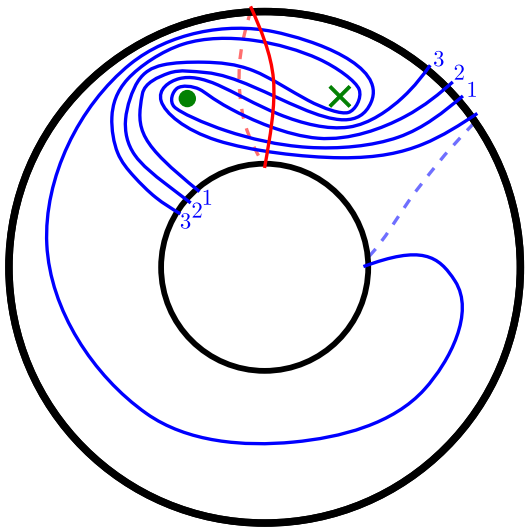

Figure 2.9: A $(1,1)$ diagram for 6_2.

Chapter 3

Knot Floer Homology

In this chapter we construct the knot Floer homology of a knot K embedded in a 3-manifold Y. The executive summary of the construction is that the knot Floer homology of a knot K is the Lagrangian intersection homology of two fixed g-dimensional tori in a $2g$-dimensional symplectic manifold associated to a genus g doubly pointed Heegaard diagram of K. The work done in this thesis is in the case $g = 1$, which is an especially simple set-up. The construction of knot Floer homology is due to P. Ozsváth & Z. Szabó, and J. Rasmussen [OS04a], [Ras03]. Note that this construction is done originally for null-homologous knots, since it is important to

Fix from now on a doubly pointed Heegaard diagram $\mathcal{D} = (\Sigma, \boldsymbol{\alpha}, \boldsymbol{\beta}, w, z)$ for a knot $K \subset Y$, and assume furthermore that the curves in $\boldsymbol{\alpha}$ intersect the curves in $\boldsymbol{\beta}$ transversely. We will start by constructing a type D structure $CFK(\mathcal{D})$ associated to $\mathcal{D}$, following [Zem17]; see also [LOT18] for the initial treatment of type D structures. Note that this is an anachronistic treatment: Ozsváth-Szabó and Rasmussen defined CFK not as a type D structure, but as a filtered chain complex, but this is a superficial difference. The filtered chain complex associated to $CFK(\mathcal{D})$ is not an invariant of K, but it is up to filtered chain homotopy; in particular, its homology is a knot invariant, denoted $HFK(K)$. In view of this, if we write $CFK(K)$, this should be

understood as the chain homotopy type of $CFK(\mathcal{D})$, for some $\mathcal{D}$ associated to K. The reader who knows of and is potentially intimidated by the various Heegaard Floer homology theories should note that the object we define extracts all the Floer theoretic information from $\mathcal{D}$ and the other versions of knot Floer homology can be obtained from it. The construction below is self-contained, although it is given without proof of invariance; such a proof may be found in [OS04a].

We will first sketch the general construction of CFK in section 3.1 for completeness and context (i.e. the construction that applies to an arbitrary knot in an arbitrary 3-manifold). In section 3.2, we will provide a different definition of the differential, appropriate for $(1,1)$ knots; its equivalence with the general definition will be relegated to Section 3.2.1.

3.1 General Definition

The notion of type D structure is a simplifying one, and a good mental model for the knot Floer complex.

Definition 3.1.1. Let $\mathcal{A}$ be a unital algebra over a field $\boldsymbol{k}$ and let $\mathbb{I}$ be the subring generated by the idempotents of $\mathcal{A}$. A **type D** structure over $\mathcal{A}$ is a finite-dimensional left $\mathbb{I}$-module V together with a morphism

$$\delta : V \to \mathcal{A} \otimes_{\mathbb{I}} V,$$

satisfying the condition

$$(\mu \otimes \mathrm{id}_V) \circ (\mathrm{id}_{\mathcal{A}} \otimes \delta) \circ \delta = 0,$$

where $\mu\colon \mathcal{A} \otimes \mathcal{A} \to \mathcal{A}$ is simply the multiplication map. The condition above is an instance of a differential squaring to 0, as in the case of chain complexes. Indeed, we call δ the **differential** of the type D structure. If there is no chance of confusion, we call V or (V, δ) the type D structure.

Notation (Abuse thereof)**.** An element of $A \otimes_{\mathbb{I}} V$ is a finite sum $\sum_i a_i \otimes x_i$. In what follows, we will usually omit the small tensor product symbol and write $\sum_i a_i \cdot x_i$ or even $\sum_i a_i x_i$ instead, especially if the subring of idempotents is $\mathbb{F}$.

Definition 3.1.2. A **differential group** is an Abelian group M together with an endomorphism $\partial\colon M \to M$ such that $\partial^2 = 0$.

Construction 3.1.3. Type D structures give rise to differential groups by the following canonical procedure. Given $\mathcal{A}$, V and δ as in definition 3.1.1, let $M = \mathcal{A} \otimes_{\mathbb{I}} V$ and define $\partial\colon M \to M$ to be the composite

$$(\mu \otimes \mathrm{id}_V) \circ (\mathrm{id}_{\mathcal{A}} \otimes \delta).$$

The type D condition ensures that $\partial^2 = 0$. We call M the **differential group associated** to the type D structure V.

Definition 3.1.4. Throughout this thesis we work with the field with two elements, which we denote by $\mathbb{F}$ and we let $\mathcal{A}$ be the polynomial ring $\mathbb{F}[U, V]$. Note that the subring of idempotents $\mathbb{I} \subset \mathcal{A}$ is the base field $\mathbb{F}$, so left $\mathbb{I}$-modules are $\mathbb{F}$-vector spaces.

Remark. U, V are a formal variables whose role will be to keep track of the information contained in $\mathcal{D}$. In particular, the differential group associated to CFK, which can be checked to be an $\mathbb{F}[U, V]$-module, will be a chain complex over $\mathbb{F}[U, V]$.

3.1.1 CFK the Vector Space

Think of Σ as a Riemann surface by endowing it with a complex structure and construct the auxiliary space $\mathrm{Sym}^g\Sigma$, which is the quotient of $\Sigma^{\times g}$ by the action of S_g, the symmetric group on g elements (S_g acts by permuting the coordinates in the Cartesian product). Even though the action of S_g on $\Sigma^{\times g}$ is not free, it turns out that $\mathrm{Sym}^g\Sigma$ is a manifold and that, furthermore, the complex structure on Σ induces a complex structure on $\mathrm{Sym}^g\Sigma$. Since

each handlebody has disjoint attaching circles, the tori

$$\mathbb{T}_\alpha := \alpha_1 \times \cdots \times \alpha_g \quad \text{and} \quad \mathbb{T}_\beta := \beta_1 \times \cdots \times \beta_g$$

survive in the quotient $\Sigma^{\times g} \to \mathrm{Sym}^g\Sigma$ as embedded g-dimensional submanifolds; we use the same symbols $\mathbb{T}_\alpha, \mathbb{T}_\beta$ to talk about their images in $\mathrm{Sym}^g\Sigma$. In the first constructions $\mathbb{T}_\alpha$ and $\mathbb{T}_\beta$, although they were not known to be Lagrangian, played the role of the Lagrangian submanifolds in Lagrangian intersection homology. It was later found out that they can be considered as honest Lagrangian submanifolds of $\mathrm{Sym}^g\Sigma$ [Per08].

Definition 3.1.5. Let $\mathcal{I} = \mathbb{T}_\alpha \cap \mathbb{T}_\beta$. We define $CFK(\mathcal{D})$ to be the $\mathbb{F}$-vector space generated by $\mathcal{I}$.

3.1.2 *CFK* the Type D Structure

To define the differential $\delta\colon CFK(\mathcal{D}) \to CFK(\mathcal{D})$, we must count holomorphic Whitney discs in $\mathrm{Sym}^g\Sigma$ (defined below). We sketch the construction, but we do not want to get stuck in thorny issues about admissible Heegaard diagrams and Maslov indices, so what follows is, although correct in spirit, possibly not sophisticated enough to yield the knot Floer theory in general. We first define topological discs.

Definition 3.1.6. Let $\mathbb{D} = \{z \in \mathbb{C} : |z| \leq 1\}$. Given $x, y \in \mathcal{I}$, a **Whitney disc** from x to y is a continuous map $u : \mathbb{D} \to \mathrm{Sym}^g\Sigma$ such that the following boundary conditions are satisfied:

$$u(-i) = x \quad u(i) = y$$

and

$$u|_{\partial\mathbb{D}}(z) \in \begin{cases} \mathbb{T}_\alpha & \text{if } \mathrm{Re}(z) \geq 0 \\ \mathbb{T}_\beta & \text{if } \mathrm{Re}(z) \leq 0 \end{cases}$$

The set of all homotopy classes of Whitney discs (rel. boundary) from x to y is denoted $\pi_2(x, y)$.

Remark. Note that if there is some $\varphi \in \pi_2(x, y)$, then, by precomposing with a reflection of the disc, there is a $\overline{\varphi} \in \pi_2(y, x)$. Whitney discs may also be composed, and this composition descends to an operation on the homotopy classes

$$* : \pi_2(x, y) \times \pi_2(y, z) \to \pi_2(x, z).$$

Finally, for all $x \in \mathcal{I}$, there is a constant disc $\varphi \in \pi_2(x, x)$. We have shown

Proposition 3.1.7. *The relation $x \sim y \iff \pi_2(x, y) \neq \varnothing$ is an equivalence relation on $\mathcal{I}$.*

A word of caution: this is not the same equivalence relation as the one used by Ozsváth and Szabó. The difference is that they define $x \sim y$ if a certain circle mapped to the ambient manifold Y is nullhomologous, whereas here, we require that the circle bounds a disc, so our relation is finer. The two are equivalent however when dealing with Heegaard diagrams of genus 1; this is explained in section 2.2 of [GLV18].

The idea is that the differential should take $x \in \mathcal{I}$ to the sum of those $y \in \mathcal{I}$ for which there is an elementary disc in $\pi_2(x, y)$:

$$\delta x = \sum_{y \in \mathcal{I}} \sum_{\varphi \in \pi_2(x,y)} c_\varphi \otimes y, \tag{3.1}$$

where c_φ is some element of $\mathcal{A}$. Some fairly difficult analysis is required first to make sense of the word "elementary" in the previous sentence and second to ensure that the set of elementary discs is finite. In short, the second task is achieved by counting elements of $\mathcal{M}(\varphi)$, **the moduli space of holomorphic representatives** of a given $\varphi \in \pi_2(x, y)$, while the first task is achieved by the **Maslov index** of discs, which is an integer $\mu(\varphi)$ associated to a moduli space. The integer $\mu(\varphi)$ is the index of some Fredholm operator and should be thought of as the dimension of $\mathcal{M}(\varphi)$; indeed, it is generically the dimension of $\mathcal{M}(\varphi)$, see [Man16]. In particular, if $\mu(\varphi) < 0$, then φ has no holomorphic representatives and if $\mu(\varphi) = 1$, then $\mathcal{M}(\varphi)$ is

1-dimensional. The Maslov index is 0 on the homotopy class of the constant disc $\varphi \in \pi_2(x, x)$ and it is additive:

$$\mu(\varphi_1 * \varphi_2) = \mu(\varphi_1) + \mu(\varphi_2)$$

We also want to keep track of how discs $\varphi \in \pi_2(x, y)$ interact with the knot $K \subset Y$. As motivation for the following definition, recall that K is the collection of the flowlines of ∇f in Y passing through w and z, where f is a Morse function associated to K.

Definition 3.1.8. Let $\varphi \in \pi_2(x, y)$ and $p \in \Sigma \setminus (\alpha \cup \beta)$ a point disjoint from the attaching circles. The number $n_p(\varphi)$ is defined to be the algebraic (i.e. oriented) intersection number of φ with

$$\{p\} \times \mathrm{Sym}^{g-1}\Sigma \hookrightarrow \mathrm{Sym}^g\Sigma.$$

In particular, we care about $n_w(\varphi)$ and $n_z(\varphi)$.

The following lemma ensures that only one of φ and $\overline{\varphi}$ has holomorphic representatives (in the notation of the remark following definition 3.1.6).

Lemma 3.1.9 (Lemma 3.2 in [OS04c])**.** *If $u \in \mathcal{M}(\varphi)$ is a holomorphic disc, then $n_p(\varphi) \geq 0$, for $p \in \{z, w\}$.*

We may now describe c_φ as follows: $c_\varphi = 0$ if $\mu(\varphi) \neq 1$ and, if $\mu(\varphi) = 1$, then

$$c_\varphi = |\widehat{\mathcal{M}}(\varphi)| \cdot U^{n_w(\varphi)} V^{n_z(\varphi)}, \tag{3.2}$$

where $\widehat{\mathcal{M}}(\varphi)$ is the quotient of $\mathcal{M}(\varphi)$ by the free action of the group of reparametrizations of $\mathbb{D}$ fixing $\pm i$ (this group is $\mathbb{R}$, so $\widehat{\mathcal{M}}(\varphi)$ is 0-dimensional; in fact it is shown in [OS04c] that $\widehat{\mathcal{M}}(\varphi)$ is a finite set). With eqs. (3.1) and (3.2) we have achieved the goal of defining the differential $\delta\colon CFK \to CFK$. Thanks to the work of [OS04a] and [Ras03], we know that δ satisfies

$$(\mu \otimes \mathrm{id}_{CFK}) \circ (\mathrm{id}_{\mathcal{A}} \otimes \delta) \circ \delta = 0,$$

so (CFK, δ) is a type D structure. In fact Ozsváth-Szabó and Rasmussen prove a slightly different but equivalent result, since their object is a filtered chain complex over $\mathbb{F}[U]$.

3.1.3 Variations on a Theme

We are in a position to explain how to obtain different Heegaard Floer chain complexes from CFK. In fact, we only show here how to obtain the differential group structure of these chain complexes, the gradings will be defined in section 3.1.5. The following objects will all be obtained by *truncating* CFK and applying construction 3.1.3.

Construction 3.1.10. Let $p \in \mathbb{F}[U,V]$ be a polynomial that is a power of a prime. A quotient $\mathbb{F}[U,V] \xrightarrow{\pi} \mathbb{F}[U,V]/(p)$ gives rise to a new type D structure, over $\mathbb{F}[U,V]/(p)$, denoted $CFK|_{p=0}$, with differential given as the composite

$$V \xrightarrow{\delta} \mathbb{F}[U,V] \otimes_{\mathbb{F}} V \xrightarrow{\pi \otimes \mathrm{id}_V} \mathbb{F}[U,V]/(p) \otimes_{\mathbb{F}} V.$$

We call $CFK|_{p=0}$ a **truncation** of CFK.

Definition 3.1.11. Define $CFK^-(\mathcal{D})$ to be the differential group associated to $CFK|_{V=1}(\mathcal{D})$.

Definition 3.1.12. Define $CFK^\infty(\mathcal{D})$ to be $CFK^-(\mathcal{D}) \otimes_{\mathbb{F}[U]} \mathbb{F}[U, U^{-1}]$.

Definition 3.1.13. Define $\widehat{CFK}(\mathcal{D})$ to be $CFK^-(K)|_{U=0}$.

Let now $\overline{\mathcal{D}} = (\Sigma, \boldsymbol{\alpha}, \boldsymbol{\beta}, w)$. This singly-pointed Heegaard diagram is the data required to construct the Heegaard Floer chain complexes of the ambient 3-manifold.

Definition 3.1.14. We define $CF^\circ(\overline{\mathcal{D}})$ to be $CFK^\circ(\mathcal{D})$, where $\circ$ is one of $\widehat{\ }, \infty$ or $-$.

There is no mistake in the above definition. The only difference between the

Heegaard Floer complex of Y and the knot Floer complex of $K \subset Y$ is the extra Alexander filtration on the knot Floer complex, defined in section 3.1.5. This extra filtration arises from the choice of z-basepoint in $\overline{\mathcal{D}}$.

We will also make use of the truncation induced by $\mathbb{F}[U,V] \to \mathbb{F}[U,V]/(UV)$ in chapter 6. This is important enough to deserve a label:

Definition 3.1.15 (cf. [KWZ20])**.** We use $\mathcal{R}$ to denote the ring $\mathbb{F}[U,V]/(UV)$ and ${}^{\mathcal{R}}CFK$ to denote the type D structure $CFK|_{UV=0}$.

3.1.4 Spin^c Structures

An important aspect of Heegaard Floer homology is that it splits over spin^c structures. According to Turaev [Tur97], these may be defined as follows for 3-manifolds:

Definition 3.1.16. Let M be a closed, oriented 3-manifold. A **spin^c structure** on M is a homology class of nowhere-vanishing vector fields X on M, where two such vector fields X, X' are said to be **homologous** if there exists an embedded ball $B \subset M$ such that, on $M \setminus B$, X is homotopic to X' through nowhere-vanishing vector fields. We denote the set of all spin^c structures on M by $\mathrm{Spin}^c(M)$.

In our case, the spin^c structures on a manifold are obtained from the vector field ∇f associated to a nice Morse function, see §2.6 of [OS04c]. We now make precise the notion of splitting. Recall that $\mathcal{D}$ is a Heegaard diagram for the manifold Y, with basepoints w and z.

Proposition 3.1.17 (See §2.6 of [OS04c])**.** *There is a natural map*

$$s_z \colon \mathcal{I} \to \mathit{Spin}^c(Y).$$

Furthermore, if $s_z(x) \neq s_z(y)$, then $\pi_2(x,y) = \varnothing$. Note that this map depends on the point $z \in \Sigma$.

Definition 3.1.18. Let $\mathfrak{s} \in \mathrm{Spin}^c(Y)$. We define $\mathcal{I}_{\mathfrak{s}}$ to be $s_z^{-1}(\mathfrak{s})$ and

$CFK(\mathcal{D},\mathfrak{s})$ to be the $\mathbb{F}$-vector space generated by $\mathcal{I}_{\mathfrak{s}}$, with differential induced from δ. This is known as the **spin^c grading** on CFK.

Corollary 3.1.19. $CFK = \bigoplus_{\mathfrak{s}\in Spin^c(Y)} CFK(\mathcal{D},\mathfrak{s})$.

Proof. By the proposition just stated, $\delta(CFK(\mathcal{D},\mathfrak{s})) \subset CFK(\mathcal{D},\mathfrak{s})$, since there are no Whitney discs between generators in different fibers of s_z. □

As a consequence, the homology of $CFK(\mathcal{D})$ splits as well:

$$HFK(K) = \bigoplus_{\mathfrak{s}\in \mathrm{Spin}^c(M)} HFK(K,\mathfrak{s}),$$

where $HFK(K,\mathfrak{s})$ is the homology of $CFK(\mathcal{D},\mathfrak{s})$.

Finally, it is important for us to know that $\mathrm{Spin}^c(Y)$ is a torsor over $H^2(Y;\mathbb{Z})$, i.e. there is a faithful and transitive action of $H^2(Y;\mathbb{Z})$ on $\mathrm{Spin}^c(Y)$; see section 2.6 of [OS04c]. By Poincaré duality, $\mathrm{Spin}^c(Y)$ is also in bijection with $H_1(Y;\mathbb{Z})$ (as a set).

3.1.5 *CFK* the Chain Complex

CFK comes equipped with two maps $a, m : CFK(\mathcal{D}) \to \mathbb{Z}$, which a student slowly comes to understand are more than just bookkeeping devices; they are the foremost means of accessing the geometric information contained in *CFK*. The second is known as the homological grading, meaning that

$$m \circ \delta = m - 1.$$

The first is known as the Alexander filtration. The maps a, m are (well-) defined on $\mathcal{I}$ up to an overall shift in each spin^c structure by

$$m(x) - m(y) = \mu(\varphi) - 2n_w(\varphi) \quad \text{and} \quad a(x) - a(y) = n_z(\varphi) - n_w(\varphi),$$

where $\varphi \in \pi_2(x, y)$. For a generic element $U^i V^j x$, the maps are determined by the rules

$$\begin{aligned} m(Ux) &= m(x) - 2, & a(Ux) &= a(x), \\ m(Vx) &= m(x), & a(Vx) &= a(x) - 1. \end{aligned}$$

This fixes the grading for homogeneous elements. For an arbitrary element $x \in CFK$, i.e. a sum of monomials $\sum_y U^{i_y} V^{j_y} y$, the Alexander filtration is defined to be

$$a(x) = \max_y (a(U^{i_y} V^{j_y} y)).$$

We point out how to see the (relative) filtration level in example 9 of section 3.3. It is mandatory in a text on Heegaard Floer theory to note at this point the most important tie between the knot Floer theory and the real world: knot Floer homology categorifies the Alexander polynomial. Precisely, there is a way to make the relative gradings a, m absolutely defined on the generators $x \in \mathcal{I}$ so that the following holds:

Theorem 3.1.20 (See [OS04a])**.** *Let $K \subset S^3$ be a knot and let $\Delta_K(t)$ be the (symmetrized) Alexander polynomial of K. Then*

$$\Delta_K(t) = \sum_{x \in \mathcal{I}} (-1)^{m(x)} t^{a(x)}.$$

3.2 Simplifications in Genus 1

From now on assume that $\mathcal{D}$ is a (1,1) diagram, i.e. that $\Sigma \simeq T^2$ and that $\boldsymbol{\alpha}$ and $\boldsymbol{\beta}$ are singletons, so that we remove the bold font and simply speak of the circles α and β embedded in T^2. Assume also that $\mathcal{D}$ is a diagram for a knot in a lens space $L_{p,q}$, for $p \geq 1$; i.e. we assume that $Y \not\simeq S^2 \times S^1$. If $p = 1$, then $L_{p,q}$ is S^3, which we also allow as a possible ambient space. Note that we will use from now on the symbol T^2 to denote the Heegaard surface Σ. The first simplification due to our assumption is that the symmetric

product and the tori $\mathbb{T}_\alpha$ and $\mathbb{T}_\beta$ become trivial:

$$\begin{aligned} \mathrm{Sym}^1 T^2 &= T^2, \\ \mathbb{T}_\alpha &= \alpha, \\ \mathbb{T}_\beta &= \beta. \end{aligned}$$

So $CFK(\mathcal{D})$ is the vector space generated by $\mathcal{I} = \alpha \cap \beta$. More importantly, the differential on $CFK(\mathcal{D})$ can be computed by counting polygons in the plane. This makes it possible to describe $CFK(\mathcal{D})$ completely combinatorially. In this section, we provide a combinatorial definition of CFK for $(1,1)$ knots; we say a word about the equivalence between the two definitions in Section 3.2.1. Another simplification is that the subtle question of "admissibility", mentioned in the first paragraph of section 3.1.2, is irrelevant to us, since it is irrelevant for manifolds whose first Betti number is 0 [OS04c], and since we agreed to exclude $S^2 \times S^1$ from our considerations.

Since $CFK(\mathcal{D})$ is an invariant of $K \subset Y$ and $K \subset Y$ is determined by $\mathcal{D}$ only up to isotopy of the curves α and β, we may apply isotopies to remove the bigons in T^2 that do not cover one of the z or w basepoints, as in figure 3.1. For details about bigon removal, see §1.2.4 in [FM12]. For convenience and not necessity, we may assume from now on that this has been done, i.e. that there are no bigons in $\Sigma \setminus \{z, w\}$. Such a $(1,1)$ diagram is called **reduced**.

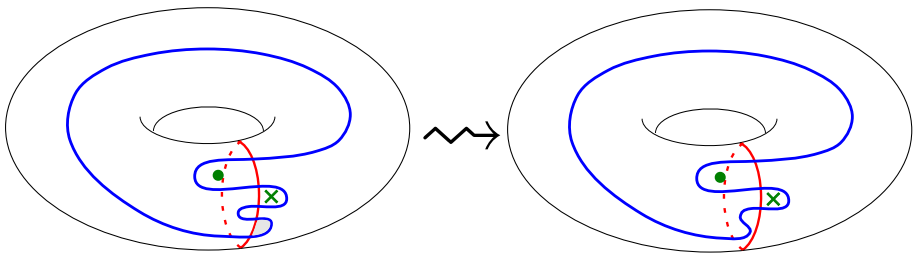

Figure 3.1: A bigon removal.

It is more convenient to map holomorphic discs into the universal cover of the torus rather than into the torus itself. We also call this the universal

cover of the diagram $\mathcal{D}$ and we use the tilde to denote lifts: for example, $\widetilde{\alpha}$ and $\widetilde{\beta}$ denote lifts of α and β, and $\widetilde{w}$ denotes a lift of the w-basepoint, etc.

Definition 3.2.1. A **Whitney bigon** is an embedding $B\colon \mathbb{D} \to \widetilde{T^2}$, which we identify with its image $B(\mathbb{D})$, such that ∂B is the union of a connected subarc arc of $\widetilde{\alpha}$ and a connected subarc of $\widetilde{\beta}$. A Whitney bigon B is said to be **from** $\widetilde{x}$ **to** $\widetilde{y}$ if $\widetilde{x}, \widetilde{y}$ are the intersection points of $\widetilde{\alpha} \cap \widetilde{\beta}$ on the boundary of B and if the path from $\widetilde{x}$ to $\widetilde{y}$ along $\widetilde{\alpha}$ followed by the path from $\widetilde{y}$ to $\widetilde{x}$ along $\widetilde{\beta}$ is a loop of winding number 1.

We will often identify Whitney bigons and their projections to the torus; the latter are in general not embeddings. Since Whitney bigons are the only kind of bigon we will talk about, we will simply call them bigons from now on. A generic bigon from x to y is illustrated in fig. 3.2.

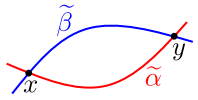

Figure 3.2: A bigon from x to y.

Definition 3.2.2. Let $x, y \in \mathcal{I}$. If there exists a pair of lifts $\widetilde{x}, \widetilde{y}$ such that there is a bigon from $\widetilde{x}$ to $\widetilde{y}$, define $\mathfrak{B}(x, y)$ to be the set of bigons from $\widetilde{x}$ to $\widetilde{y}$ in the universal cover. If such a pair of lifts does not exist, define $\mathfrak{B}(x, y)$ to be empty. We use the notation

$$\mathfrak{B} = \bigcup_{x,y \in \mathcal{I}} \mathfrak{B}(x, y).$$

Remark. The maps n_z and n_w defined in the general case still make sense as maps $\mathfrak{B} \to \mathbb{Z}$. If $B \in \mathfrak{B}$, then $n_z(B)$ (resp. $n_w(B)$) is simply the number of lifts of z (resp. w) contained in B.

Definition 3.2.3. For the class of $(1, 1)$ knots, we still define CFK to be the $\mathbb{F}$-module generated by $\mathcal{I} = \alpha \cap \beta$, but we define a new differential, $\overline{\delta}$,

by

$$\overline{\delta}x = \sum_{y\in\mathcal{I}} \sum_{B\in\mathfrak{B}(x,y)} U^{n_w(B)}V^{n_z(B)}y.$$

Ultimately, we will write δ instead of $\overline{\delta}$ since the two are equal; see section 3.2.1.

Fix from now on a curve $\lambda \subset T^2$ with the property that $\{[\alpha],[\lambda]\}$ is a basis for $H_1(T^2;\mathbb{Z})$ and fix a cover $\mathbb{R}^2 \to T^2$ where α lifts to horizontal lines. In the chosen basis, we have

$$[\beta] = p[\lambda] + q[\alpha],$$

for some relatively prime $p, q \in \mathbb{Z}$. Note that $p \neq 0$ $\mathcal{D}$, since is not a Heegaard diagram for $S^2 \times S^1$. The ambient manifold Y is the lens space $L_{p,q}$ (which may be S^3). Note also that β is periodic with period p. Indeed, this is how the splitting of $\mathcal{I}$ along spin^c structures manifests itself in our case: if we fix $x \in \alpha \cap \beta$ and a lift $\widetilde{x} \subset \mathbb{R}^2$, then β, thought of as a path from x to x, lifts to a path from $\widetilde{x}$ to another lift of x, $\widetilde{x}'$, such that the lifts of the $y \in \alpha \cap \beta$ occur as intersection points of $\widetilde{\beta}$ with p different lifts of α, one for each element of $H_1(Y;\mathbb{Z}) \simeq \mathbb{Z}/p\mathbb{Z}$. This is illustrated in the following example.

Example 7 (A knot in $L_{3,1}$)**.** Consider the $(1,1)$ diagram in fig. 3.3, where the left and right hand sides of the square are identified as usual, and the top and bottom are identified according to the labelling of the intersection points. The diagram on the right shows three lifts of β to the universal cover. The lift which exhibits the partitioning of $\alpha \cap \beta$ along spin^c structures is the central one, drawn in a darker shade of blue. The diagonal lines are lifts of λ. Note the 3-periodicity of β.

Remark. Let us pause here to explain the second half of the title. At the end of section 2.3 we saw a heuristic method for constructing $(1,1)$ diagrams by sliding the endpoints • and ✕ along the torus and thereby pushing the β curve. One should lift this method to the universal abelian cover of the

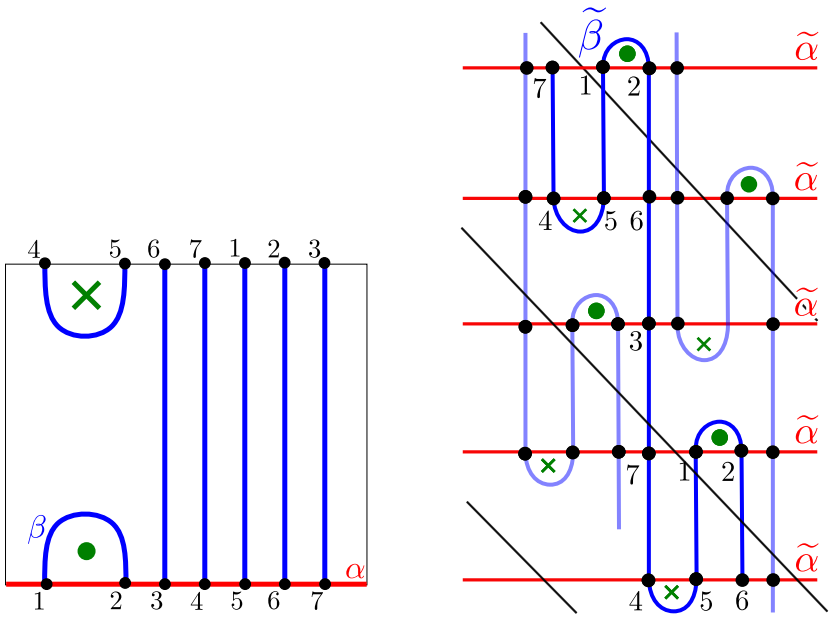

Figure 3.3: A $(1,1)$ diagram for a knot in $L_{3,1}$ and a lift of β to the universal cover. The numbers indicated are the indices of the lifted intersection points.

twice-punctured torus and think of $(1,1)$ diagrams as constructed by taking a grid in $\mathbb{R}^2$, where the horizontal lines are fixed lifts of α and the vertical lines are lifts of β which can be pushed around by isotopies. If one then puts a toothpick at every lift of $\times$, say, and slides these toothpicks along the plane, pushing the lifts of β around, one obtains a picture such as the one in fig. 3.3. This is akin to how the iconic pattern in the glazing of a mille-feuille is produced.

3.2.1 $CFK = CFK$

In this footnote to section 3.2 we wish to provide an aide-memoire for the proof of the following, somewhat folklore theorem.

Theorem 3.2.4. *Let $\mathcal{D}$ be a reduced $(1,1)$ diagram and recall the definitions*

of δ in section 3.1 and of $\overline{\delta}$ in section 3.2. We have

$$\overline{\delta} = \delta.$$

Definition 3.2.5. We call a Whitney disc $\varphi \in \pi_2(x, y)$ **primitive** if there is no $z \in \alpha \cap \beta \setminus \{x, y\}$ such that $\varphi = \varphi_1 * \varphi_2$, for some $\varphi_1 \in \pi_2(x, z)$ and $\varphi_2 \in \pi_2(z, y)$.

A proof of Theorem 3.2.4 requires showing that homotopy classes of Whitney discs of Maslov index 1 are in bijection with Whitney bigons, and that in the genus-1 case, such discs have unique holomorphic representatives. To provide a correspondence, the idea is to lift a primitive Whitney disc until it becomes an embedding of a disc in a surface covered by $\mathbb{C}$. In Proposition 6.4 of [OS04a], the Riemann mapping theorem is used to show that Whitney discs in the torus have unique holomorphic representatives.; this proposition, along with its method of proof, justify our combinatorial definition of knot Floer homology for $(1, 1)$ knots.

3.3 Some Sample Computations

Example 8. Consider the unknot $\mathbb{U} \subset S^3$. It has the $(1, 1)$ diagram in fig. 3.4. Since $|\alpha \cap \beta| = 1$, the dimension of $CFK(\mathbb{U})$ is 1. Since $\mathfrak{B} = \varnothing$, we have $\delta = 0$.

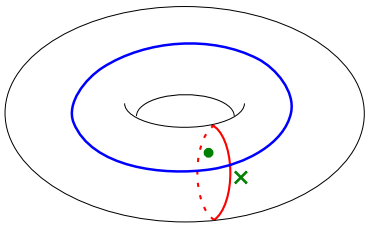

Figure 3.4: $(1, 1)$ diagram for $\mathbb{U}$.

Example 9. We compute the knot Floer chain complex for the left-handed and right-handed trefoil knots side-by-side, for comparison. Their $(1,1)$ diagrams are drawn in fig. 3.5. The reader may check that these are indeed diagrams for the two trefoils by connecting the $w = \bullet$ and $z = \times$ basepoints to form the knots, as explained in section 2.3.

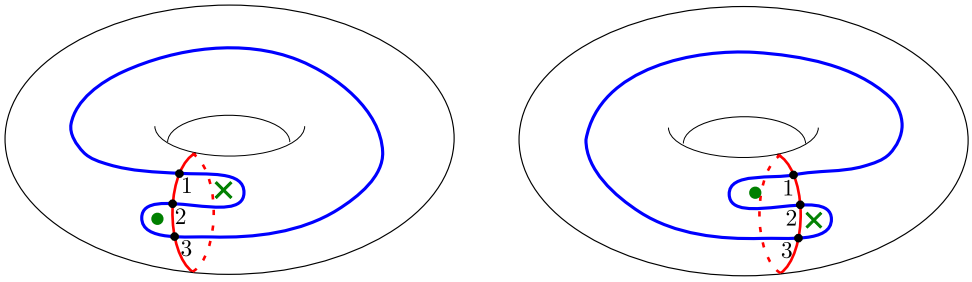

Figure 3.5: $(1,1)$ diagrams for the trefoil knots. Left: for the left-handed trefoil. Right: for the right-handed trefoil.

Let $\{x_1, x_2, x_3\}$ and $\{y_1, y_2, y_3\}$ be the generators of CFK for the left-handed and right-handed trefoil, respectively. There are precisely two bigons in each diagram, and these determine the differential:

$$\begin{aligned} \delta x_1 &= V x_2 & \delta y_1 &= 0 \\ \delta x_2 &= 0 & \delta y_2 &= U y_1 + V y_3 \\ \delta x_3 &= U x_2 & \delta y_3 &= 0 \end{aligned}$$

Notation. Type D structures V over $\mathcal{A} = \mathbb{F}[U, V]$ can be represented concisely by directed, labelled graphs whose vertices are generators of V and where there is an edge from v to v' precisely when v' is a summand of $\delta(v)$. Such graphs satisfy the following

1. Every vertex is a point in $\mathbb{R}^2$ with integer entries.
2. If $U^i V^j y$ is a summand of $\delta(x)$, the vertex corresponding to x is (a, b) and the vertex corresponding to y is (a, b), then $c - a = i$ and $d - b = j$.

For example, the type D structures of the two trefoil knots are encoded by

the following graphs.

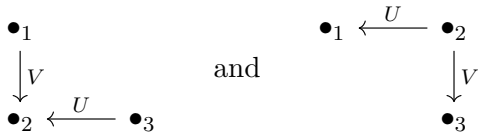

Since the arrows labelled by powers of U are always horizontal and the arrows labelled by powers of V are always vertical, the convention is to drop the labels on the arrows.

Using similar notation, the chain complexes CFK^- are pictorially represented by the following graphs. The vertical arrow labelled $\mathcal{F}_z$ is drawn to indicate the Alexander filtration level, which is induced by the z-basepoint.

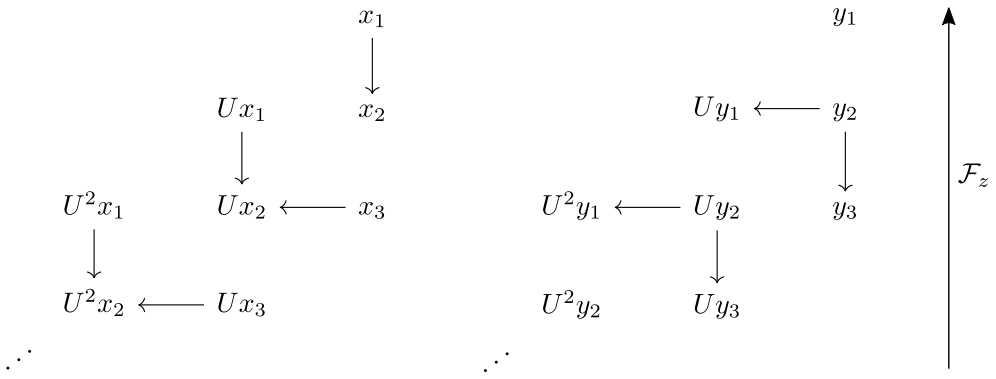

Example 10. The figure-8 knot is the first knot for which CFK has an acyclic summand. We leave it as an exercise to check that the following is a $(1,1)$ diagram for the figure-8 knot and that $CFK(4_1)$ is given by the adjacent graph.

Let the generators be labeled $x_1, \ldots, x_5$, according to the figure. The acyclic summand can be found by using the basis $\{y_1, \ldots, y_5\}$, where

$$y_i = \begin{cases} x_i & \text{if } i \neq 5, \\ x_1 + x_5 & \text{if } i = 5. \end{cases}$$

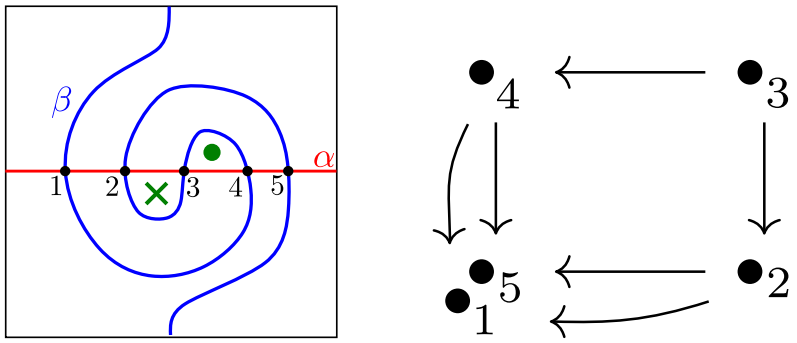

Figure 3.6: $(1,1)$ diagram for 4_1 and $CFK(4_1)$.

In this basis, the differential vanishes on y_1 and $\{y_2, y_3, y_4, y_5\}$ generates an acyclic subcomplex of CFK^-, since $\ker(\delta) = \mathrm{im}(\delta) = \mathbb{F}\langle y_2 + y_4, y_5\rangle$. The filtered complex $CFK^-(4_1)$ is illustrated in fig. 3.7.

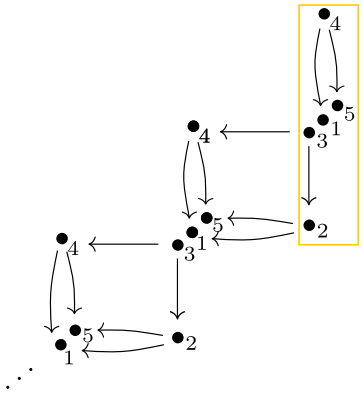

Figure 3.7: The complex $CFK^-(4_1)$, with powers of U omitted on the generators, to ease the notation. Boxed in yellow is the subcomplex $\widehat{CFK}(4_1)$.

Chapter 4

On $(1,1)$ L-space Knots

L-spaces (see definition 4.1.4) are Heegaard Floer homology lens spaces and they are at the centre of a conjecture currently driving some of the developments in low-dimensional topology; see [Juh15] [BGW13]. In the scope of obtaining a bank of computable and varied examples, it is worthwhile to know quickly whether a knot can be used to produce an L-space. In [GLV18], Greene, Lewallen and Vafee (henceforth GLV) presented a pleasant result enabling one to read immediately from a $(1,1)$ diagram drawn in a standard fashion whether there exists some Dehn surgery on the corresponding knot producing an L-space. In this chapter, after reviewing Dehn surgery in section 4.1, we will explain in section 4.2 the standard fashion of drawing $(1,1)$ diagrams, sketch in section 4.3 the main result from [GLV18], which is a characterization of $(1,1)$ L-space knots, and, in section 4.4, present the author's implementation of the characterization as a computer program.

Let us assume from now on that our knots $K \subset Y$ are *null-homologous* $(1,1)$ knots. This is the original set-up of knot Floer homology and allows one to make canonical choices which simplify the discussion.

4.1 An Overview of Dehn Surgery

A practical way to construct new 3-manifolds is via Dehn surgery, a classic construction which we review here. Some good references are [FM97], [Rol03] and especially [Sav12].

Let $K\colon S^1 \hookrightarrow Y$ be a knot and $\nu(K)$ a tubular neighbourhood of K. Drilling out this tubular neighbourhood, we obtain $Y \setminus \nu(K)$, a manifold with torus boundary. To construct a closed manifold, we need another manifold with torus boundary and an identification of the two boundaries.

Definition 4.1.1. Maintaining the notation above, **Dehn surgery** is the passage from the manifold Y to the manifold

$$Y \setminus \nu(K) \cup_h D^2 \times S^1,$$

where h is a homeomorphism $\partial(D^2 \times S^1) \to \partial(Y \setminus \nu(K))$.

Recall from Proposition 2.1.6 that the homeomorphism type of the resulting 3-manifold depends on the mapping class of h. The mapping class group of T^2 is isomorphic to the group of automorphisms of $H_1(T^2;\mathbb{Z})$, which is $SL_2(\mathbb{Z})$; see [Rol03]. The isomorphism $\mathrm{MCG}(T^2) \simeq SL_2(\mathbb{Z})$ is specified once a basis is chosen for $H_1(T^2;\mathbb{Z})$. This is because a choice of basis specifies an isomorphism $H_1(T^2;\mathbb{Z}) \simeq \mathbb{Z} \oplus \mathbb{Z}$, so an automorphism of $H_1(T^2;\mathbb{Z})$ can be encoded as an invertible 2-by-2 matrix with integer entries. Let $\mu \subset \partial\nu(K)$ be a **meridian**, i.e. a circle bounding a disc in $\nu(K)$ and fix a curve $\lambda \subset \partial\nu(K)$ so that $\{[\mu],[\lambda]\}$ forms a basis for $H_1(\partial\nu(K);\mathbb{Z})$ and $\mu \cdot \lambda = 1$ (see Definition 4.2.5). Such a pair of curves is called a **meridian-longitude pair**. The curve λ is known as a **longitude**. Note that, once $\nu(K)$ is fixed, μ is canonical, but a choice must be made to obtain λ. Two different choices are drawn on the boundary of a knot complement in fig. 4.1.

In our case, there is a canonical choice of longitude as well:

Definition 4.1.2. Let K be a null-homologous knot in a 3-manifold Y.

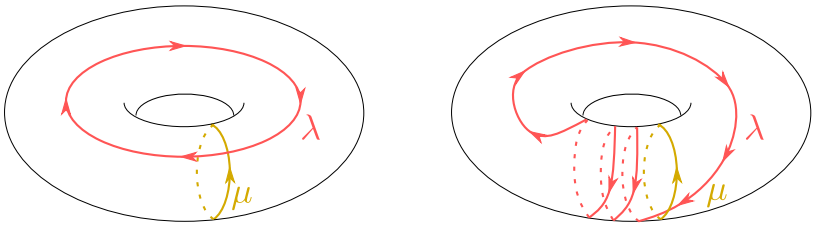

Figure 4.1: Two possible choices of curves μ, λ on the boundary of $\partial\nu(K)$ such that $\{[\mu], [\lambda]\}$ is a basis for $H_1(\partial\nu(K); \mathbb{Z})$ and $\mu \cdot \lambda = 1$.

The **standard meridian-longitude pair** on the knot complement $K^c := Y \setminus \nu(K)$ is the meridian-longitude pair (μ, λ_0), where $\lambda_0 \subset \partial(K^c)$ is the longitude that is null-homologous in K^c.

Remark. The longitude λ_0 in the definition above is unique up to isotopy, and it is known as the **Seifert longitude**. This justifies our use of the definite articles in the above definition.

Remark. The convention that $\mu \cdot \lambda = 1$ is consistent with [Rol03] and [RR17], but it is opposite from the convention in [HRW16] and [HRW18]. This causes no issue, as long as one is aware of the difference.

Fix also the curves $m = \partial D^2 \times \{*\} \subset D^2 \times S^1$ and $\ell = \{1\} \times S^1 \subset D^2 \times S^1$. With bases chosen, an element $A \in SL_2(\mathbb{Z})$ corresponds to a map $h_A \colon H_1(\partial D^2 \times S^1; \mathbb{Z}) \to H_1(\partial Y \setminus \nu(K); \mathbb{Z})$ given by matrix multiplication.

Proposition 4.1.3 (Lemma 1.6 in [Sav12])**.** *Let p, q be arbitrary coprime integers and let $r, s \in \mathbb{Z}$ be such that $ps - qr = 1$, i.e. such that $\left(\begin{smallmatrix} p & r \\ q & s \end{smallmatrix}\right) \in SL_2(\mathbb{Z})$. Then the assignment $[m] \mapsto p[\mu] + q[\lambda]$ determines the manifold $Y \setminus \nu(K) \cup_{h_A} D^2 \times S^1$ up to homeomorphism.*

The upshot of Proposition 4.1.3 is that, once a homological basis is chosen for $\partial(\nu(K))$, a Dehn surgery on K is determined by a pair of coprime integers p, q. By the correspondence between pairs of coprime integers and elements of $\mathbb{Q}$, we see that every Dehn surgery on a knot corresponds to an element of $\mathbb{Q}P^1 := \mathbb{Q} \cup \{1/0\}$. The standard notation for $1/0$ is ∞, since $\mathbb{Q}P^1 \subset$

$\mathbb{R}P^1 \simeq S^1 \simeq \mathbb{R} \cup \{*\}$; cf. example 1.

Notation. Let $K \subset Y$ be a null-homologous knot and let $\{\mu, \lambda_0\} \subset \partial\nu(K)$ be the standard meridian-longitude pair. We denote the Dehn surgery $[m] \mapsto p[\mu] + q[\lambda_0]$ by $Y_{p/q}(K)$.

Remark. ∞-surgery on any knot $K \subset Y$ is the passage from Y to itself.

Remark. There are potentially infinitely many choices of surgery yielding 3-manifolds distinct from the one given. Many open questions spring out of this observation, including botany and geography questions and the Berge conjecture, which is a proposed answer, in the form of a list of knots, to the following question of J. Berge:

Question. Which surgeries on which knots in S^3 result in lens spaces?

The same spirit of inquiry leads to questions about L-spaces, such as:

Question. Which surgeries on which knots result in L-spaces?

GLV give a partial answer and this is the result we wish to present in this chapter.

Definition 4.1.4. An **L-space** is a rational homology sphere Y such that $\widehat{HF}(Y)$[1] is an $\mathbb{F}$-vector space of dimension $|H_1(Y;\mathbb{Z})|$.

Remark. If Y is a rational-homology 3-sphere, it turns out that, for every $\mathfrak{s} \in \mathrm{Spin}^c(Y)$, we have $|\widehat{HF}(Y,\mathfrak{s})| \geq 1$; see §10 in [OS04b]. This, together with the bijection $H^2(Y) \leftrightarrow \mathrm{Spin}^c(Y)$ and the splitting of $\widehat{HF}(Y)$ along spin^c structures, implies that if Y is an L-space, then

$$\widehat{HF}(Y,\mathfrak{s}) \simeq \mathbb{F},$$

for every spin^c structure $\mathfrak{s} \in \mathrm{Spin}^c(Y)$.

Definition 4.1.5. Let Y be closed, oriented 3-manifold and let $K\colon S^1 \to Y$

[1] We remind the reader that the various Heegaard Floer homologies were defined in section 3.1.3.

be a null-homologous knot K is called an **L-space knot** if K admits a non-trivial Dehn surgery yielding an L-space.

Remark. The word "non-trivial" in the definition above is necessary to exclude ∞-surgery, in the case that Y is already an L-space.

Definition 4.1.6. Let Y be an L-space and $K \subset Y$ an L-space knot with the standard meridian-longitude pair. We say that K is a **positive** (resp. **negative**) L-space knot if there exists a positive (resp. negative) slope p/q for which $Y_{p/q}(K)$ is an L-space.

Remark. The standardization of the longitude of a null-homologous knot and the convention $\mu \cdot \lambda = 1$ are required to make sense of the words "positive" and "negative" in the definition above.

4.2 The Normal Form

There is a standard manner of drawing doubly pointed Heegaard diagrams for $(1,1)$ knots that is referred to the *normal form*. In fact, this is more generally a standard manner for drawing a connected curve embedded in the boundary of a solid torus. D. H. Choi and K. H. Ko found this normal form in [CK03] and applied it to the knot itself. A description of the normal form for $(1,1)$ diagrams may be found in [Ras05].

Definition 4.2.1. A $(1,1)$ diagram is said to be in **normal form** if it is drawn as in fig. 4.2. A $(1,1)$ diagram in normal form is characterized by a quadruple (p,q,r,s), where $p = |\alpha \cap \beta|$, q is the number of **rainbow arcs** (labelled in fig. 4.2), r is the number of arcs running from the top left of the diagram to the bottom, next to the rainbow arcs; we call these **curvy arcs**. Finally, s is the twist factor: it is a number satisfying $0 \leq s < p$ and it encodes how the top and the bottom of the diagram should be identified: the i^{th} intersection point on the top of the diagram is identified with the $(i+s)^{th}$ intersection point on bottom.

Remark. (1) The etymology of "twist factor" can be found by picturing how one must identify the ends of the cylinder obtained by identifying the left and right hand sides of a normal form diagram.

Notation. We call the $p-2q$ non-rainbow arcs in a normal form the **vertical arcs**. The vertical arcs which are not curvy are called **straight**. We will say that two vertical arcs are of the **same kind** if both are curvy or both are straight. This is vocabulary that we will use especially in Chapter 5.

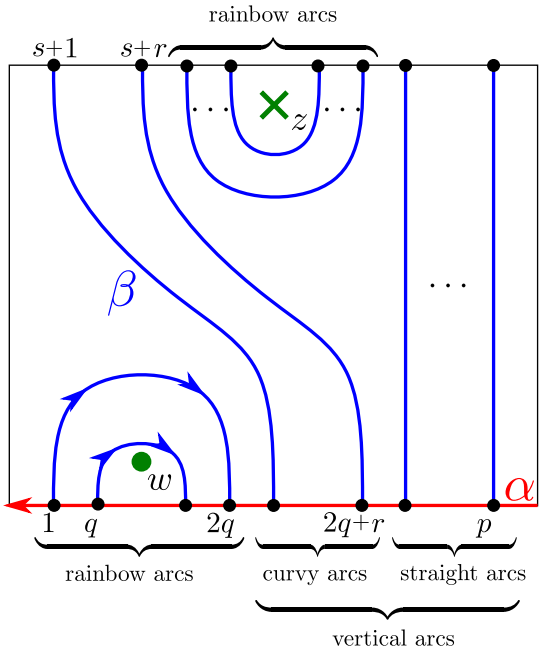

Figure 4.2: A $(1,1)$ diagram in normal form. The left and right sides of the square are identified as usual, and the top and bottom are identified after a rotation of one end of the cylinder.

Definition 4.2.2. We let $\mathcal{D}(p,q,r,s)$ denote the $(1,1)$ diagram in normal form corresponding to (p,q,r,s). We let $K(p,q,r,s)$ denote the knot described by $\mathcal{D}(p,q,r,s)$.

Before proving that $(1,1)$ diagrams admit normal forms, we need the following remark. See fig. 4.3 for an example of a Dehn twist, and see [Sav12] for a precise definition.

Remark. Let $\mathcal{D} = (T^2, \alpha, \beta, w, z)$ be a $(1,1)$ diagram for a knot $K \hookrightarrow Y$. Applying a Dehn twist along α or β to $\mathcal{D}$ produces a new diagram $\mathcal{D}'$ which contains the same bigons as $\mathcal{D}$, hence produces the same knot Floer type D structure. In fact, Dehn twists along α or β leave the embedding $K \hookrightarrow Y$ unchanged, but we do not need this. One should be able to prove this by analyzing how a Dehn twist along an attaching circle affects the construction of a nice Morse function associated with $\mathcal{D}$. Note that the *projection* of a knot is definitely affected by a Dehn twist, see fig. 2.4.

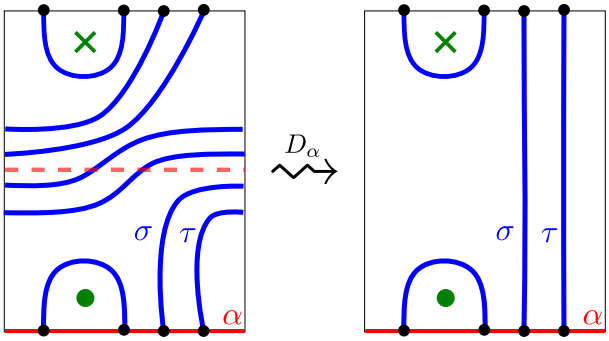

Figure 4.3: An application of D_α, the Dehn twist along α.

Lemma 4.2.3. *Every* $(1,1)$ *knot admits a* $(1,1)$ *diagram in normal form.*

Proof. (cf. §2.1 in [CK03]) Let K be a $(1,1)$ knot and $\mathcal{D} = (T^2, \alpha, \beta, w, z)$ a $(1,1)$ diagram for K. Suppose furthermore, without loss of generality, that $\mathcal{D}$ is reduced. We may let $p = |\alpha \cap \beta|$.

Consider the cylinder $\mathcal{C} := T^2 \setminus \nu(\alpha)$. Note that since β is connected, its image under the operation $\mathcal{D} \rightsquigarrow \mathcal{C}$ is a collection of arcs of two kinds: rainbow arcs, which have both endpoints on a connected component of $\partial\mathcal{C}$, and non-rainbow arcs, which have each endpoint on a different component of $\partial\mathcal{C}$. Let S_1 and S_2 denote the two connected components of $\partial\mathcal{C}$. There are as many rainbow arcs with their endpoints on S_1 as there are with endpoints on S_2, since both S_1 and S_2 contain p endpoints of arcs of β. So we may let q be the number of rainbow arcs with endpoints on S_1.

Next, since $\mathcal{D}$ is reduced, every rainbow arc cobounds a disc embedded in $\mathcal{C}$ that contains the z or the w basepoint. Claim: no rainbow arc cobounds a disc that contains both basepoints. Proof: by contradiction, suppose $\rho \subset \mathcal{C}$ is such a rainbow arc and suppose $\partial\rho \subset S_1$. On the one hand, since β is embedded, a rainbow arc ρ' with endpoints on S_2 cannot cobound a disc containing any basepoint, lest ρ' intersect ρ; this contradicts our assumption that $\mathcal{D}$ is reduced. On the other hand, if there are no rainbow arcs with endpoints on S_2, we contradict our earlier observation that there are as many rainbow arcs with endpoints on S_1 as there are rainbow arcs with endpoints on S_2. This proves the claim.

Finally, since β is an attaching circle for a solid torus in the Heegaard splitting of a lens space $L_{m,n}$[2], after negleting the basepoints, β is isotopic to the (m, n) torus knot. Thus there exists a non-rainbow arc, σ. Apply sufficiently many Dehn twists along α to the diagram so that σ is isotopic to a straight line, exemplified in fig. 4.3. The remaining non-rainbow arcs fall into two kinds. Those parallel to σ and those arcs τ which cannot be made parallel to σ, because both connected components of $\mathcal{C} \setminus (\tau \cup \sigma)$ contain rainbow arcs. We may let r be the number of non-rainbow arcs parallel to σ (including σ) and we let s be the appropriate twist factor with $0 \leq s < p$. $\square$

Definition 4.2.4. Let $\mathcal{D} = (T^2, \alpha, \beta, z.w)$ be a $(1, 1)$ diagram in normal form and suppose furthermore that it is **oriented**, i.e. that orientations have been chosen on α and β. The diagram $\mathcal{D}$ is **coherent** if each of the rainbow arcs is oriented the same way (left to right or right to left).

Definition 4.2.5. Let γ_1 and γ_2 be two smooth curves in a surface S such that γ_1 and γ_2 intersect transversely. Suppose S is oriented so, at every $c \in S$, the tangent space T_cS is equipped with class of bases on which $GL_2^+(\mathbb{R})$ acts freely and transitively. To every $c \in \gamma_1 \cap \gamma_2$, assign the integer

$$\deg(c) = \begin{cases} 1 & \text{if the pair } (\gamma_1'(c), \gamma_2'(c)) \text{ is an oriented basis for } T_cS \\ -1 & \text{otherwise.} \end{cases}$$

[2]The letters p, q are unavailable

So $\deg(c) = -1$ if $(\gamma_2'(c), \gamma_1'(c))$ is in the orientation class of T_cS. The **algebraic intersection number** $\gamma_1 \cdot \gamma_2$ is defined to be

$$\sum_{c \in \gamma_1 \cap \gamma_2} \deg(c).$$

Definition 4.2.6. Every bigon B in an oriented $(1,1)$ diagram $\mathcal{D}$ has two oriented arcs in its boundary: $\partial B \cap \beta$ and $\partial B \cap \alpha$. The orientation on these arcs may be given by an orientation on ∂B, in which case we say that α and β **orient** ∂B. Suppose $\mathcal{D}$ is coherent and the orientations on α, β are such that, for every bigon B with $\partial B \cap \beta$ a rainbow arc, α and β orient ∂B. In this case, we say that $\mathcal{D}$ is **positive-coherent** if $\mathcal{D}$ is coherent and $\alpha \cdot \beta > 0$ and **negative-coherent** if $\alpha \cdot \beta < 0$.

Example 11. The $(1,1)$ diagrams in section 3.3 are good examples illustrating coherence. The trefoils are redrawn in fig. 4.4 for the reader's convenience. For the left-handed trefoil, $\alpha \cdot \beta = -1$, so it is negative-coherent. The right-handed trefoil is positive-coherent, with $\alpha \cdot \beta = 1$. We leave it to the reader to check that the figure-8 knot is incoherent, using fig. 3.6.

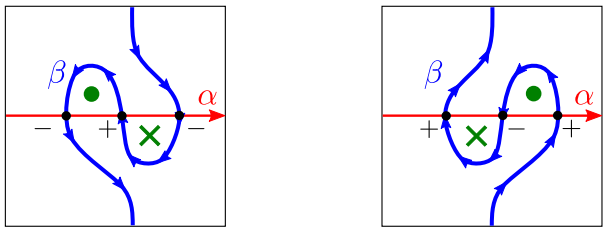

Figure 4.4: Oriented $(1,1)$ diagrams for the two trefoil knots. Left: for the left-handed trefoil. Right: for the right-handed trefoil. The sign next to each intersection point c indicates the value of $\deg(c)$.

Now we can state the main result of GLV:

Theorem 4.2.7 (Theorem 1.2 in [GLV18])**.** *Let K be a $(1,1)$ knot and $\mathcal{D}$ a $(1,1)$ diagram for K in normal form. Then K is a positive (resp. negative) L-space knot if and only if $\mathcal{D}$ is positive (resp. negative)-coherent.*

Remark. Knots with $(1,1)$ diagrams $\mathcal{D}(p,0,r,s)$ are automatically both positive-coherent and negative-coherent. Thus the above result allows for $(1,1)$ knots which admit both positive and negative surgery slopes resulting in L-spaces. This is consistent with [RR17], where is shown that the set slopes on a knot for which Dehn surgery results in an L-space is either empty, a singleton or an interval in $\mathbb{Q}P^1$. In this latter case, the interval may contain both negative and positive slopes. For example, there exists a knot in $L_{4,1}$ such that the interval of L-space surgery slopes is $\mathbb{Q}P^1 \setminus \{pt\}$. See [HRW18]; the property of a knot in an L-space having a single surgery slope which does not yield an L-space is equivalent to the knot complement being a Heegaard Floer solid torus.

We will sketch the proof of this result in the following section, focusing on the salient features. We will provide another proof of this result after describing the immersed curve formalism in chapter 6, so will not consider the statements in section 4.3 as established, except when computing examples.

4.3 Sketch of the Proof of Theorem 4.2.7

The proof of GLV depends crucially on Theorem 4.3.2, which characterizes the shape of CFK for L-space knots. J. and S. Rasmussen were able to prove this general result using work of Ozsváth-Szabó and Boileau-Boyer-Cebanu-Walsh, see [RR17]. It is now possible to prove this result using the immersed curve formalism of chapter 6.

4.3.1 The Staircase Characterization

Definition 4.3.1. Let $K\colon S^1 \to Y$ be a knot and fix a spin^c structure $\mathfrak{s} \in \mathrm{Spin}^c(Y)$. $CFK(K,\mathfrak{s})$ is said to be a **positive staircase** if there is a

basis $\{x_1, \dots, x_{2n+1}\}$ for $CFK(K, \mathfrak{s})$ such that

$$\delta x_i = \begin{cases} U^{n_i} x_{i+1} + V^{m_i} x_{i-1} & \text{if } i \text{ is even} \\ 0 & \text{otherwise,} \end{cases}$$

where n_i and m_i are positive integers. $CFK(K, \mathfrak{s})$ is said to be a **negative staircase** if it becomes a positive staircase once all the arrows are flipped. More formally, it is a negative staircase if it admits a basis $\{x_1, \dots, x_{2n+1}\}$ such that

$$\delta x_i = \begin{cases} U^{n_i} x_2 & \text{if } i = 1 \\ 0 & \text{if } i \text{ is even} \\ V^{m_i} x_{2n} & \text{if } i = 2n+1 \\ U^{n_i} x_{i+1} + V^{m_i} x_{i-1} & \text{otherwise} \end{cases}$$

Again, m_i, n_i are positive integers. If $CFK(K, s)$ is a positive staircase for every s, then we say that CFK **consists of positive staircases**. The expression "CFK consists of negative staircases" is defined similarly.

For some simple examples, we refer again to section 3.3. The type D structure $CFK(3_1^L)$, where 3_1^L denotes the left-handed trefoil, is a negative staircase, $CFK(3_1^R)$ is a positive staircase and $CFK(4_1)$ is not a staircase. A more interesting example is the following

Example 12. The $(3, 4)$ torus knot $T(3, 4)$ appears as 8_{19} in Rolfsen's table [Rol03]. It is also the knot $K(5, 1, 1, 1)$, whose $(1, 1)$ diagram is drawn in fig. 4.5. It is left as an exercise to check that the graph in the same figure is $CFK(8_{19})$; to this end, it may be helpful to consider the universal cover, drawn in fig. 4.6. Note the power of 2 appearing in the differential:

$$\delta x_5 = U^2 x_3 + V^2 x_2.$$

Checking the definition, one sees that $CFK(8_{19})$ is a negative staircase. By theorem 4.3.2, this implies that 8_{19} is a negative L-space knot.

Another example is $CFK(\mathcal{D}(19, 2, 1, 7))$, partially computed in section 5.2,

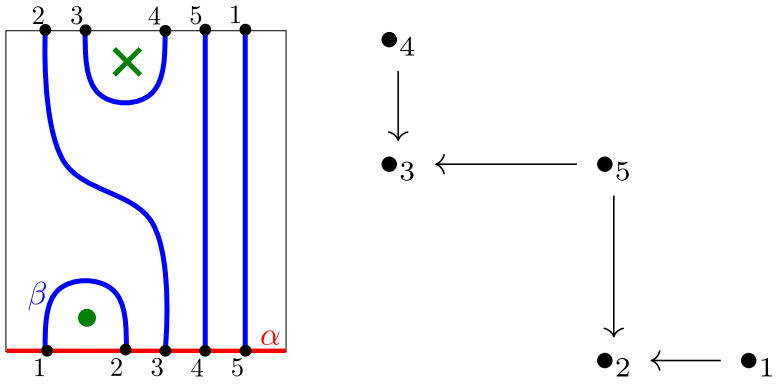

Figure 4.5: A $(1,1)$ diagram for 8_{19} and $CFK(8_{19})$. Note that each of the two arrows out of $\bullet_5$ has length 2.

although the graph for CFK is not drawn.

The following theorem is modified from its original source because in our context $\widehat{HFK}$, as defined in [RR17], is isomorphic to CFK.

Theorem 4.3.2 (Lemmas 3.2, 3.3 and 3.5 in [RR17])**.** *A knot K in an L-space Y is a positive (resp. negative) L-space knot if and only if $CFK(K)$ consists of positive (resp. negative) staircases.*

Remark. In [RR17] and [GLV18], staircases are called chains, but given our representation of CFK as a graph in the plane, we find our terminology more descriptive.

4.3.2 The Proof

To prove that coherent diagrams describe L-space knots, the idea is to get enough control on the possible bigons by lifting them to the universal cover $\mathbb{C} \to T^2$, and we will do this in detail in section 7.1. Conversely, to prove that $(1,1)$ L-space knots admit only coherent diagrams, GLV prove the following technical lemma:

Lemma 4.3.3 (Lemma 2.3 in [GLV18])**.** *Suppose $CFK(\mathcal{D}, \mathfrak{s})$ is a positive*

staircase and $\mathcal{D}$ is a reduced $(1,1)$ diagram. Let $\{x_1, \ldots, x_{2n+1}\}$ be a basis satisfying definition 4.3.1. If $x, y \in \mathcal{I}$ are generators and $\varphi \in \pi_2(x,y)$ has a holomorphic representative with $\mu(\varphi) = 1$, then $x = x_{2i}$ for some i and $y = x_{2i\pm1}$. Moreover, $y = x_{2i+1}$ if $n_z(\varphi) = 0$ and $y = x_{2i-1}$ if $n_w(\varphi) = 0$.

The above lemma is proved through a careful analysis the Maslov and Alexander gradings of the x_i, x and y. Its conclusion is that the intersection points $x \in \alpha \cap \beta$, once properly labeled, form a basis exhibiting $CFK(\mathcal{D})$ as a collection of staircases of the same sign. This is an important bridge between the algebraic data of $CFK(\mathcal{D})$ and the geometric data of $\mathcal{D}$.

Next, suppose that K is a $(1,1)$, positive L-space knot and $\mathcal{D}$ is its $(1,1)$ diagram. By Theorem 4.3.2, $CFK(\mathcal{D})$ consists of positive staircases. By the above lemma, there is a labelling on the elements of $\alpha \cap \beta$ so that they form a staircase basis and the bigons in $\mathcal{D}$ are thus restricted: there exists a unique bigon between subsequent basepoints, once they are labelled. The final steps are to show that the bigons are arranged such that, for every $\mathfrak{s}$, $(\widetilde{\alpha}_{\mathfrak{s}}, \widetilde{\beta})$ is positive graphic in the sense of the definition below and to apply lemma 4.3.6.

Definition 4.3.4. Let γ_1, γ_2 be two copies of $\mathbb{R}$ embedded in $\mathbb{R}^2$ which intersect transversely and let $\mathbb{R} \subset \mathbb{R}^2$ be the x-axis with the standard orientation. We say that the pair (γ_1, γ_2) is **graphic**, if there is an orientation-preserving homeomorphism $\mathbb{R}^2 \to \mathbb{R}^2$ which takes γ_1 into $\mathbb{R} \times \{0\}$ and γ_2 into the graph of some polynomial $p(x) \in \mathbb{R}[x]$. In addition, we say that the pair is **positive-graphic** if the leading coefficient of $p(x)$ is negative and **negative graphic** if the leading coefficient is positive. In the case that $\gamma_1 = \mathbb{R} \times \{*\}$, we say that γ_2 is graphic to mean that the pair (γ_1, γ_2) is.

Example 13. Consider the diagram $\mathcal{D}(5,1,1,1)$, drawn in fig. 4.5, and take a horizontal lift $\widetilde{\alpha}$ of α to the universal cover $\mathbb{C}$. Take also a lift $\widetilde{\beta}$ of β. The pair $(\widetilde{\alpha}, \widetilde{\beta})$ is negative-graphic, as can be seen in fig. 4.6.

GLV point out the following characterization of graphic curves:

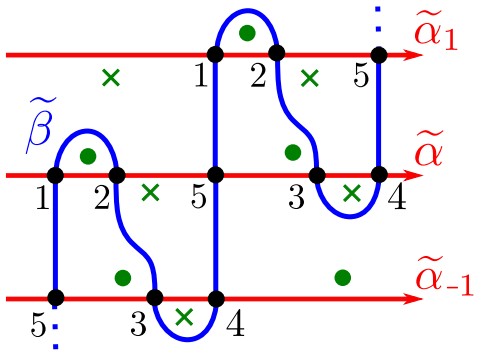

Figure 4.6: The pair $(\widetilde{\beta}, \widetilde{\alpha})$ for the diagram $\mathcal{D}(5,1,1,1)$.

Proposition 4.3.5. *The pair (γ_1, γ_2) is graphic if and only if γ_1 and γ_2 can be oriented so that the intersection points $x \in \gamma_1 \cap \gamma_2$ occur in opposite order along γ_1 and γ_2.*

Proof. The "only if" direction is obvious, because the intersection data is preserved by orientation-preserving homeomorphisms and it is true in the case of polynomials. For the "if" direction suppose, without loss of generality, that $\gamma_1 = \mathbb{R}$ is oriented from left to right and the intersection points occur in opposite order along γ_1 and γ_2. The case $\gamma_1 \cap \gamma_2 \neq \varnothing$ can be dealt with separately and easily, so we may suppose that there is an intersection point. Label the intersection points x_i in the order in which they occur along γ_1 and consider the polynomials $c(x-x_1)(x-x_2)\dots(x-x_n)$, where $n = |\gamma_1 \cap \gamma_2|$ and $c \in \mathbb{R}$ can be chosen small enough so that $\gamma_2 \cap p([x_1, x_n]) = \gamma_2 \cap \gamma_1$. Applying a straight line homotopy then yields a desired homeomorphism. □

For example, consider the central lift $\widetilde{\alpha}$ in fig. 4.6 and its intersections points with $\widetilde{\beta}$. Orienting $\widetilde{\beta}$ so that $\widetilde{\alpha} \cdot \widetilde{\beta} = -1$, the intersection points along $\widetilde{\beta}$ are, in order, x_4, x_3, x_5, x_2, x_1, which is the opposite order in which they are encountered along $\widetilde{\alpha}$. This characterization of graphic curves serves to prove the following key lemma, which we will absorb in Theorem 7.1.1.

Lemma 4.3.6. *Let $\mathcal{D} = (T^2, \alpha, \beta, w, z)$ be a $(1,1)$ diagram for a knot $K \subset Y$, let $\mathfrak{s} \in Spin^c(Y)$ and take the lifts $\widetilde{\alpha}_{\mathfrak{s}}$, $\widetilde{\beta}$ of α and β, respectively, to*

the universal cover such that α is lifted to a horizontal line and oriented from left to right. Then $\mathcal{D}$ is $\pm$-coherent if and only if the pair $(\widetilde{\alpha}_{\mathfrak{s}}, \widetilde{\beta})$ is $\pm$-graphic, for every $\mathfrak{s} \in Spin^c(Y)$.

4.4 Algorithmic Implementation

The result of GLV makes it easy to write a computer program to list potential $(1,1)$ diagrams and to decide whether they are diagrams for L-space knots or not. Let us explain the algorithm here. The idea is very simple: start at an intersection point $x \in \alpha \cap \beta$, walk along the β curve, and record the intersection points in the order in which they occur. This list of intersection points is almost equivalent to the quadruple (p,q,r,s), but not quite: see the example following the notation.

Notation. For this section, we want to compute explicitly the action of $\mathbb{Z}/p\mathbb{Z}$ on $\alpha \cap \beta$, so the elements of $\alpha \cap \beta$ are labelled $x_0, x_1, \ldots x_{p-1}$, according to their order along the bottom of the normal form diagram.

Notation. We agree to orient α from *right to left*, contrary to what we have done so far, and to orient β so that the first rainbow arc is from x_0 to x_{2q-1} and thus co-orients its rainbow bigon with α.

In both $\mathcal{D}(3,1,1,0)$ and $\mathcal{D}(3,1,1,1)$, the intersection points are encountered in the order (x_0, x_1, x_2), but $K(3,1,1,0)$ is the left-handed trefoil knot, whereas $K(3,1,1,1)$ is the right-handed trefoil knot (cf. section 3.3). Adding an extra bit of information to the intersection points provides a list from which (p,q,r,s) can be recovered.

The main methods are the unfortunately named `check`, which transforms a quadruple of non-negative integers (p,q,r,s) into a p-tuple of oriented elements of $\alpha \cap \beta$, and the method `nextPoint`, which walks along β from one intersection point to the next. For the program to work as intended, we should restrict (p,q,r,s) so that $p \geq 2q + r$ and $0 \leq s < p$, but that is it. The helper method `isHeegaard` can then be used to check whether

the quadruple (p, q, r, s) corresponds to a doubly-pointed Heegaard diagram. With these methods, it is possible to generate a large number of quadruples (p, q, r, s), to pick out those which correspond to doubly pointed Heegaard diagrams and, among these latter, to pick out either the incoherent or the coherent diagrams.

`check`

This method takes as input a quadruple of integers (p, q, r, s) and returns a p-tuple, called `pathCycleOr`, of pairs $(x_i, \epsilon_i) \in \alpha \cap \beta \times \{0, 1\}$, where ϵ_i is the information of the direction of β at x_i. Our convention is to set

$$\epsilon_i = \frac{\deg(x_i) + 1}{2}.$$

So, looking at $\mathcal{D}(p, q, r, s)$ drawn in normal form, $(x_i, 0)$ is the point x_i with β running up. For example, `check` always starts at the intersection point x_0, so the first entry of `pathCycleOr` is $(x_0, 0)$ and the second entry is invariably $(x_{2q-1}, 1)$. The third entry depends on the specific value of $2q-1$. The method `check` constructs `pathCycleOr` one point at a time, using the method `nextPoint` to find the next pair (intersection point, ϵ).

`nextPoint`

This method takes an oriented point (x_i, ϵ_i) and a quadruple (p, q, r, s) and returns the next point encountered along the β curve of $\mathcal{D}(p, q, r, s)$. The formulas used in this method can be found using the normal form. For example if $\epsilon_i = 0$, then the following holds: if $0 \leq i \leq 2q - 1$, then x_i is the endpoint of a rainbow arc and the next point along β, x_j, can be found using the identity $i + j = 2q - 1$; if $2q \leq i \leq 2q + r - 1$, then x_i is the endpoint of one of the vertical arcs and the next endpoint x_j may be found using the identity $i = j - s + 2q$; see fig. 4.7.

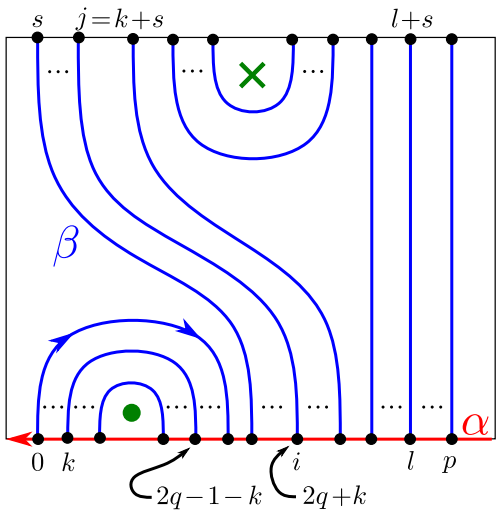

Figure 4.7: Illustration of the identities satisfied by the indices of intersection points. Given i satisfying $2q \leq i < 2q + r$, we define k to be $2q - i$ and j to be the other endpoint of the arc starting at i.

`isHeegaard` and `isCoherent`

Both methods take as input a p-tuple of pairs `pathCycleOr`. The method `isHeegaard` returns `true` if the p-tuple corresponds to a doubly pointed Heegaard diagram and `isCoherent` returns `true` if the diagram is coherent. The first method checks whether x_0 appears twice in the p-tuple, as this indicates that β is disconnected. The method `isCoherent` checks whether one of the rainbow arcs is oriented from right to left. This is done by checking whether, in the p-tuple of pairs, there exist two subsequent pairs $(x_i, 0)$ and $(x_j, 1)$ with $i > j$.

An add-on

It is also possible to compute the algebraic intersection number $\alpha \cdot \beta$. We have

$$\alpha \cdot \beta = \sum_i (2\epsilon_i - 1).$$

This allows us to restrict the fundamental group of the ambient manifold Y.

4.4.1 Discussion

The above algorithm is helpful for finding potentially interesting examples that are too large to compute by hand. It is a fact that the complexity of $(1,1)$ knots (and knots in general) becomes apparent only in large examples. In our case, it is helpful to know right away whether a quadruple of integers can be the quadruple of a $(1,1)$ diagram in normal form and to know whether the knot represented is an L-space knot or not. Having an algorithm on hand makes it easy to look for L-space knots with particular characteristics, like a large r/q ratio, which allows for certain complications to occur. For instance, $K(19,2,1,7)$ from example 5.1 was found in this manner.

Chapter 5

The Structure of Bigons in $(1,1)$ Diagrams

In this chapter we want to establish the vocabulary required to pursue a careful analysis of the bigons $(1,1)$ diagrams. This work, and especially conjecture 1, will be the cornerstone of our alternative proof of Theorem 4.2.7 in chapter 7.

Definition 5.0.1. Let $\mathcal{D} = \mathcal{D}(p,q,r,s)$. A **rainbow bigon** is a bigon whose boundary consists of a single rainbow arc and a subarc of α. If a rainbow bigon B has $n_w(B) = 1$, we call it **locally maximal**. Otherwise, $n_z(B) = 1$ and we call it **locally minimal**.

Remark. There are $2q$ rainbow bigons in $\mathcal{D}(p,q,r,s)$, one for every rainbow arc.

Definition 5.0.2. By a **polygon** in $\mathcal{D}(p,q,r,s)$, we mean an embedding of an even-sided polygon in T^2 such that the edges of the polygon alternate between subarcs of α and subarcs of β.

Definition 5.0.3. Let P be a polygon in $\mathcal{D}(p,q,r,s)$ We use the following

notation:

$$\partial_\alpha P := \alpha \cap \partial P,$$
$$\partial_\beta P := \beta \cap \partial P.$$

Lemma 5.0.4 (§3.2 in [Doy05])**.** *Let $B \in \mathfrak{B}(x, y)$ be a bigon. We have the following bounds:*

$$|\partial_\alpha B \cap \beta| < p,$$
$$|\partial_\beta B \cap \alpha| < p.$$

Proof. We show that if $|\partial_\alpha B \cap \beta| \geq p$, then β is not embedded in T^2, a contradiction. The second inequality follows by symmetry.

Fix a lift $\widetilde{x} \in \mathbb{R}^2$ of x, and let $\widetilde{\alpha}$ and $\widetilde{\beta}$ be the lifts of α and β which contain $\widetilde{x}$. By assumption, there is a lift $\widetilde{x}'$ of x in $\partial_\alpha \widetilde{u}$ which is distinct from $\widetilde{x}$. The path along $\widetilde{\alpha}$ from $\widetilde{x}$ to $\widetilde{x}'$ projects down to $[\alpha]^n \in \pi_1(T^2, x)$, for some integer n. Let $\sigma \colon \mathbb{R}^2 \to \mathbb{R}^2$ be the deck transformation corresponding to $[\alpha]^n$. If $\widetilde{x}'$ is in the interior of $\partial_\alpha B$, then, by the Jordan curve theorem applied to ∂B, $\widetilde{\beta}$ intersects $\sigma\widetilde{\beta}$ nontrivially. Otherwise, $\widetilde{x}'$ is the other endpoint of $\partial_\alpha B$, in which case $\widetilde{\beta}$ also intersects $\sigma\widetilde{\beta}$ nontrivially. Projecting to T^2, we see that β is not embedded. □

5.1 From $(1, 1)$ to *CFK*

Part of G. Doyle's algorithm from [Doy05] lists all the bigons in a given $(1, 1)$ diagram. We briefly outline this part of the algorithm in the following list. The input is a normal form $(1, 1)$ diagram $\mathcal{D} = \mathcal{D}(p, q, r, s)$.

1. Form the set $\mathbb{P}$ of all the polygons in $\mathcal{D}$. Form also the set $\mathbb{B}$ of the $2q$ rainbow bigons of $\mathcal{D}$.

2. Pick an element $P \in \mathbb{P}$ and, for every element $B \in \mathbb{B}$, check if $\partial_\alpha B$ is equal an arc in $\partial_\alpha P$. If it is, it is possible to attach B to P along this

common α-arc. If it is possible to do this until the resulting polygon is a bigon, add this resulting bigon to $\mathbb{B}$.

3. Iterate step 2 over all elements of $\mathbb{P}$.

4. Return the set $\mathbb{B}$.

Doyle argues that the algorithm terminates in finite time and that $\mathbb{B} = \mathfrak{B}$, the set of all bigons in $\mathcal{D}$. In this thesis, we are interested in extracting the type D structure ${}^{\mathcal{R}}CFK(K)$, given the same input of a $(1,1)$ diagram $\mathcal{D}$ in normal form. Obviously, it is possible to apply Doyle's algorithm to extract $CFK(\mathcal{D})$ and then take the quotient to obtain ${}^{\mathcal{R}}CFK(\mathcal{D})$. The hope is that, given that we need less information from the $(1,1)$ diagram to extract ${}^{\mathcal{R}}CFK(\mathcal{D})$, a simpler or faster algorithm should be available.

5.2 The Knot $K(19,2,1,7)$

This section is devoted to the computation of CFK for an L-space knot which has a feature not present in low-rank examples. We hope to convince the reader that the combinatorics of a $(1,1)$ diagram in normal form can be complicated, even in the case of L-space knots, where CFK is already isomorphic to ${}^{\mathcal{R}}CFK$.

Example 14. Consider the $(1,1)$ diagram $\mathcal{D}(19,2,1,7)$. First of all, it can be checked that the β curve is connected, so this quadruple indeed produces a $(1,1)$ diagram. By applying the GLV criterion, we see that this is the diagram of an L-space knot. Coherent orientations have been drawn in figure 5.1. It's easy to check that $\alpha \cdot \beta = -1$, so $K(19,2,1,7)$ is a negative L-space knot in S^3, by Theorem 4.2.7.

To compute $CFK(19,2,1,7)$, we apply Doyle's pseudo-algorithm. We will only compute half of CFK; the rest of the computation is analogous and does not add educational value. Start with the two locally maximal rainbow bigons, which cover the w basepoint; this basepoint is drawn in the diagram

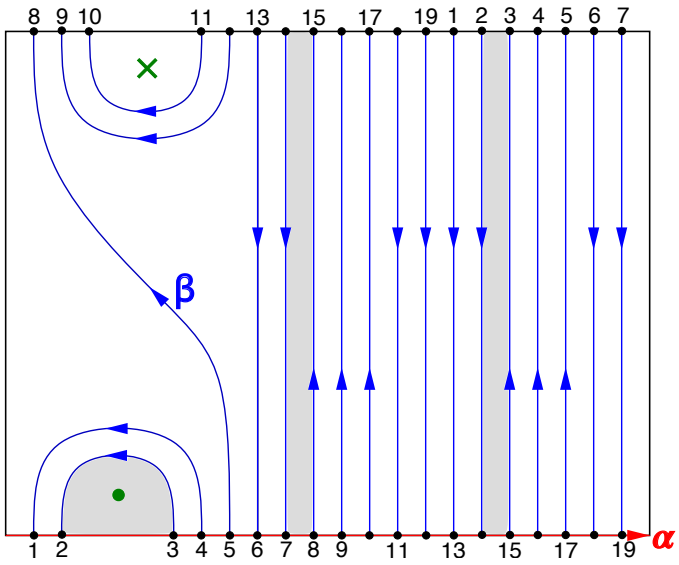

Figure 5.1: $(1,1)$ diagram for $K(19,2,1,7)$. The bigon $\bullet_7 \to \bullet_8$ is shaded.

as $\bullet$. Each of these bigons contributes a horizontal arrow of length 1 to CFK.

Now we check to see how these bigons extend throughout our diagram; take the bigon which contributes $\bullet_2 \to \bullet_3$ to the differential, for instance. By running along the β arcs, it is immediate that the bigon $\bullet_2 \to \bullet_3$ extends to a bigon which contributes $\bullet_{14} \to \bullet_{15}$, by gluing it to the 4-gon with vertex set $\{\bullet_2, \bullet_3, \bullet_{14}, \bullet_{15}\}$. Continuing in this fashion, we obtain the following (incomplete) list of arrows:

$$\bullet_2 \xrightarrow{U} \bullet_3 \qquad \bullet_1 \xrightarrow{U} \bullet_4$$
$$\bullet_{14} \xrightarrow{U} \bullet_{15} \qquad \bullet_{13} \xrightarrow{U} \bullet_{16}$$
$$\bullet_7 \xrightarrow{U} \bullet_8 \qquad \bullet_6 \xrightarrow{U} \bullet_9$$
$$\bullet_{19} \xrightarrow{U^2} \bullet_5$$
$$\bullet_{12} \xrightarrow{U^2} \bullet_{17}$$

Remark. These arrows are in a sense the most obvious ones, obtained

from the rainbow bigons $\bullet_1 \to \bullet_4$ and $\bullet_2 \to \bullet_3$ by extending the bigons through the vertical arcs. Recall our definition of curvy and straight arcs in section 4.2; for instance, there is a single curvy arc in fig. 5.1. Note here that, in general, we have

Lemma 5.2.1. *Suppose B is a locally maximal rainbow bigon in a reduced $(1,1)$ diagram $\mathcal{D}$ and suppose that B may be extended to a bigon B' through vertical arcs c_1, c_2. If c_1 and c_2 are of the same kind (i.e. both are straight or both are curvy), then $n_w(B) = n_w(B') = 1$ and $n_z(B) = n_z(B') = 0$. If one of c_1 or c_2 is straight and the other is curvy, then $n_w(B') = n_w(B) + 1$ and $n_z(B) = n_z(B') = 0$.*

Proof. The rainbow bigon B has boundary $\rho \cup a$, where ρ is a rainbow arc and $a \subset \alpha$ is a subarc. Let $\partial\rho = \{x_i, x_{2q+1-i}\}$, with $i < 2q+1-i$ and suppose that c_1 has $\partial c_1 = \{x_i, x_k\}$ and c_2 has $\partial c_2 = \{x_{2q+1-i}, x_l\}$; a possible sketch of B' is drawn in fig. 5.2. If c_1 and c_2 are both straight or both curvy, we have

$$l - k = (2q + 1 - i) - i < 2q.$$

Thus c_1, c_2 are arcs in the same fundamental domain of the tiling of $\mathbb{C}$ by the diagram in normal form and B' is obtained by gluing B to a 4-gon which does not cover any basepoints. This shows that $n_w(B) = n_w(B') = 1$ and $n_z(B) = n_z(B') = 0$.

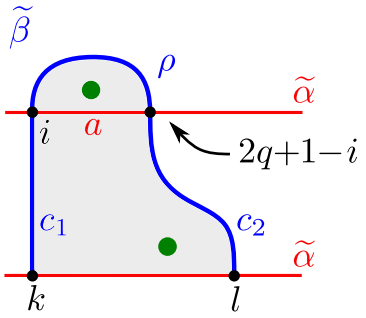

Figure 5.2: A sketch of the bigon B'.

Suppose now that one of c_1, c_2 is straight and the other curvy. Since the indices of the endpoints of ρ satisfy $(2q+1-i)-i < 2q$, it is not possible for c_1 to be curvy and c_2 to be straight, as this would require a larger difference between the top endpoints of c_1 and c_2. In short, fig. 5.2 is an accurate sketch of B'. Since ρ is a rainbow arc, c_1 and c_2 must be in adjacent fundamental domains, so B' is obtained by gluing B and a 4-gon which covers a single lift of the w-basepoint. This proves the result. □

If the diagram is for an L-space knot, then every bigon covers basepoints of only one type, by lemma 5.2.3. Let us put a name to this type of bigon.

Definition 5.2.2. If a bigon B has $n_z(B) = 0$ or $n_w(B) = 0$, then we say that the bigon is **pure**.

In the current example, the bigon $\bullet_{12} \to \bullet_{17}$ is obtained from $\bullet_{19} \to \bullet_5$ by extending along vertical arcs of the same kind, whereas the bigon $\bullet_{19} \to \bullet_5$ is obtained from $\bullet_7 \to \bullet_8$ by extending along vertical arcs which are not of the same kind.

There is an additional arrow

$$\bullet_{18} \xrightarrow{\qquad\qquad U^4 \qquad\qquad} \bullet_{10} \ ,$$

obtained by extending the bigons $\bullet_6 \to \bullet_9$ and $\bullet_{12} \to \bullet_{17}$ along the straight arcs connecting $\bullet_6$ to $\bullet_{18}$ and $\bullet_{17}$ to $\bullet_{10}$. This last bigon is the hardest to see, so we draw its lift to a universal cover of the torus in which the straight arcs are straight in fig. 5.3.
Finally, we claim that these are all the horizontal arrows. This follows from the following lemma. This thesis relies neither on its proof nor on its result.

Lemma 5.2.3. *Suppose K is a $(1,1)$ knot and $\mathcal{D} = (T^2, \alpha, \beta, w, z)$ is a $(1,1)$ diagram for K. If K is an L-space knot, then $CFK(K) =^{\mathcal{R}} CFK(K)$ and, furthermore, there are $p-1$ bigons in $\mathcal{D}$, each contributing a distinct arrow $\bullet_i \to \bullet_j$ to CFK.*

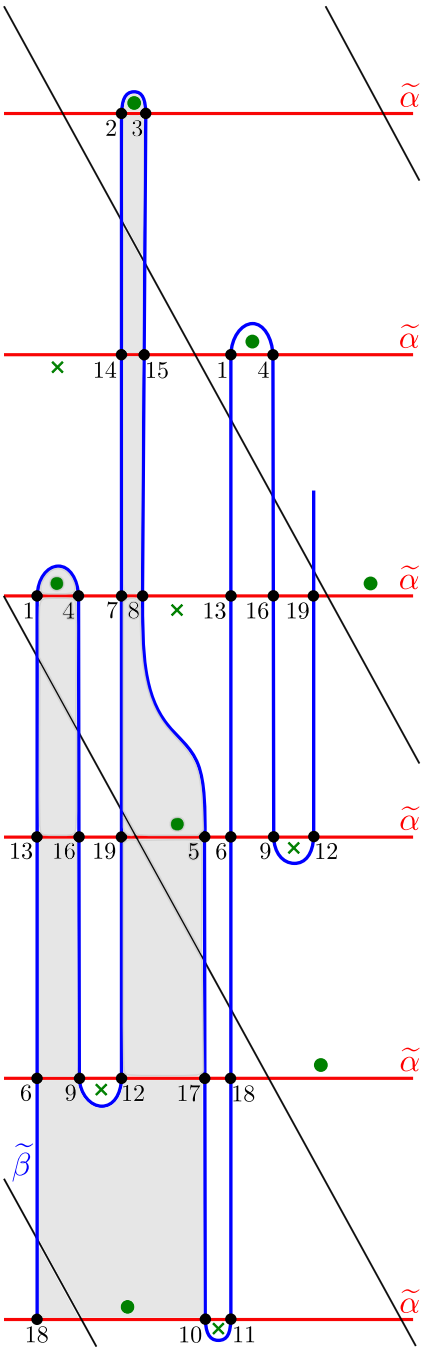

Figure 5.3: The bigon $\bullet_{18} \xrightarrow{U^4} \bullet_{10}$.

Proof. This follows from Theorem 4.3.2 and Lemma 2.3 in [GLV18]. □

5.3 Purity Conjecture

Let us now make one more observation about the structure of bigons, necessary for the proof of Theorem 7.1.1. Fix $x \in \alpha \cap \beta$, a lift $\widetilde{\beta}$, a lift $\widetilde{x}$ and the lift $\widetilde{\alpha}_{\mathfrak{s}}$ that contains $\widetilde{x}$, where $\mathfrak{s} = s_z(x)$. The line $\widetilde{\alpha}_{\mathfrak{s}}$ splits the plane into two half-planes: H_+ and H_- and $\widetilde{\beta}$ intersects each half plane in n compact arcs and a closed ray. Let $\{\gamma_i^-\} = \widetilde{\beta} \cap H_-$ and $\{\gamma_i^+\} = \widetilde{\beta} \cap H_+$, and let B_i^+ (resp. B_i^-) be the bigon cobounded by γ_i^+ (resp. γ_i^-) and a subarc of $\widetilde{\alpha}_{\mathfrak{s}}$. Each γ_i^+ attains a local maximum, hence contains a lift of a locally maximal rainbow arc. Similarly, each γ_i^- contains a lift of a locally minimal rainbow arc. One may be tempted to conclude from this that $n_w(B_i^+) > 0$ and $n_z(B_i^-) > 0$ for all i. This is not true, since bigons such as the one drawn in fig. 5.4 exist. This is a small gap in [GLV18], but they only use this false statement in the context where *CFK* is a staircase, in which case the statement is true:

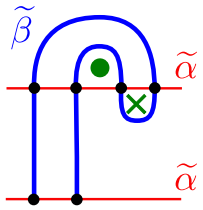

Figure 5.4: A bigon B in H^+ s.t. $n_w(B) = 0$.

Lemma 5.3.1 (cf. §2.3 in [GLV18])**.** *With the notation above, and under the additional hypothesis that $CFK(\mathcal{D})$ consists of positive staircases (or consists of negative staircases), we have that, for all i,*

$$n_w(B_i^+) > 0 \quad \text{and} \quad n_z(B_i^-) > 0.$$

Proof. Suppose also that there is a bigon $B_i^+ \subset H_+$ such that $n_w(B_i^+) = 0$ and let x, y be the labels of the generators on ∂B_i^+, so that the bigon is from x to y. If B_i^+ is the bigon drawn in fig. 5.4, then the 4 intersection points of the top lift of α with $\widetilde{\beta}$ provide the following subgraph of the type

D structure $CFK(K)$:

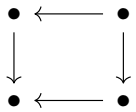

This contradicts the assumption that $CFK(\mathcal{D})$ consists of staircases, proving the lemma for this particular bigon. The idea is that if $B_i^+ \subset H_+$ is a bigon with $n_w(B_i^+) = 0$, then some subarc of $\partial_\beta B_i^+$ is hook-shaped, like the bigon in fig. 5.4. Precisely, we claim that there exists a subarc $\gamma \subset \partial_\beta B_i^+$ and a lift $\widetilde{\alpha}$ such that γ and α intersect in at least 4 points and produce a subgraph of $CFK(\mathcal{D})$ which contradicts the staircase assumption. Since $\mathcal{D}$ is reduced and we assume that $n_w(B_i^+) = 0$, we have $n_z(B_i^+) > 0$, therefore $\partial_\beta B_i^+$ contains a locally minimal rainbow arc, ρ. Let γ be the smallest connected subarc of $\widetilde{\beta}$ containing ρ and two locally maximal rainbow arcs. Since B_i^+ does not cover any lifts of the $w = \bullet$ basepoint, we have the following two cases for γ, up to mirroring: Note that the bigon under the lift of α may

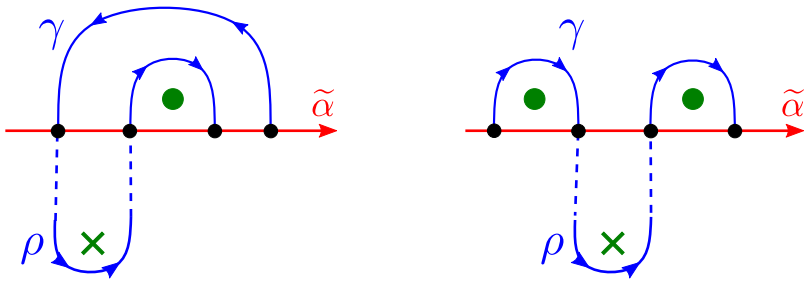

Figure 5.5: Two possible cases for γ.

cover multiple copies of the $\times$ basepoint. The arc γ and the lift $\widetilde{\alpha}$ in left-hand figure, produce a box subgraph of $CFK(\mathcal{D})$, just like the one obtained above from fig. 5.4. The reader may check that, in the case on the right-hand side of the figure above, it is possible to find another arc $\gamma' \subset \partial_\beta B_i^+$ such that γ' is as in the left-hand side of the figure. This is because B_i^+ is a bigon which does not cover any $\bullet$ basepoint and because $\partial_\alpha B_i^+$ is a subarc of a lift of α which is below the lift in fig. 5.5. □

Finally, we make what seems to be a more than reasonable conjecture, that

extends Lemma 5.2.1. Recall that we are still assuming that we are working with a reduced $(1,1)$ diagram $\mathcal{D}$ such that the ambient manifold is not $S^2 \times S^1$.

Definition 5.3.2. Let B be a bigon in $\mathcal{D}$ and orient α from left to right. We say that B is **graphic**, if it is possible to orient β such that every one of the rainbow arcs in $\partial_\beta B$ co-orients its rainbow bigon with α.

Conjecture 1. Graphic bigons are pure.

Some evidence for the conjecture: note that all the bigons in a $(1,1)$ L-space knot are pure, by lemma 4.3.3. By the main result of GLV, every bigon in a $(1,1)$ L-space knot is graphic. So the conjecture is true for $(1,1)$ L-space knots. The conjecture is also true for all examples that the author has encountered. It appears however that a combinatorial proof of Conjecture 1 would be rather involved.

If there exists a non-coherent $(1,1)$ diagram which contains a bigon that is graphic and not pure, then the existence of this bigon, which already obstructs the existence of L-space surgery slopes, implies that coherence is broken elsewhere in the diagram. This would be interesting, but troublesome for the following reason: in chapter 7, we take a diagram that is not coherent and walk along β to look for an obstruction to ${}^{\mathcal{R}}CFK(K)$ consisting of $\pm$-staircases, which obstructs the existence of L-space surgery slopes by theorem 4.3.2. We remind the reader that ${}^{\mathcal{R}}CFK$ is the truncation of CFK by the ideal (UV), so only pure bigons contribute to the differential of ${}^{\mathcal{R}}CFK$. The existence of a graphic non-pure bigon would make the argument in chapter 7 require some serious fixing. Since we will need to work with knots having the conjectured property, we make the following definition.

Definition 5.3.3. A **GP diagram** $\mathcal{D}$ is a $(1,1)$ diagram such that all graphic bigons in $\mathcal{D}$ are pure. Of course, GP stands for "Graphic-Pure". A GP knot is a knot which admits a GP diagram. Whenever we talk about a $(1,1)$ diagram for a GP knot, we assume that it is a GP diagram.

Chapter 6

Immersed Curves

There is another criterion for checking whether a $(1,1)$ knot admits a (non-trivial) surgery to an L-space, which in a sense supersedes GLV's criterion. This comes through the analysis of the bordered Heegaard Floer invariant assigned to the knot complement. In this chapter we describe this (algebraic) invariant and its reinterpretation as a geometric object.

The second way to characterize L-space knots is via the bordered theory and the work in [HRW16]. In short, bordered Heegaard Floer theory is the adaptation of Heegaard Floer theory to cut-and-paste techniques. It assigns algebraic invariants to manifolds with boundary and describes how to obtain the Heegaard Floer homology of a closed manifold $Y = Y_1 \cup_h Y_2$ by pairing the bordered invariants of Y_1 and Y_2 using the diffeomorphism $h\colon \partial Y_2 \xrightarrow{\sim} -\partial Y_1$; this is known in the literature as the *pairing theorem*. Note that we now explicitly take our manifolds to be *oriented*, as opposed to *orientable*. In [HRW16], the bordered theory of a manifold with torus boundary is interpreted in a pleasing and simple manner as an immersed 1-manifold in the torus. We now turn to this theory, as it provides a particularly simple method for computing the effect of Dehn surgery on the Heegaard Floer homology of a manifold.

6.1 The Immersed Curve $\widehat{HF}$

Let Y be a compact oriented 3-manifold with $\partial Y \simeq T^2$ and suppose that (μ, λ) is a pair of curves in ∂Y which induce a basis in homology and such that $\mu \cdot \lambda = -1$. Fix also a point $z \in \partial Y \setminus \{\mu, \lambda\}$. The pair (μ, λ) is often called a **framing**.

Remark. In the case that Y is a knot complement and (μ, λ) is a choice of framing, the pair $(\mu, -\lambda)$ forms a meridian-longitude pair; see section 4.1.

Notation. The **standard framing** on a knot complement is the pair $(\mu, -\lambda_0)$, where (μ, λ_0) is the standard meridian-longitude pair.

The bordered theory assigns to Y a type D structure $\widehat{CFD}(Y)$ over an algebra $\mathcal{A}$. In general, $\mathcal{A}$ depends on the homeomorphism class of the boundary of the 3-manifold. In our case, $\mathcal{A}$ is an 8-dimensional $\mathbb{F}$-vector space generated by two idempotents

$$\iota_\bullet \quad \text{and} \quad \iota_\circ,$$

and six so-called Reeb elements

$$\rho_1, \rho_2, \rho_3, \rho_{12}, \rho_{23}, \rho_{123}.$$

The Reeb elements satisfy the relations

$$\rho_1\rho_2 = \rho_{12}, \quad \rho_2\rho_3 = \rho_{23}, \quad \rho_1\rho_{23} = \rho_{12}\rho_3 = \rho_{123},$$

and other products of Reeb elements are 0. The full multiplication relations may be found in [LOT18]; we will not make use of them, except implicitly, to justify that the differential satisfies the type D relation. Let us note here that, in contrast with the type D structure CFK, there are nontrivial idempotents in $\mathcal{A}$, so a type D structure over $\mathcal{A}$ is a vector space V that decomposes as

$$V = V_\bullet \oplus V_\circ,$$

where $V_\bullet = \iota_\bullet V$ and $V_\circ = \iota_\circ V$. Similarly to the convention in section 3.3,

type D structures (V, δ) over $\mathcal{A}$ are depicted as labelled, directed graphs whose vertices correspond to basis elements of $V_\bullet$ and $V_\circ$, accordingly labelled $\bullet$ or $\circ$, and where there is an arrow $x \xrightarrow{\rho_i} y$ if $\rho_i \otimes y$ is a summand of δx. Note that there is no need to label arrows by the idempotents, since a basis vector $x \in V$ has $\iota_\bullet x = 0$ or $\iota_\circ x = 0$, and the differential respects the decomposition $V = V_\bullet \oplus V_\circ$.

Example 15. Let K be the right-handed trefoil knot and K^c its the complement in S^3. For a choice of framing (namely the standard one, Definition 4.1.2), the type D structure $\widehat{CFD}(K^c)$ is given by the graph below. It also appears as figure 5 in [HRW16].

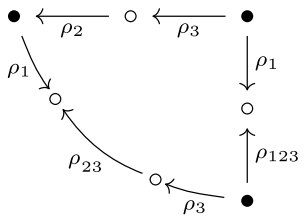

Let T_Y be the complement of 0 in the torus $H_1(\partial Y; \mathbb{R})/H_1(\partial Y; \mathbb{Z})$, as in [HRW16], and note that T_Y may be identified with $\partial Y \setminus z$, up to isotopy. Given the work of J. Hanselman, J. Rasmussen and L. Watson, $\widehat{CFD}(Y)$ is equivalent to a 1-dimensional manifold $\widehat{HF}(Y) \looparrowright T_Y$[3], decorated with local systems, meaning that each connected component of $\widehat{HF}(Y)$ is decorated with a finite-dimensional $\mathbb{F}$-vector space V and an automorphism $V \to V$. The object $\widehat{HF}(Y)$ is well-defined up to regular homotopy and isomorphism of the local systems. Moreover, under their reinterpretation of the bordered invariants as immersed curves, the pairing theorem is also reinterpreted as follows:

Theorem 6.1.1 (Theorem 2 in [HRW18])**.** *Let Y_1 and Y_2 be 3-manifolds with torus boundary, $h\colon \partial Y_2 \to -\partial Y_1$ a diffeomorphism, and let $\gamma_1 = \widehat{HF}(Y_1)$,*

[3]Note that there is no ambiguity in notation here, since the Heegaard Floer homology $\widehat{HF}(Y)$ is only defined for closed manifolds, whereas the immersed curves $\widehat{HF}(Y)$ are only defined for manifolds with torus boundary.

$\gamma_2 = \widehat{HF}(Y_2)$. *Then*

$$\widehat{HF}(Y_1 \cup_h Y_2) \simeq HF(\gamma_1, h(\gamma_2)),$$

where $HF(\gamma_1, \gamma_2)$ *is the immersed Lagrangian intersection homology of the Lagrangian submanifolds* γ_1 *and* γ_2*, computed in* $\partial Y_1 \setminus z_1$.

It should be stressed here that $HF(\gamma_1, \gamma_2)$, the Lagrangian intersection homology, is often easier to compute than the original pairing between the algebraic invariants of the bordered theory. In general, Lagrangain intersection homology, which we encountered in Chapter 3, is the homology of a chain complex generated by the intersection points of two Lagrangian submanifolds of a symplectic manifold, with a differential that counts pseudoholomorphic discs between intersection points. In the present context, the symplectic manifold is the punctured torus $T^2 \setminus z$ with its area form, which is symplectic, and every unobstructed immersed curve in T^2 is an immersed Lagrangian submanifold. So $HF(\gamma_1, \gamma_2)$ is the homology of a chain complex generated by the set $\gamma_1 \cap \gamma_2$. For our purposes, the differential is immaterial and we can usually check whether a knot surgery yields an L-space by counting the minimal intersection number between two 1-dimensional manifolds immersed in a torus, cf. Lemma 6.1.2. Let us illustrate this idea immediately by explaining how to pass from $\widehat{CFD}(Y)$ to $\widehat{HF}(Y)$ and by computing the effect of $(+2)$-surgery on the right-handed trefoil.

Lemma 6.1.2 (Corollary 3 in [HRW16])**.** *If* $\widehat{HF}(Y)$ *has trivial local systems and if no two components of* $\widehat{HF}(Y)$ *are parallel, then dim*$(\widehat{HF}(Y \cup_h D^2 \times S^1)$ *is the minimal intersection number between* $\widehat{HF}(Y)$ *and* $h(\widehat{HF}(D^2 \times S^1)$.

Construction 6.1.3. Let Y be a 3-manifold with (μ, λ)-framed torus boundary. The collection of curves $\widehat{HF}(Y)$ can be defined as an embedding of the graph associated to $\widehat{CFD}(Y)$, thought of as a 1-dimensional CW complex, into T_Y. The recipe is: (i) embed the generators of $V_\bullet$ in μ and the generators of $V_\circ$ in λ, (ii) cut open T_Y along μ, λ, and embed the edges of the graph in T_Y according to the rules illustrated in fig. 6.1.

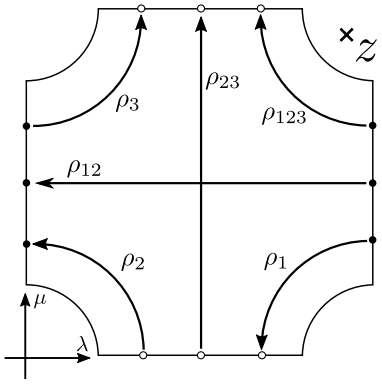

Figure 6.1: Mnemonic for immersing $\widehat{CFD}(Y)$ into T_Y.

Remark. The justification for construction 6.1.3 is to be found in the papers [HRW16] and [HRW18], and we do not go into it beyond the following remarks. First, note that there is no loss of information due to immersing the *directed* graph of $\widehat{HF}(Y)$ as an immersed CW-complex in the framed torus: the direction of the arc is information contained in the direction in which the arcs wrap around the puncture. Second, construction 6.1.3 does not mention local systems. Third, there is no reason for the graph of $\widehat{CFD}(Y)$ to immerse as a 1-manifold in the torus. Indeed, it is possible for this graph to have vertices of valence > 2, in which case construction 6.1.3 produces an immersed *train track* (cf. Definition 6.2.2). The point is that there is a type D structure homotopic to $\widehat{CFD}(Y)$ such that the construction applied to it either produces an immersed 1-manifold or a train track that is equivalent to an immersed 1-manifold decorated with local systems. The reader should also note that examples where a non-trivial local system is required have not been found.

Example 16. If we apply construction 6.1.3 to the type D structure in example 15, we find the immersed curve in fig. 6.2. Note that this type D structure corresponds to a particular framing (μ, λ), indicated by the axes.

Example 17. Consider $D^2 \times S^1$, the complement of the unknot in S^3, and let $\mu, \lambda \subset \partial D^2 \times S^1$ be the **standard meridian and longitude** for the knot.

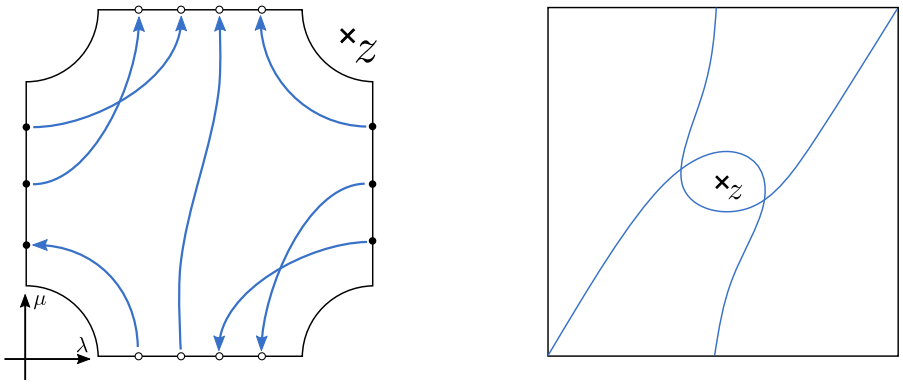

Figure 6.2: The immersed curve $\widehat{HF}$ for the right-handed trefoil. Left: the type D structure as an immersed graph in the punctured torus. Right: another view of the curve $\widehat{HF}$. The boundaries of both squares are identified in the standard fashion to form a punctured torus.

Thus $\mu = \{*\} \times S^1$, and $\lambda = \partial D^2 \times \{*\}$. Fix also $z \in \partial(D^2 \times S^1) \setminus (\mu \cup \lambda)$. Since there is justice in the world, $\widehat{CFD}(D^2 \times S^1)$ is as simple as possible: it is a 1-dimensional vector space V. The subspace $V_\circ$ is trivial and the differential may be read off of the associated graph:

Applying construction 6.1.3, we find that the immersed curve $\widehat{HF}(D^2 \times S^1)$ is the longitude $\lambda = \partial D^2 \times \{*\} \subset \partial(D^2 \times S^1) \setminus z$, illustrated in fig. 6.3.

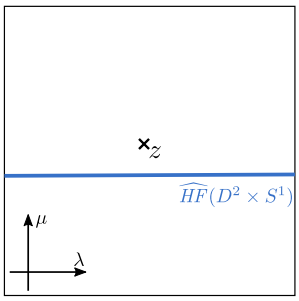

Figure 6.3: $\widehat{HF}(D^2 \times S^1)$, with the standard framing.

6.1.1 2-surgery on the Right-handed Trefoil Knot

Let $K \subset S^3$ be the right-handed trefoil knot and let $K^c = S^3 \setminus \nu(K)$ have the standard framing. This is the framing for which $\widehat{CFD}(K^c)$ is given by the graph in example 15. For convenience, let $\ell = \widehat{HF}(D^2 \times S^1)$, as computed in example 17. Using the previous two examples, we can compute the $+2$-surgery on K by applying Theorem 6.1.1, cf. Example 30 in [HRW18]. Such a surgery is given by a map $h\colon \partial(D^2 \times S^1) \to -\partial(K^c)$ such that, in homology we have:

$$h_*\colon [\ell] \mapsto 2[\mu] + [\lambda],$$

where (μ, λ) is a meridian-longitude pair in the knot complement. According to Theorem 6.1.1, to compute $\widehat{HF}(S^3_{+2}(K))$, we draw the following picture, from which it is clear that the minimal intersection number between $\widehat{HF}(K^c)$ and ℓ is 2, so $\mathrm{rk}\widehat{HF}(S^3_{+2}(K)) = 2$. It is convenient to draw lifts of these curves to the universal Abelian cover of T_Y, or a subcover of it, as sketched on the right in the same figure. Note here that two different lifts of $h(\ell)$ are required in order to lift both intersection points. By Proposition 6.1.4, this implies that $\widehat{HF}(S^3_{+2}(K))$, as a vector space, is isomorphic to $\mathbb{F}^2$, so that $S^3_{+2}(K)$ is an L-space.[4]

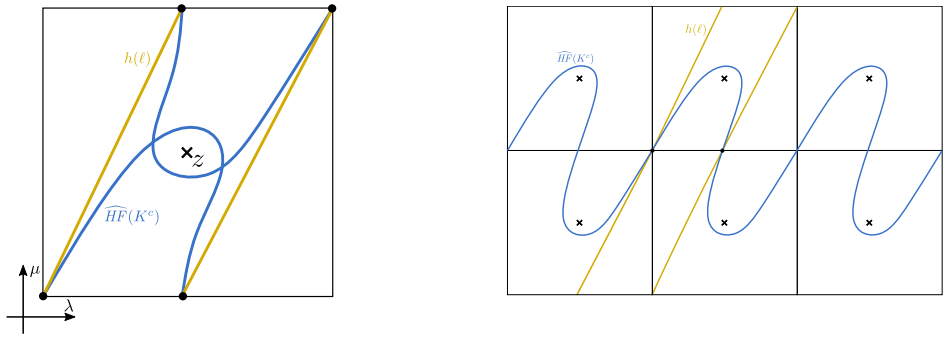

Figure 6.4: The curves $\widehat{HF}(K^c)$ and $h(\ell)$, in ∂K^c and their lifts to a $\mathbb{Z}$-cover thereof. Intersection points are indicated by dots.

[4]This follows from the remark following Definition 4.1.4 and the computation $H_1(S^3_{p/q}(K)) \simeq \mathbb{Z}/p\mathbb{Z}$.

For the next proposition, let Y_1, Y_2 and h be as in Theorem 6.1.1 and let $\boldsymbol{\gamma}_i = \widehat{HF}(Y_i)$. For each i, suppose $\boldsymbol{\gamma}_i$ is a collection of n_i immersed curves. It is then possible to attach $n_i - 1$ oriented arcs to $\boldsymbol{\gamma}_i$, so that the result is a path-connected graph off of which the Heegaard Floer gradings can be read, including the spin^c grading; cf. §2.1 of [HRW18], where the oriented arcs are called **grading arrows**. Assume in the proposition below that the immersed curve invariants are decorated with grading arrows, for the purpose of constructing a path from x to y in $\boldsymbol{\gamma}_i$. To check the computation of $\widehat{HF}(S^3_{+2}(K))$ above, this assumption is not needed, since each of $\widehat{HF}(K^c)$ and $\widehat{HF}(D^2 \times S^1)$ is connected.

Proposition 6.1.4 (§2.1 in [HRW18])**.** *With the notation above, suppose that $\boldsymbol{\gamma}_1$ and $h(\boldsymbol{\gamma}_2)$ are in minimal position. Two elements $x, y \in \boldsymbol{\gamma}_1 \cap h(\boldsymbol{\gamma}_2)$ have the same spin^c grading if and only if there are lifts $\widetilde{\boldsymbol{\gamma}_1}$ and $\widetilde{h(\boldsymbol{\gamma}_2)}$ of $\boldsymbol{\gamma}_1$ and $h(\boldsymbol{\gamma}_2)$ which pass through a lift of x and a lift of y.*

Remark. One should think of the right-hand picture in fig. 6.4 as a peg-board, with a small circular peg at every puncture, and where the lift of $\widehat{HF}(K^c)$ is to be thought of as an elastic band wrapping around the pegs. This idea is useful for computing the minimal intersection number between the immersed curve and a surgery slope. As the radii of the pegs goes to 0, we see that the set of slopes which yield an L-space is the interval $[1, \infty]$, as a slope outside this interval would intersect $\widehat{HF}(K^c)$ in multiple points. To avoid a pitfall with this computation, one needs to count the intersection points between $\widehat{HF}(K^c)$ and $h(\ell)$ in the torus.

Theorem 6.1.5 (Theorem 11.26 in [LOT18])**.** *There is an algorithm which takes the graph $CFK(K)$ and yields the graph of $\widehat{CFD}(K^c)$.*

Notation. Let us use the symbol $\mathbb{A}$ to denote the algorithm mentioned above.

Definition 6.1.6. Let $K \subset S^3$ be an L-space knot. Let $\{x_1, \ldots, x_{2n+1}\}$ be a basis for $CFK(K)$, and let n_i and m_i be the exponents on the variables

U, V which appear in δx_i, as defined in Definition 4.3.1. Let

$$L(CFK(K)) = \sum_{i=1}^{2n+1} n_i + m_i.$$

Example 18. Recall that 3_1 denotes either trefoil knot $\mathbb{U}$ denotes the unknot. It is not hard to see that $L(3_1) = 2$ and $L(\mathbb{U}) = 0$.

Remark. Ozsváth and Szabó define a knot invariant $\tau(K)$ in [OS03]. It follows essentially from the definitions (of τ and L) that $L(K) = |2\tau(K)|$. Thus, we will write $L(K)$ instead of $L(CFK(K))$.

Theorem 6.1.7. *Suppose $K \subset S^3$ is a strictly positive (resp. negative) L-space knot, in the sense that K admits a positive surgery, but no negative surgery yielding an L-space, and let K have the standard meridian-longitude pair. Then the set of surgery slopes on K yielding an L-space is the interval $[L(K) - 1, \infty] \cap \mathbb{Q}P^1$ (resp. $[\infty, 1 - L(K)] \cap \mathbb{Q}P^1$). If K is a positive and negative L-space, then the set of surgery slopes on K yielding an L-space is $\mathbb{Q}P^1 \setminus \{0\}$.*

Proof. Suppose K is a positive L-space knot. It is not hard to see that construction 6.1.3 applied to $\mathbb{A}(CFK(K))$ yields a graphic, periodic curve like the one fig. 6.4, with the difference that the height of $\widehat{HF}(K^c)$, once pulled tight, is $L - 1$. By the same argument as for the right-handed trefoil, the L-space surgery slopes on K form the interval $[L - 1, \infty] \subset \mathbb{Q}P^1$. An analogous argument works in the case that K is a negative L-space knot. □

The invariant $\widehat{HF}(Y)$ splits over spin^c structures: the algorithm $\mathbb{A}$ applies to $CFK(K, \mathfrak{s})$ for every $\mathfrak{s} \in \text{Spin}^c(Y)$ and yields a type D structure $\widehat{CFD}(K^c, \mathfrak{s})$. This is important in our case, since $(1, 1)$ knots are embedded in lens spaces, and the lens space $L_{p,q}$ has p spin^c structures. Recall that the set of spin^c structures on Y is in bijection with $H^2(Y; \mathbb{Z}) \simeq H_1(Y, \partial Y; \mathbb{Z})$.

Definition 6.1.8. We let $\widehat{HF}(Y, \mathfrak{s})$ denote the immersed curve obtained by applying construction 6.1.3 to $\mathbb{A}(CFK(K, \mathfrak{s}))$.

Notation. If $K \subset Y$ is an L-space knot in a lens space, then, for every $\mathfrak{s} \in \mathrm{Spin}^c(Y)$, we may define $L(CFK(K), \mathfrak{s})$ and let $\mathcal{L}(K, \mathfrak{s}) \subset \mathbb{Q}P^1$ denote the interval of surgery slopes which intersect $\widehat{HF}(K^c, \mathfrak{s})$ in points that lie in distinct spin^c gradings.

If $Y = S^3$, then there is a unique spin^c structure $\mathfrak{s} \in \mathrm{Spin}^c(Y)$ and $\mathcal{L}(K, \mathfrak{s})$ is one of $[L-1, \infty]$, $[\infty, 1-L]$ or $\mathbb{Q}P^1 \setminus \{0\}$, as mentioned above. We can now state what the interval of L-space surgery slopes is on a $(1,1)$ L-space knot. The proof of the following theorem follows from the algorithm $\mathbb{A}$ and the construction of $\widehat{HF}$ in [HRW18].

Theorem 6.1.9. *Suppose K is a $(1,1)$ L-space knot and let K^c is the knot complement, with the standard framing. The interval of L-space slopes on K is*

$$\mathcal{L}(K) := \bigcap_{\mathfrak{s} \in Spin^c(Y)} \mathcal{L}(K, \mathfrak{s}).$$

Remark. In the above theorem, unless K is both a positive and a negative L-space knot, there set of L-space surgery slopes on K is either $[L-1, \infty]$ or $[\infty, 1-L]$, where

$$L = \min_{\mathfrak{s} \in \mathrm{Spin}^c(Y)} L(CFK(K), \mathfrak{s}).$$

6.2 The ⦶ Formalism

In the same way that the type D structure $\widehat{CFD}(Y)$ is equivalent to an immersed 1-manifold $\widehat{HF}(Y)$ in the punctured torus (for Y a manifold with torus boundary), the type D structure ${}^{\mathcal{R}}CFK(K)$ is equivalent to an immersed 1-manifold in a surface, this time the twice-punctured disc. The larger framework here is that of marked surfaces with full arc systems; see [KWZ20] and the references therein for more details.

Definition 6.2.1. We define ⦶ to be an oriented disc with two punctures and an arc $\boldsymbol{a}$ drawn in red. The orientation is chosen so that it restricts to

the counter-clockwise orientation on the boundary. The surface  $\setminus \nu(\boldsymbol{a})$ is a disjoint union of two annuli: we denote the left-hand annulus by A_v and the right-hand annulus by A_u, and we call them the V**-annulus** and the U**-annulus**, respectively.

Definition 6.2.2. A **train track** in a surface Σ is a collection of immersed curves $\gamma_i \looparrowright \Sigma$ such that, for all i, j, $\gamma_i \cap \gamma_j$ is either a single point where γ_i and γ_j intersect transversely or else it is a **switch**, a point where at more than two arcs intersect such that their tangents at the switch agree; see fig. 6.5.

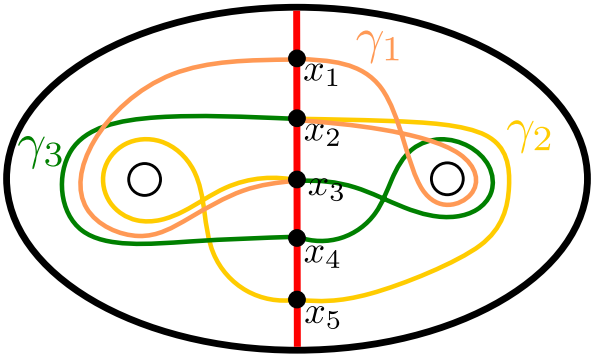

Figure 6.5: An example of a train track in  . The switches occur at the labels x_2 and x_3. The other labelled points are the intersection points of the γ_i with $A \subset$  .

We will be concerned with train tracks in  . Note that for our applications, the train tracks may be compact, as in fig. 6.5, or they may have non-compact ends at the punctures. They will not have their endpoints on the boundary of the disc; see Construction 6.2.6.

Theorem 6.2.3 (Theorem 1 in [KWZ20])**.** *Let $K \subset Y$ be a knot. The type D structure $^{\mathcal{R}}CFK(K)$ is equivalent to an immersed 1-manifold (as opposed to just a train track) $\Upsilon \subset$*  *, decorated with local systems and defined up to regular homotopy and equivalence of local systems.*

Remark. The above theorem has various proofs; see the references in

[KWZ20].

Definition 6.2.4. We denote the immersed curve associated to the type D structure ${}^{\mathcal{R}}CFK(K)$ by $\curlyvee(K)$.

The relationship between $\curlyvee$ and $\widehat{HF}$ is given by a handle attachment, denoted by $\curvearrowright$. The handle is attached at the punctures (enlarged into boundary components), it takes  into a torus with a disc removed, and it connects the endpoints of the non-compact arcs through arcs passing over the handle; see [KWZ20] for some beautiful illustrations. Note that there is some ambiguity in the choice of arcs connecting the endpoints of $\curlyvee$ at the punctures. This is equivalent to the dependence of $\widehat{HF}$ on a choice of framing.

Theorem 6.2.5 (Theorem 2 in [KWZ20])**.** *Let K be a knot in S^3 and let K^c be the knot complement. If $\curlyvee \subset$*  *is a curve representing the knot Floer invariant ${}^{\mathcal{R}}CFK(K)$, then $\curvearrowright(\curlyvee)$ is equivalent to $\widehat{HF}(K^c)$.*

Remark. The above theorem generalizes to knots in lens spaces; see [KWZ20] and [HL16].

The way to associate an immersed curve to ${}^{\mathcal{R}}CFK$ is to first associate to it a train track using construction 6.2.6 and then to resolve the switches using the basis simplification algorithm, nicely written up by J. Hom as the proof of Lemma 2.1 in [Hom13].

Construction 6.2.6. Given a type D structure V over $\mathcal{R}$, we construct a train track $\widetilde{\curlyvee} \subset$  as follows: pick a basis $\mathcal{B}$ for V. Note that, by definition of type D structure, $\mathcal{B}$ is finite. For every $x \in \mathcal{B}$, draw a dot labelled by x on $\boldsymbol{a} \subset$  . For every arrow $x \xrightarrow{U^i} y$, draw an arc in the U-annulus from x to y, winding i times around the puncture with an orientation equal to the orientation on ∂  . Similarly, for every arrow $x \xrightarrow{V^j} y$, draw an arc winding j times around the puncture in the V-annulus, with the same orientation. Finally, for every basis element x that is not the endpoint of an arc in A_u, draw an arc from x to the puncture in A_u and do the same for every element that is not the endpoint of an arc in A_v.

Example 19. Figure 6.5 is the construction applied to ${}^{\mathcal{R}}CFK(\mathcal{D}(5,2,1,0))$, which the reader may check is CFK of a $(1,1)$ diagram for the figure-8 knot. The type D structure is drawn in fig. 6.6. The arc γ_1 in fig. 6.5 corresponds to the arrows $x_1 \xrightarrow{U} x_3$ and $x_1 \xrightarrow{V} x_2$, for example.

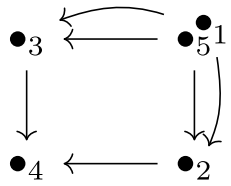

Figure 6.6: The type D structure $CFK(\mathcal{D}(5,2,1,0))$.

Note that there is a change of basis, namely the change of basis

$$\{x_1, x_2, x_3, x_4, x_5\} \mapsto \{x_1, x_2, x_3, x_4, x_1 + x_5\},$$

that simplifies the type D structure:

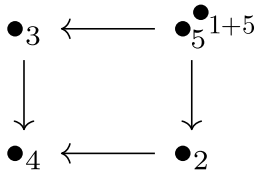

Figure 6.7: The simplified type D structure $CFK(\mathcal{D}(5,2,1,0))$.

It can be checked that applying construction 6.2.6 to the type D structure in fig. 6.7 yields the immersed 1-manifold in fig. 6.8. The point is that there exists a canonical way to change the basis of the type D structure $CFK(K)$ so that the switches in $\curlyvee(K)$ become manageable enough to be expressible as local systems, as explained in [KWZ20]. The change of basis is the basis simplification algorithm alluded to before the construction, also known in the literature as the "cancellation lemma".

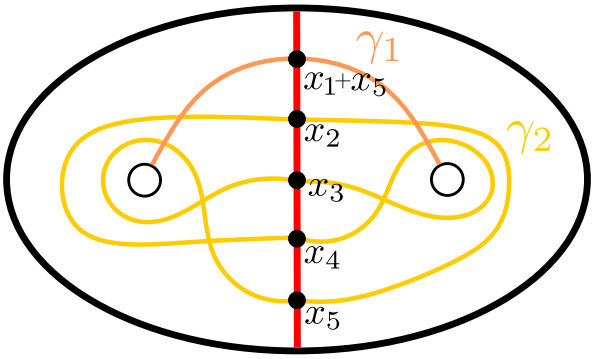

Figure 6.8: The immersed curve invariant $\Upsilon(4_1)$.

6.2.1 The Basis Simplification Algorithm

Definition 6.2.7. Consider a type D structure $CFK(\mathcal{D})$ and construct the type D structures $C^v := CFK(\mathcal{D})|_{U=0}$ and $C^h := CFK(\mathcal{D})|_{V=0}$. We call C^v the **vertical** type D structure and C^h the **horizontal** type D structure and denote the induced differentials by δ^v and δ^h.

Remark. If $CFK(K)$ is a positive staircase with basis $\{x_1, \dots, x_{2n+1}\}$ as in Definition 4.3.1, then $H_*(C^v) \simeq \langle x_{2n+1} \rangle$ and $H_*(C^h) \simeq \langle x_1 \rangle$. If $CFK(K)$ is a negative staircase, then $H_*(C^v) \simeq \langle x_1 \rangle$ and $H_*(C^h) \simeq \langle x_{2n+1} \rangle$.

Definition 6.2.8 (Taken from §2 of [Hom13])**.** A **vertically simplified basis** is a basis $\{x_i\}$ for C^v, such that for each element x_i, exactly one of the following holds:

1. There exists a unique basis element, x_{i-1}, such that $\delta^v x_{i-1} = x_i$.
2. The element x_i is in the kernel, but not in the image of δ^v.
3. There is a basis element x_{i+1} such that $\delta^v(x_i) = x_{i+1}$.

Horizontally simplified bases are defined similarly for C^h.

Lemma 6.2.9 (Lemma 2.1 in [Hom13])**.** *Each of C^v and C^h admits a simplified basis.*

Note that it is not known whether it is possible to find a basis of $CFK(K)$

that simultaneously simplifies C^v and C^h. We have the following (see [KWZ20]), where $H^v(K) := H_*(C^v)$:

$$H^v(K) \simeq \widehat{HFK}(K) \simeq H^h(K).$$

The above identifications are given by the Heegaard Floer theory and provide us with an isomorphism from a basis of $CFK(K)$ that simplifies C^v to a basis that simplifies C^h. With this in hand, we may apply construction 6.2.6 to C^v (resp. C^h), with a simplified basis, to obtain a collection of immersed curves in the annulus A_u (resp. A_v). The isomorphism $H^v \simeq H^h$ may be encoded by a train track connecting the basis simplifying C^h to the basis simplifying C^v [KWZ20] and it turns out that it is possible to resolve all the switches in the train tracks or to encode them as local systems on the curves. The result is an immersed curve in 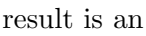 (decorated with local systems) which is an invariant of K.

Remark. There is a refinement of the invariant $\mathfrak{Y}(K)$ over the spin^c structures of the ambient manifold:

$$\mathfrak{Y}(K) = \bigsqcup_{\mathfrak{s}\in \mathrm{Spin}^c(Y)} \mathfrak{Y}(K,\mathfrak{s}).$$

The curve $\mathfrak{Y}(K,\mathfrak{s})$ is not necessarily connected, but it is if $CFK(K,\mathfrak{s})$ is a staircase since, in this case, construction 6.2.6 produces a single non-compact immersed curve, as the reader may check.

Remark (cf. [KWZ20])**.** Only the compact components of $\mathfrak{Y}(K)$ may carry nontrivial local systems.

Proposition 6.2.10. *The existence of compact components in $\mathfrak{Y}(K)$ obstructs the existence of a surgery slope resulting in an L-space.*

Proof. Let $\gamma \subset \mathfrak{Y}(K)$ be compact and connected. Under  , the curve γ maps to a compact curve in the punctured torus which lifts to a curve $\widetilde{\gamma}$ in $\mathbb{C}\backslash\mathbb{Z}^2$. The lift $\widetilde{\gamma}$ necessarily intersects multiple fundamental domains in such

a way that at least one fundamental domain contains multiple subarcs of $\widetilde{\gamma}$. This obstructs the existence of L-space surgery slopes, by Proposition 6.1.4. □

By the above three statements, if $K \subset Y$ is a $(1,1)$ L-space knot, then $\mathfrak{Y}(K)$ is a collection of $|H_1(Y;\mathbb{Z})|$ immersed non-compact curves (with trivial local systems) in  , where the ends of each curve lie on the two punctures. Since we are only interested in detecting L-space knots in this thesis, this implies that we may completely disregard the existence of local systems and think of $\mathfrak{Y}(K)$ as a collection of honest, immersed curves.

6.2.2 Monotonicity

We now wish to reinterpret the staircase condition in terms of immersed curves in  . To motivate the definition, we construct the immersed curve invariant of the knot 8_{19}, for which a $(1,1)$ diagram is illustrated in fig. 4.5, along with $CFK(8_{19})$. Construction 6.2.6 applied to $CFK(8_{19})$, illustrated in fig. 4.5, yields the immersed curve in fig. 6.9, where the labels on the generators are the same as in fig. 4.5.

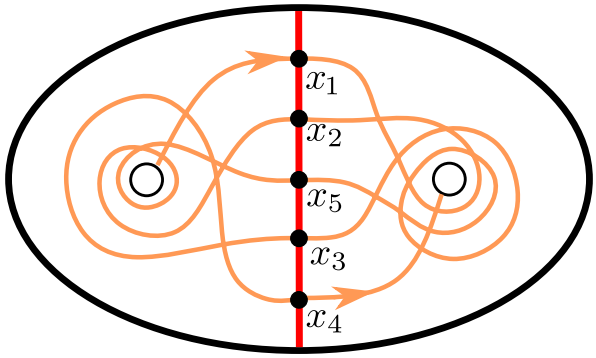

Figure 6.9: An illustration of $\mathfrak{Y}(8_{19})$, oriented to illustrate monotonicity.

If we orient the curve $\mathfrak{Y}(8_{19})$ so that the starting point is at the puncture in A_v and the endpoint is at the puncture in A_u, then the restriction of the

curve to the annulus A_u is oriented consistently with the orientation on  and the restriction of the curve to A_v is opposite to the orientation on  . This property characterizes $\gamma(8_{19})$ as the immersed curve associated to a negative staircase. In the case of a positive staircase, the immersed curve, oriented from the A_v-puncture to the A_u-puncture, is oriented consistently in the V-annulus and inconsistently in the U-annulus. Thus we make the following definition.

Definition 6.2.11. Let $K \subset Y$ be a $(1,1)$ knot. We say that $\gamma(K)$ is **positive-monotone** (resp. **negative-monotone**) if it is a collection of $|\mathrm{Spin}^c|$ non-compact immersed curve in  such that, when we orient the curves from the A_v-puncture to the A_u-puncture, they are oriented consistently in the A_v annulus (resp. in the A_u annulus) and their orientation is opposite the orientation on  in the A_u annulus (resp. the A_v annulus). We say that $\gamma(K)$ is monotone if it is either positive- or negative-monotone.

Chapter 7

The Reproof

Let $\mathcal{D} = (T^2, \alpha, \beta, w, z)$ be a reduced $(1,1)$ diagram of a knot $K \subset Y$ throughout this chapter, which we assume to be GP. We will give a complete proof of theorem 4.2.7. This is in two steps, theorem 7.1.1 and theorem 7.2.1. We prove theorem 7.1.1 by showing, following GLV, that if $\mathcal{D}$ is $\pm$-coherent, then, for every $s \in \mathrm{Spin}^c(Y)$, $(\widetilde{\alpha}_s, \widetilde{\beta})$ is $\pm$-graphic; this then implies that $\boldsymbol{\gamma}(K)$ is monotone. We part from the argument in GLV to prove the converse: we show that if $\mathcal{D}$ is not coherent, then we can find an obstruction to the monotonicity of $\boldsymbol{\gamma}(K) \subset$  . We note here that, other than being a novel argument, this new proof also has the advantage of being more elementary, in the sense that it only requires combinatorial lemmas about $(1,1)$ diagrams, as opposed to a careful analysis of the Alexander and Maslov gradings of the generators of $CFK(\mathcal{D})$, but at present this new proof requires the assumption that the knot is GP. Finally, in theorem 7.2.1 we transfer the monotonicity of $\boldsymbol{\gamma}(K)$ to the setting of $\widehat{HF}(Y \setminus \nu(K)) \subset T^2$ to complete the proof.

Notation. Let us make the convention that the lifts of α are the lines $L_n := \{z \in \mathbb{C} : \mathrm{Im}(z) = n\}$, for $n \in \mathbb{Z}$. If $\widetilde{\alpha}_1$ and $\widetilde{\alpha}_2$ are lifts of α, it makes sense to talk about the (Euclidean) distance between the two lifts, which we denote by $d(\widetilde{\alpha}_1, \widetilde{\alpha}_2)$. Let now $\widetilde{\beta}$ be a lift of β and let $R, R' \subset \widetilde{\beta}$ be lifts of

rainbow arcs. We define $d(R, R')$ to be the distance $d(\widetilde{\alpha}_R, \widetilde{\alpha}_{R'})$, where $\widetilde{\alpha}_R$ is the lift of α which cobounds a rainbow bigon with R.

7.1 Coherence of $\mathcal{D}$ is equivalent to monotonicity of $\curlyvee$

We split the proof following theorem into the two subsequent lemmas.

Theorem 7.1.1. *Let $\mathcal{D}$ be a GP diagram for a knot K. The diagram $\mathcal{D}$ is coherent if and only if $\curlyvee(K)$ is monotone. Moreover, $\mathcal{D}$ is $\pm$-coherent if and only if $\curlyvee(K)$ is $\pm$-monotone.*

Note that the following lemma does not require that the knot be GP.

Lemma 7.1.2. *If $\mathcal{D}$ is a $\pm$-coherent $(1,1)$ diagram for a knot $K \subset Y$, then $\curlyvee(K)$ is $\pm$-monotone.*

Proof. This argument is taken from [GLV18] Fix a lift $\widetilde{\beta}$ of β to the universal cover of T^2 and an element $\mathfrak{s} \in \mathrm{Spin}^c(Y)$. Pick a point $x \in \alpha \cap \beta$ with $s_z(x) = \mathfrak{s}$ and lift $\widetilde{x}$ of x. Let $\widetilde{\alpha}_{\mathfrak{s}}$ be the corresponding lift of α. Orient α and β so that $\widetilde{\alpha}$ orients from left to right and α and β orient the bigons in $\mathcal{D}$. $\widetilde{x}$ is the endpoint of a subarc of $\widetilde{\beta}$ oriented out of $\widetilde{x}$. Suppose this subarc intersects $\widetilde{\alpha}_{\mathfrak{s}}$ in another point and let y be the first such point along $\widetilde{\beta}$. One of two cases occurs: along $\widetilde{\alpha}_{\mathfrak{s}}$, either $y < \widetilde{x}$ or $y > \widetilde{x}$. If $y > \widetilde{x}$, then the subarcs of $\widetilde{\beta}$ and $\widetilde{\alpha}_{\mathfrak{s}}$ from $\widetilde{x}$ to y cobound a bigon B whose boundary is not oriented by $\widetilde{\beta}$ and $\widetilde{\alpha}_{\mathfrak{s}}$. The bigon B attains an extremal point, which is the lift of an extremal point of one of the rainbow arcs of $\mathcal{D}$. Projecting to $\mathcal{D}$, we find a rainbow arc which does not orient its rainbow bigon, which contradicts coherence. Thus the intersection points occur in increasing order along $\widetilde{\beta}$ and in decreasing order along $\widetilde{\alpha}_{\mathfrak{s}}$. This proves that $\widetilde{\beta}$ is positive-graphic, by proposition 4.3.5. We now show that if $(\widetilde{\alpha}_{\mathfrak{s}}, \widetilde{\beta})$ is positive graphic, then the curve $\curlyvee(K, \mathfrak{s})$ is positive-monotone. Label the elements $\widetilde{\alpha}_{\mathfrak{s}} \cap \widetilde{\beta}$ as $x_1, \ldots, x_{2n+1}$, in the order

in which they occur along $\widetilde{\alpha}_{\mathfrak{s}}$. Then the differential on CFK is given by

$$\begin{aligned}\partial x_{2i} &= U^{n_{2i-1}}V^{m_{2i-1}}x_{2i-1} + U^{n_{2i+1}}V^{m_{2i+1}}x_{2i+1}\\ \partial x_{2i-1} &= 0\end{aligned}$$

Since $H_*(CFK|_{U=0}) \simeq H_*(CFK|_{V=0}) \simeq \mathbb{F}$, it follows that, for all i, either $n_{2i-1} = m_{2i+1} = 0$ or $m_{2i-1} = n_{2i+1} = 0$. Moreover, by lemma 5.3.1, the differential evaluates to

$$\partial x_{2i} = U^{n_{2i-1}}x_{2i-1} + V^{m_{2i+1}}x_{2i+1},$$

so that $\Upsilon(K,\mathfrak{s}) \subset$  is a monotone, immersed curve. Furthermore, since $(\widetilde{\alpha}_{\mathfrak{s}}, \widetilde{\beta})$ is $+$-graphic, the element of $CFK(\mathcal{D},\mathfrak{s})$ that generates the vertical homology is x_1, proving that $\Upsilon(K,\mathfrak{s})$ is positive-monotone for every $\mathfrak{s} \in \mathrm{Spin}^c(Y)$, so that $\Upsilon(K)$ is positive-monotone. An analogous argument shows that if $\mathcal{D}$ is negative-coherent, then $\Upsilon(K)$ is negative-monotone. □

Lemma 7.1.3. *Suppose $K \subset Y$ is a $(1,1)$ knot such that $\Upsilon(K)$ is not monotone and $\mathcal{D}$ is a GP $(1,1)$ diagram in normal form for K. Then $\mathcal{D}$ is not coherent.*

Proof. Orient α from left to right and orient β so that the innermost locally maximal rainbow arc co-orients the innermost rainbow bigon. Fix a lift $\widetilde{\beta}$ and label the rainbow arcs R_i, in the order in which they occur when traversing $\widetilde{\beta}$ along its orientation, with R_1 some fixed lift of the innermost locally maximal rainbow arc. The last lift of a distinct rainbow arc is R_{2q}, where $\mathcal{D} = \mathcal{D}(p,q,r,s)$. Note that R_i is a locally maximal rainbow arc if i is odd and a locally minimal rainbow arc if i is even. Since $\mathcal{D}$ is not coherent, there exist indices j such that R_j is locally maximal and does not co-orient its rainbow bigon. Let us put a name to this local manifestation of non-coherence.

Definition 7.1.4. In the notation of the above discussion, let R_{j-2}, R_{j-1}, R_j be such that one and only one of R_{j-2} and R_j co-orients its rainbow bigon. We call the minimal subarc of β containing R_{j-2}, R_{j-1} and R_j a **snail** from

R_{j-2} to R_j. We define the **girth** of the snail to be

$$\max\{d(R_{j-2}, R_{j-1}), d(R_{j-1}, R_j)\}.$$

See fig. 7.1 for sketches of two snails.

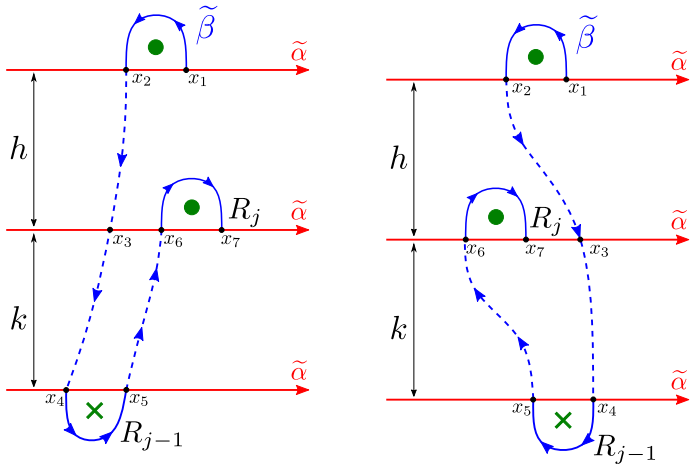

Figure 7.1: Sketch of the snail from R_{j-2} to R_j in the universal cover. Left: case (1), R_{j-1} does not orient its rainbow bigon. Right: case (2), R_{j-1} orients its rainbow bigon.

Let j be the smallest index such that R_j is locally maximal and does not co-orient its rainbow bigon. Note that $j \geq 3$ and there is a snail from R_{j-2} to R_j. We have two cases: (1) R_{j-1} doesn't orient its rainbow bigon or (2) it does. If we suppose that

$$d(R_{j-2}, R_{j-1}) \geq d(R_{j-1}, R_j), \tag{7.1}$$

then the two cases are illustrated in fig. 7.1. If instead of the inequality eq. (7.1), we have $d(R_{j-2}, R_{j-1}) \leq d(R_{j-1}, R_j)$, then the reader may check that we obtain completely analogous sketches of the snail and the following argument applies as is. It is therefore without loss of generality that we assume eq. (7.1). Note that each of the dotted arcs in fig. 7.1 consists of some number, $h + k$ or k, of vertical arcs, with $h, k \geq 0$. Let us label by

x_i the lifts of elements of $\alpha \cap \beta$ which occur along the snail, in the order in which they appear.

If the snail is as in case (2), this immediately obstructs the monotonicity of $\curlyvee(K)$: the bigons $x_3 \to x_6$ and $x_6 \to x_7$ in fig. 7.1 are pure, since the bigon $x_3 \to x_6$ is graphic and we are assuming that $\mathcal{D}$ is GP. Therefore these two bigons contribute an arc γ to $\curlyvee$. Furthermore, once we orient $\curlyvee$, the arc γ is either consistently oriented in both annuli or inconsistently oriented in both annuli. Thus $\curlyvee$ cannot be monotone.

We will prove that case (1) obstructs the monotonicity of $\curlyvee(K)$ by induction on $h + k$, i.e. the girth of the snail.

Suppose first that $h = k = 0$, so the three lifts of α in fig. 7.1 coincide and the snail in the universal cover looks like one of the snails in fig. 7.2. Each

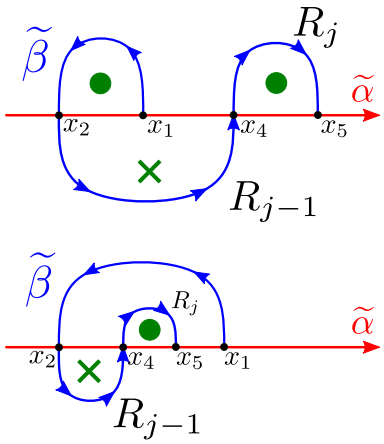

Figure 7.2: Sketch of the possible snails in case (1) if $h = k = 0$.

of the snails in 7.2 contributes an obstructing subarc to $\curlyvee(K)$, as in fig. 7.3.

Indeed, only part of any of these snails is required to obstruct monotonicity: the parts illustrated in fig. 7.3 contribute a subarc $\gamma \subset \curlyvee(K)$, also indicated in the figure. Depending on the orientation of $\curlyvee(K)$, the arc γ is either oriented consistently in both the U- and the V-annulus, or it is oriented

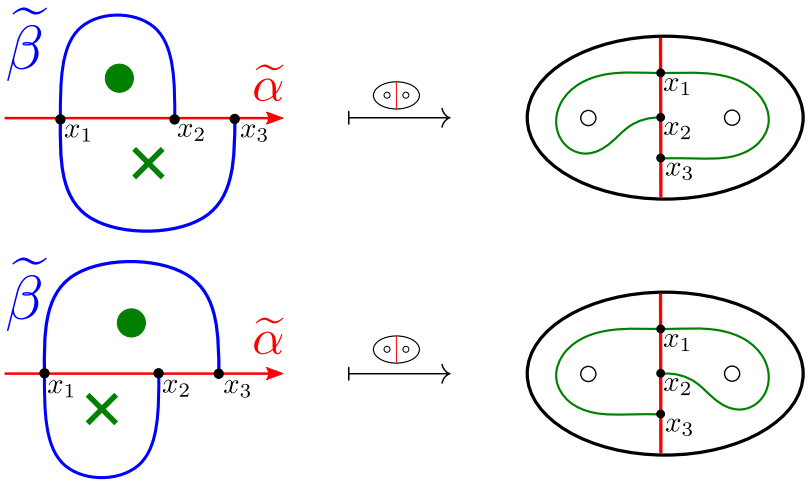

Figure 7.3: The disc transformation applied to a subarc of $\widetilde{\beta}$.

inconsistently in both annuli. This proves the base case. We remark here that the bigons in fig. 7.3 would still provide an obstruction if they contained more lifts of the basepoints, as long as the bigons remained pure.

Suppose next that $h + k > 0$. To find an obstruction, we walk backwards along $\widetilde{\beta}$ and pick out the first intersection point with one of the lifts of α drawn in fig. 7.1. Let us call this point y and denote by Γ the subarc of $\widetilde{\beta}$ from y to x_1. We proceed by cases, depending on where y lies. These are drawn in fig. 7.4.

To access the induction hypothesis, we need the following.

Lemma 7.1.5. *Suppose a subarc $\gamma \subset \widetilde{\beta}$ is non-graphic, in the sense of definition 5.3.2. Suppose furthermore that γ is contained between two lifts of α which are a distance d apart. Then there is a snail in $\widetilde{\beta}$ of girth less than d.*

We postpone the proof and now proceed to prove the statement in each of the subcases (1.1) through (1.4). For all subcases, if Γ is not graphic, lemma 7.1.5 provides us with a snail whose girth is strictly smaller than h. The induction hypothesis then lets us conclude that there exists a sub-

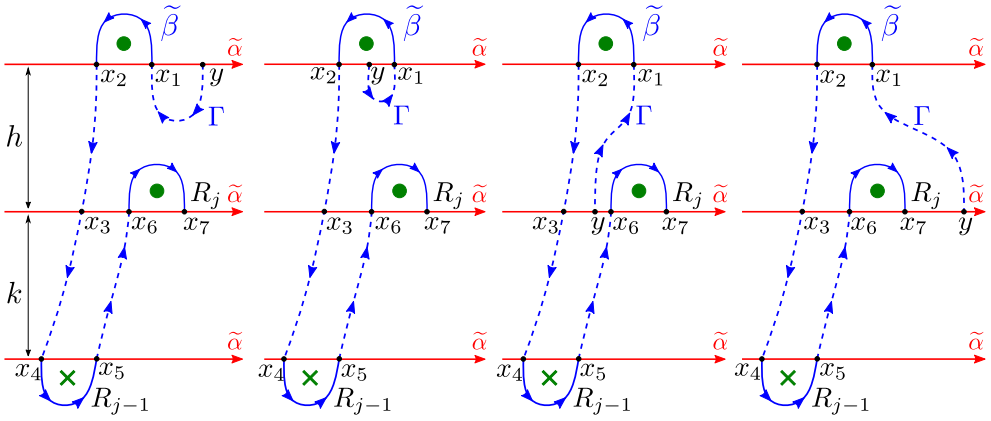

Figure 7.4: Possible extensions of the snail from case (1). Note that Γ may contain both rainbow and vertical arcs, whereas the other dotted arcs consist only of vertical arcs.

curve in $\curlyvee(K)$ obstructing its monotonicity. Let us suppose then that Γ is graphic. In every subcase other than (1.1), we invoke conjecture 1 to obtain an obstructing subcurve of $\curlyvee(K)$. In subcase (1.2), Γ cobounds with the top lift of $\widetilde{\alpha}$ a pure bigon $x_1 \xrightarrow{V^k} y$, for some $k \geq 1$. This bigon together with the bigon $x_1 \xrightarrow{U} x_2$ produce an obstruction as in fig. 7.3. In subcase (1.3), the obstruction is due to the bigons $x_3 \to y$ and $x_6 \to x_3$. In subcase (1.4), the obstruction comes from the bigons $x_3 \to y$ and $x_6 \to x_3$.

Let us suppose finally that we are in case (1.1) and Γ is graphic. Let us also denote the top lift of α in fig. 7.4 by $\widetilde{\alpha}_1$ and the bottom lift by $\widetilde{\alpha}_2$. In this case, the only way both $(\widetilde{\alpha}_1, \widetilde{\beta})$ and $(\widetilde{\alpha}_2, \widetilde{\beta})$ can be graphic is if $(\widetilde{\alpha}_1, \widetilde{\beta})$ is negative-graphic and $(\widetilde{\alpha}_2, \widetilde{\beta})$ is positive-graphic. In this case it is therefore also not possible for $\curlyvee(K)$ to be monotone, since, it would contain two connected components which are not both positive-monotone or both negative-monotone. This completes the proof of the lemma and of Theorem 7.1.1. □

Proof of Lemma 7.1.5. Let $\widetilde{\alpha}_1$ and $\widetilde{\alpha}_2$ be the two lifts bounding γ and orient

them from left to right. Orient $\widetilde{\beta}$ as well and let $\{R_i\}_{i=1}^n$ be the set of rainbow arcs in γ, in the order in which they are encountered along γ with the chosen orientation. The statement that γ is not graphic is equivalent to the statement that the map $\Psi\colon \{1,\dots,n\} \to \{0,1\}$, given by

$$\Psi(i) = \begin{cases} 0 & \text{if } R_i \text{ co-orients its rainbow bigon with } \widetilde{\alpha} \\ 1 & \text{otherwise} \end{cases}$$

is surjective.

If there is a snail in γ, then we are done, since γ is bounded by lifts of α which are a distance d apart, so the mentioned snail has girth strictly bounded above by d. Conversely, suppose there is no snail in γ. Note that the existence of a snail in γ is equivalent to the existence of one of the substrings $(0,1,1)$, $(0,0,1)$, $(1,1,0)$ or $(1,0,0)$ in the n-tuple $(\Psi(1),\dots,\Psi(n))$. Since Ψ is surjective, the n-tuple $(\Psi(i))$ must be alternating, i.e. either $(1,0,1,\dots)$ or $(0,1,0,\dots)$. In either case, this implies that the curve γ is, up to isotopy in $\mathbb{R}^2$ punctured at the lifts of w and z, a spiral such as the one in fig. 7.5.

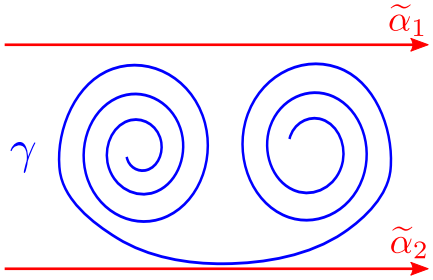

Figure 7.5: Possible γ with $(\Psi(i))$ an alternating string of 1 and 0.

In other words, we may say, once we put a metric on $\mathbb{R}^2$, that $(\Psi(i))$ is alternating if and only if γ is either right-veering everywhere or left-veering everywhere. It is certainly possible for γ to be a right- or left-veering curve with an arbitrary number of local maxima and minima, but, since there are finitely many rainbow arcs in a normal form $(1,1)$ diagram and the complement $\gamma' := \widetilde{\beta} \setminus \gamma$ intersects $\widetilde{\alpha}_1$ and $\widetilde{\alpha}_2$, γ' needs to veer in the opposite

direction of γ, so there is a snail in $\gamma' \cup \gamma$ between the lifts $\widetilde{\alpha}_1$ and $\widetilde{\alpha}_2$, providing us with a snail of girth strictly smaller than d. □

7.2 Υ detects L-space knots

Theorem 7.2.1. *Suppose $K \subset Y$ is a $(1,1)$ knot. The curve $\Upsilon(K)$ is monotone in*  *if and only if K is an L-space knot. Moreover, $\Upsilon(K)$ is $\pm$-monotone if and only if K is a $\pm$ L-space knot.*

Proof. Suppose first that $\Upsilon(K)$ is $+$-monotone in  , so that $\Upsilon(K)$ consists of $|\mathrm{Spin}^c(Y)|$ immersed, non-compact, connected curves. Equivalently, $CFK(K)$ is a collection of $|\mathrm{Spin}^c|$ positive staircases. By Theorem 6.1.9, the set of L-space slopes on K^c is the interval $[L(K)-1, \infty]$, proving that K is a positive L-space knot. A similar argument shows that if $\Upsilon(K)$ is negative-monotone, then K is a negative L-space knot.

Conversely, suppose that $\Upsilon(K)$ is not monotone. In this case, there is a subarc $\gamma \subset \Upsilon$ like the green arc in the right-hand side of fig. 7.3, namely an arc which, after choosing an orientation on $\Upsilon(K)$, is oriented coherently in both A_v and A_u. In this case, by the same argument as the one in Proposition 6.2.10, this arc obstructs the existence of a nontrivial L-space slope. We briefly restate this argument. The map  takes γ to a subarc $\overline{\gamma}$ of $\widehat{HF}(K^c)$ and a $\overline{\gamma}$ lifts to a curve $\widetilde{\gamma}$ in $\mathbb{C} \setminus \mathbb{Z}^2$ with the following property: it crosses a fundamental domain twice, in such a way that every line of non-infinite slope in $\mathbb{C}$ which intersects $\widetilde{\gamma}$ transversely, intersects it in two points. By Proposition 6.1.4, these two intersection points lie in the same spin^c grading of the surgered manifold, so the result of the Dehn surgery is not an L-space. □

Chapter 8

Conclusion

The goal of this thesis was, broadly, to explain the similarities between the characterization of L-space knots provided by Theorem 1.2 in [GLV18] and the formalism of immersed curves constructed in [HRW16], [HRW18] and [KWZ20]. This goal was partially achieved, after a long build up, by equating the notion of coherence in a GP $(1,1)$ diagram with the notion of monotonicity of the immersed curve invariant γ in Theorems 7.1.1 and 7.2.1. The author still hopes that in the very near future, he will prove Conjecture 1, establishing the results of this paper in general, and erasing the letters GP from the statements of the main results.

At the start of this project, the author had in mind a more ambitious means of achieving the stated goal. This was to build a general correspondence which takes knot Floer chain complexes of knots into curves immersed in a surface. Building such a correspondence would fit nicely into the program of relating some of the modern homology theories to Fukaya categories of surfaces. To this program belong many recent research efforts, listed in the references of [KWZ20], and including immersed curve invariants constructed for 4-ended tangles by C. Zibrowius and immersed curve invariants for Khovanov homology by A. Kotelskiy, L. Watson and Zibrowius. The following open question lurks in the background of this body of work:

Question. Given an algebraic invariant (for knots, tangles or manifolds, for example) that admits an interpretation as an immersed curve in some surface, is there a path of least resistance from the object to the immersed curve? In other words, is there a way to obtain the immersed curve invariant from the object itself, without passing through the algebraic invariant?

It is still a goal of the author to understand the general framework for turning relative homological invariants into immersed curves which pair up using Lagrangian intersection homology.

Finally, let us mention that despite the shortcoming of requiring that the knots be GP, the direct method developed in this thesis for analysing the bigons in $(1,1)$ diagrams seems likely to be useful to a future researcher in the knot Floer theory of $(1,1)$ knots. It certainly points to some unexpectedly complex combinatorics for $(1,1)$ diagrams.

Bibliography

BGW13. Steven Boyer, Cameron McA. Gordon, and Liam Watson. On L-spaces and left-orderable fundamental groups. *Mathematische Annalen*, 356(4):1213–1245, 2013.

CK03. Doo Ho Choi and Ki Hyoung Ko. Parameterizations of 1-bridge torus knots. *Journal of Knot Theory and Its Ramifications*, 12(04):463–491, jun 2003.

Dol92. Helmut Doll. A generalized bridge number for links in 3-manifolds. *Mathematische Annalen*, 294:701–717, 1992.

Doy05. Gabriel Doyle. Calculating the Knot Floer Homology of (1, 1) Knots, 2005. BSc. Thesis, Princeton University.

FM97. A. T. Fomenko and S. V. Matveev. *Algorithmic and Computer Methods for Three-Manifolds*, volume 425 of *Mathematics and Its Applications*. Springer Netherlands, 1997.

FM12. Benson Farb and Dan Margalit. *A primer on mapping class groups*. Princeton University Press, Princeton, 2012.

Fuj96. Hirozumi Fujii. Geometric indices and the Alexander polynomial of a knot. *Proceedings of the American Mathematical Society*, 124(9):2923–2933, 1996.

GLV18. Joshua Greene, Sam Lewallen, and Faramarz Vafaee. $(1,1)$ L-space knots. *Compositio Mathematica*, 154(5):918–933, 2018.

GMM05. Hiroshi Goda, Hiroshi Matsuda, and Takayuki Morifuji. Knot Floer homology of (1, 1)-knots. *Geometriae Dedicata*, 112(1):197–214, 2005.

Hir76. Morris W. Hirsch. *Differential Topology*. Springer New York, 1976.

HL16. Matthew Hedden and Adam Simon Levine. Splicing knot complements and bordered Floer homology. *Journal fr die reine und angewandte Mathematik (Crelles Journal)*, 2016(720), jan 2016.

Hom13. Jennifer Hom. Bordered heegaard floer homology and the tau-invariant of cable knots. *Journal of Topology*, 7(2):287–326, aug 2013.

HRW16. Jonathan Hanselman, Jacob Rasmussen, and Liam Watson. Bordered Floer homology for manifolds with torus boundary via immersed curves, 2016. arXiv:1604.03466.

HRW18. Jonathan Hanselman, Jacob Rasmussen, and Liam Watson. Heegaard Floer homology for manifolds with torus boundary: properties and examples, 2018. ArXiv:1810.10355v1.

Juh15. András Juhász. A survey of Heegaard Floer homology. In *New ideas in low dimensional topology*, volume 56 of *Ser. Knots Everything*, pages 237–296. World Sci. Publ., Hackensack, NJ, 2015.

KWZ20. Artem Kotelskiy, Liam Watson, and Claudius Zibrowius. A mnemonic for the Lipshitz-Ozsvth-Thurston correspondence, 2020. arXiv:2005.02792.

LOT18. Robert Lipshitz, Peter Ozsvath, and Dylan Thurston. Bordered Heegaard Floer homology. *Memoirs of the American Mathematical Society*, 254(1216):0–0, jul 2018.

Man16. Ciprian Manolescu. An introduction to knot Floer homology. In *Physics and Mathematics of Link Homology*, volume 680 of *Contemporary Mathematics*, Providence, Rhode Island Montreal, Quebec, Canada, 2016. American Mathematical Society Centre de Recherches Mathematiques.

Mat02. Hiroshi Matsuda. Genus one knots which admit (1,1)-decompositions. *Proceedings of the American Mathematical Society*, 130(07):2155–2164, 2002.

Mil63. John W. Milnor. *Morse Theory*. Princeton University Press, dec 1963.

Mil16. John Milnor. *Lectures on the H-Cobordism Theorem*. Princeton University Press, 2016.

Moi77. Edwin E. Moise. *Geometric Topology in Dimensions 2 and 3*. Springer New York, 1977.

Mor60. Marston Morse. The existence of polar non-degenerate functions on differentiable manifolds. *Annals of Mathematics*, pages 352–383, 1960.

MS91. Kanji Morimoto and Makoto Sakuma. On unknotting tunnels for knots. *Mathematische Annalen*, 289(1):143–167, mar 1991.

Ord06. Philip J. P. Ording. *On knot Floer homology of satellite (1,1) knots*. PhD thesis, Columbia University, 2006.

OS03. Peter Ozsváth and Zoltán Szabó. Knot Floer homology and the four-ball genus. *Geometry & Topology*, 7(2):615–639, oct 2003.

OS04a. Peter Ozsváth and Zoltán Szabó. Holomorphic disks and knot invariants. *Advances in Mathematics*, 186(1):58–116, aug 2004.

OS04b. Peter Ozsváth and Zoltán Szabó. Holomorphic disks and three-manifolds invariants: Properties and applications. *Annals of Mathematics*, 159(3):1159–1245, may 2004.

OS04c. Peter Ozsváth and Zoltán Szabó. Holomorphic disks and topological invariants for closed three-manifolds. *Annals of Mathematics*, 159(3):1027–1158, may 2004.

Per08. Timothy Perutz. Hamiltonian handleslides for Heegaard Floer homology. In *Proceedings of Gökova Geometry-Topology Conference 2007*, pages 15–35. Gökova Geometry/Topology Conference (GGT), Gökova, 2008.

Rác15. Béla András Rácz. *Geometry of (1, 1)-knots and knot Floer homology.* PhD thesis, Princeton University, 2015.

Ras03. Jacob Rasmussen. *Floer homology and knot complements.* PhD thesis, Hardvard University, 2003.

Ras05. Jacob Rasmussen. Knot polynomials and knot homologies. In *Geometry and topology of manifolds*, volume 47 of *Fields Inst. Commun.*, pages 261–280. Amer. Math. Soc., Providence, RI, 2005.

Rol03. Dale Rolfsen. *Knots and Links.* AMS Chelsea, 2003.

RR17. Jacob Rasmussen and Sarah Dean Rasmussen. Floer simple manifolds and L-space intervals. *Advances in Mathematics*, 322:738–805, dec 2017.

Sav12. Nikolai Saveliev. *Lectures on the Topology of 3-Manifolds.* De Gruyter, Berlin, Boston, 2012.

Sch54. Horst Schubert. Über eine numerische Knoteninvariante. *Mathematische Zeitschrift*, 61(1):245–288, dec 1954.

Sch93. Matthias Schwarz. *Morse Homology.* Birkhäuser Basel, 1993.

Thu97. William P. Thurston. *Three-Dimensional Geometry and Topology, Volume 1.* Princeton University Press, dec 1997.

Tur97. Vladimir Turaev. Torsion invariants of Spin^c-structures on 3-manifolds. *Mathematical Research Letters*, 4(5):679–695, 1997.

Zem17. Ian Zemke. Connected sums and involutive knot Floer homology. 2017.